**Title**
The Effect of Lipid Chemistry and Structure on Liposome Formation



**Author**
Perttu, Emily

**Publication Date**
2012

Peer reviewed|Thesis/dissertation

The Effect of Lipid Chemistry and Structure on Liposome Formation

by

Emily K Perttu

DISSERTATION

Submitted in partial satisfaction of the requirements for the degree of

DOCTOR OF PHILOSOPHY

in

Bioengineering

in the

GRADUATE DIVISION

of the

UNIVERSITY OF CALIFORNIA, SAN FRANCISCO

AND

UNIVERSITY OF CALIFORNIA, BERKELEY

To my mother, for without her selfless love, I would not be who I am or where I am today. To my father for his unmatched display of unconditional love and support. And, for Sully, my Brown Eyed Girl, "standing in the sunlight, laughing."

~Little Children Love Each Other~
Acknowledgements (I)

The text of Chapter 2 is in part a reprint of materials submitted to the Journal of the American Chemical Society. Emily K. Perttu wrote the paper and Frank C. Szoka, Jr. revised the manuscript.

The text of Chapter 3 is in part a reprint of materials published in the journal Chemical Communications. Emily K. Perttu wrote the paper Frank C. Szoka, Jr. revised the manuscript. Emily K. Perttu and Francis C. Szoka Jr. *Zwitterionic sulfobetaine lipids that form vesicles with salt-dependent thermotropic properties. Chem. Commun.*, 2011, **47**, 12613-12615.

Acknowledgements (II)

Dr. Francis C. Szoka, Jr.—For his mentorship, breadth of knowledge, and steadfast guidance throughout the completion of this work.

Dr. Tejal Desai—For serving as my graduate advisor and member of my qualification exam and thesis committees, as well as for her helpful support along the way.

Dr. Seung-Wuk Lee—For serving as a member of my qualification exam and thesis committees and for his belief in me and my abilities.

Dr. Ken Dill, Dr. Brian Shoichet, and Dr. Chris Diederich—For serving on my qualification exam committee.

To the current and past members of the Szoka lab who have made my time in lab enjoyable and memorable: Kat Jerger, Colin Walsh, Vincent Venditto, Doug Watson, Derek van der Poll, Darren Chan, Juliane Nguyen, Kareen Riviere, Matt Tiffany, Aditya Kohli, Jonothan Sockolosky, Bo Chen, and Michael Motion.

Dr. Daniel Sheehan—For his inspiring mentorship, support, and ability to nurture a lasting desire for research within me.

Dr. Peter Iovine—For providing me with a strong foundation in chemical research and many outstanding opportunities to mature as a scientist.

To my friends and family who have supported me throughout my work while only occasionally asking me when I would be finished.

This work was support by the National Science Foundation Graduate Research Fellowship Program and NIH grants EB003008; GM061851 and a UCSF-QB3 Pfizer grant.

Abstract

Lipids have been known to self-assemble into vesicles for over four decades; a process that has been exploited in fields ranging from drug delivery to the study of cellular mimics. The supramolecular properties of the liposome are primarily determined by the individual lipids which comprise it. Small changes to the architecture or chemistry of the lipid can result in significant alterations to both liposomal properties and the ease of liposome formation, and sometimes result in the formation of an entirely different aggregation phase (micelle, fiber, tube, etc…). Both experimental and theoretical methods have been employed to devise a framework for predicting how a given lipid will assemble in water and how the resulting liposomal will behave. To date, a number of basic principles exist that focus primarily on traditional phospholipids systems. My thesis work has added a number of new lipids that might be used to further test the properties of bilayer formation.

In the first chapter of this thesis, I discuss how lipid structure can affect liposomal properties relevant to drug delivery. In the second and third chapters, I report on novel lipids that explore how alterations to the charge-orientation and type of anion in the lipid headgroup affect the liposome's biophysical characteristics (i.e. transition temperature, permeability, surface potential, interaction with divalent cations) and in one case, even eliminates the lipid's ability to form vesicles under standard conditions. In the fourth and fifth chapters of this thesis, I describe a class of synthetic zwitterionic bolaamphiphiles that is capable of forming small diameter vesicles and discuss the possible configurations of the compounds within the vesicle wall as well as modifications to the bolaamphiphile that may enable them to be used in drug delivery. Each of these four classes of new

lipids produced vesicles with unpredicted and interesting properties. They should provide biophysical chemists additional tools to study the physical and chemical properties of membranes and could contribute to the development of new liposome therapeutics.

Table of Contents

# List of Tables

# List of Figures

CHAPTER 1

# The Impact of Lipid Design and Self-Assembly on Liposomal Drug Delivery Systems

## 1.1 Introduction to Liposomes

All naturally occurring lipids self-assemble into supramolecular aggregates such as micelles and bilayers. In 1965, Bangham[1] published that lipid bilayers formed from phospholipids assemble into vesicles which he named liposomes (Fig. 1-1). In the intervening decades, liposomes have become the most successful nanoparticle therapeutic, with several FDA-approved liposomal therapies for the treatment of a variety of cancer types and fungal infections[2]. Liposomes can encapsulate a wide variety of substrates from small molecules to large biopolymers, such as RNA and DNA[3]. Encapsulation of these compounds can dramatically increase their circulation time, alter their biodistribution and reduce their degradation. Unlike their cargo, liposomes, which are typically ~80-150 nm in diameter, are not subject to renal clearance and can passively accumulate at sites of inflammation and in tumors through the Enhanced Permeability and Retention (EPR) effect[4].

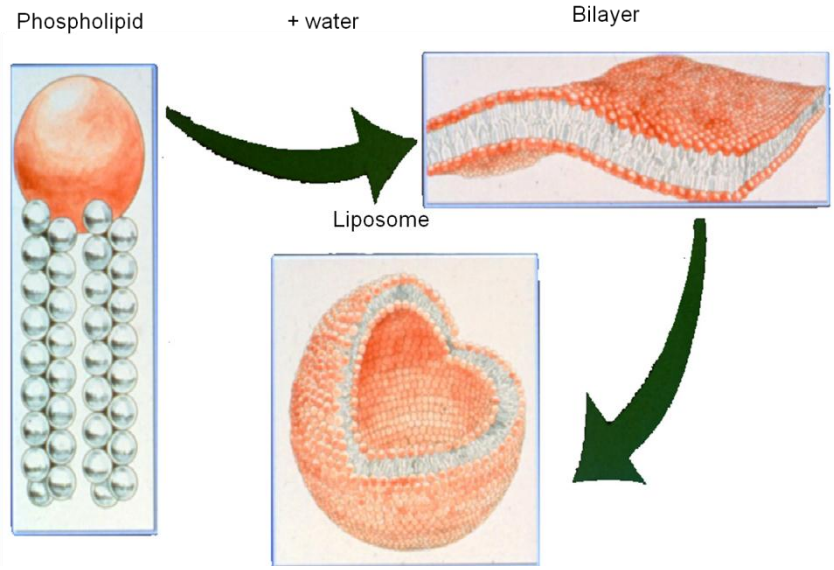


**Figure 1-1: Process of phospholipid assembly to form bilayers and liposomes**

Liposomes are easily prepared from formulations containing commonly used lipids, such as phosphocholine (PC), phosphatidylglycerol (PG), phosphatidylethanolamine (PE), and cholesterol through a variety of methods, such as thin film hydration, ethanol dilution, and reverse-phase evaporation[5]. While traditional lipids are able to form stable liposomes and encapsulate a variety of molecules; in order for the liposome field to continue to advance and take on more therapeutic challenges, new lipids with a variety of structures and functionalities should be pursued to overcome current roadblocks, such as site-specific delivery, cellular uptake, endosomal escape, and controlled release.

The liposomal properties that are most desirable can vary depending on the type of therapy (i.e. targeted delivery vs. systemic or small molecule drug vs. biopolymer). Often, advantageous liposome characteristics can be easily outlined on paper; however, the next steps of (1) designing a lipid structure that is likely to meet those requirements, (2) synthesizing the lipid, and then (3) being able to form liposomes that behave as predicted, are much more complex. The properties of the liposome, not just the individual lipids are the key to a successful delivery system, especially for mixed-lipid systems. It is very difficult to predict *a priori* how a newly synthesized lipid will affect both the formation and the resulting properties of a liposome. Many of the overall liposomal attributes are affected by multiple aspects of the individual lipid. For instance, in Chapter 3 of this thesis, I will discuss how both the lipid headgroup and the length of the hydrocarbon chain affect the liposome transition temperature ($T_m$). Therefore, designing a portion of a lipid with one favorable property in mind may result in a

disadvantageous change in another property. Additionally, some alterations to a lipid structure may improve the process of liposome formation or drug loading, but lead to disadvantageous effects when administered *in vivo*. An example of this is the use of cationic headgroups in the delivery of oligonucleotides. The incorporation of a positive charge in the lipid headgroup enables the efficient loading of anionic biopolymers through electrostatic interactions; however, cationic lipid headgroups have proven to be toxic *in vivo*[6]. It is not only difficult to predict the overall liposomal properties based on an individual lipid structure, it can also be challenging to predict how easily the lipids will form a vesicle, if at all.

When discussing lipid design and liposome formation, it is advantageous to have a basic understanding of the properties of a liposome that have the greatest impact on its biological fate and success as a drug delivery vehicle. In general, the most important aspects of liposome are: (1) the liposome surface (i.e. charge, hydration, presence of bioactive molecules, etc…), (2) the permeability of the bilayer and (3) the diameter. Each of these three aspects is important and any of them alone can cause a potential liposome therapeutic to fail if not appropriately addressed. Furthermore, changes to any region of the lipid (the headgroup, the hydrophobic tails, or the linkage between the two) can affect any of these three general characteristics or even the phase that a lipid adopts when dispersed in water. The work presented in this thesis touches on all three of these liposomal attributes as well as the process of liposome formation, which has a significant impact on the final diameter of a liposome. In Chapters 2 and 3, I report on lipids with headgroup modifications that result in significant alterations to properties of the liposome surface, the permeability, and the capacity to form liposomes altogether. In Chapter 4 I

describe lipid-like molecules designed to form small-diameter vesicles and discuss the possible configurations of the molecule in the vesicle wall. In the remainder of this introduction, I will provide a brief background on two general areas. In section 1.2.1, I present an overview on importance of lipid headgroup chemistry and discuss how alterations to a headgroup can result in changes to the overall nature of the liposome. In Section 1.2.2, I discuss the predominant theories behind vesicle formation and the lipid traits that may promote the formation of small vesicles within the context of each of the theories presented.

**1.2 The Lipid Headgroup**

The nature of a lipid headgroup influences how it interacts with the biological environment, the encapsulated cargo (and its permeability), and other lipid headgroups. It also contributes to the overall lipid geometry, the transition temperature and the phase a given lipid preferentially adopts when dispersed in an aqueous environment.

The interactions of the lipid headgroup with the biological environment can be detrimental to its efficacy as a drug carrier. How a host recognizes and reacts toward a liposome is largely based on its overall surface charge, which strongly impacts the circulation time, biodistribution and toxicity of a liposome. Many non-specific interactions and immune responses are, in part, driven by the overall charge of a foreign particle. Generally, neutral hedgroups interact to a lesser extent with components in the biological medium and have longer circulation times. Relative to neutral liposomes, anionic liposomes of the same size are more rapidly recognized by reticuloendothelial system macrophages which results in a faster clearance and higher mononuclear

phagocyte system uptake[7-9]. Furthermore, both anionic and cationic lipids activate complement to a greater extent than neutral liposomes[10].

Anionic lipids that occur naturally in small amounts often act as signaling molecules for a variety of biological mechanisms including apoptosis and cell growth[11, 12]. Anionic lipids can also interact with divalent cations (i.e $Ca^{2+}$ and $Mg^{2+}$), which can mediate liposome aggregation and fusion[13]. Even zwitter-neutral phosphocholine (PC) liposomes can coordinate with $Ca^{2+}$ (without aggregating) resulting in a positive surface potential at physiologically relevant $Ca^{2+}$ concentrations[14]. Chapters 2 and 3 report on two different zwitter-neutral headgroups, similar to PC, which have an inversion of the charged headgroup moieties at the bilayer surface. The lipids in Chapter 2 (CP lipids), have an anionic phosphate group while those in Chapter 3 (sulfobetaine or SB lipids), have an anionic sulfonate group. These two lipids interact with $Ca^{2+}$ to a lesser extent than PC lipids and their liposomes maintain a negative surface potential in up to 10 mM $Ca^{2+}$. This difference in $Ca^{2+}$ interaction highlights shows how subtle changes to a headgroup can result in significant changes to the overall liposome.

Unlike anionic lipids, there are no significant cationic lipids found naturally in humans (the cationic sphingosine is a precursor to ceramides and sphingolipids, but is present in very low concentrations). Cationic lipids can lead to aggregation in the presence of anionic serum proteins and can result in embolisms when they become trapped in the lungs[7, 15]. Cationic lipids can also interact with natural anionic lipids and bilayers, leading to bilayer destabilization and cell lysis.

The interactions of the biological environment discussed above significantly impact the pharmacokinetics of a liposome *in vivo*, but it is ultimately the

pharmacokinetics of the cargo that matter and so the permeability of a liposome is also of great importance. The lipid headgroup can have a significant impact on the permeability of a molecule with the functional group closest the bilayer surface being of greatest importance. When the region of the headgroup closest to the bilayer interface interacts with a molecule, usually through electrostatics, it increases its local concentration at the bilayer surface and in turn, its probability of permeation. If the charge adjacent to the bilayer is negative, as in the case of phospholipids headgroups like PC, cationic molecules pass through the bilayer at a faster rate than anionic molecules. Likewise, for lipids with a cationic group adjacent to the bilayer, anionic molecules have increased permeabilities[16]. This affect is highlighted in Chapters 2 and 3, which show that zwitter-neutral CP and SB lipids with an inverted headgroup charge (cation adjacent to the bilayer) are more permeable than PC liposomes to an anionic, water-soluble dye, carboxyfluorescein. When mixtures of a PC and a charge-inverted lipid are formulated together, an intermediate release rate is observed.

In addition to the electrostatic "ushering" of charged solutes across the bilayer, the headgroup size can also influence the passage of solutes across the bilayer[17] and an increase in permeability has been correlated with an increase in the average lipid headgroup area.

During a phase transition, the bilayer moves from a crystalline state to a fluid state and the temperature at which that occurs is determined in part by the length and packing of the hydrocarbon chains[18]. The energy required to melt the chains and disrupt the associated van der Waals attractive forces increases with increasing chain length and packing order. Additionally, high headgroup interaction energies can affect the $T_m$ of a

bilayer. When a headgroup interacts with other headgroups more than solutes and water molecules in solution, the $T_m$ of the bilayer is increased and the hydration of the liposome surface is reduced. In addition to chain-chain attractions, strong headgroup interactions, due to either hydrogen bonding or ion pairing, must also be overcome for the bilayer to adopt a fluid phase[19]. The headgroup interactions can create a considerable energy barrier as is demonstrated in the large differences in $T_m$ for PE and PC bilayers with the same hydrocarbon chain lengths. PE bilayers have much higher $T_m$ than PC bilayers and the increase is due to strong hydrogen bonding between the protonated amine and the phosphate groups on adjacent lipids[20-22]. Phosphatidic acid headgroups, which are also able to hydrogen bond when partially protonated, have elevated $T_m$ relative to PC headgroups[21].

The PC headgroup is not able to hydrogen bond with its neighbors; however, it could potentially form ion pairs. The transition temperatures for the PA, PE, and PC lipid bilayers alone might suggest that elevated $T_m$ are only observed for lipids that can hydrogen bond. However, as I discovered in the work covered in Chapters 2 and 3, predicting which headgroups will form strong interactions with the neighboring headgroups is not straightforward. In Chapter 3, I report that SB lipids, which cannot directly hydrogen bond to each other, interact with one another via electrostatic interactions and have $T_m$ close to PE lipids with the same chain lengths. In Chapter 2, I show that the CP lipids have no increase in $T_m$ relative to PC lipids. Therefore, ion pairing in the SB lipids leads to increased $T_m$ and the orientation of the charge does not affect the $T_m$. A result like this (ion paring in the SB lipids, but not the CP or PC lipids) would be difficult to foretell based solely on lipid structure and it highlights the difficulty

associated with the design of new lipids for liposomal delivery systems. It remains unclear whether the difference in behavior is due to the hydration of the headgroup moieties, the strength interaction between the two anions and the quaternary amine, sterics, or another phenomenon.

The above properties relate primarily to the headgroup chemistry and its impact on molecular interactions. The last headgroup property we will discuss—the headgroup volume—does not specifically take into consideration the chemistry of the headgroup, just its size. As will be discussed in more detail in section 1.3.3, the geometric contribution of the headgroup to the lipid's overall hydrophilic/hydrophobic volume ratio influences the ability of the lipid to form liposomes over other aggregate phases. The size, hydration, and charge of a headgroup determine the average surface area per lipid in a liposome. For a given chain length, an increase in the headgroup surface area promotes greater curvature of the monolayer while a decrease in headgroup area can favor the formation of a hexagonal phase. These two scenarios are observed for the naturally occurring headgroups: PG and PE. The addition of a small percent (5-10%) of the anionic PG lipid can promote the formation of small diameter liposomes, while PE lipids, which have a small surface area, are often exploited for their fusogenic properties as they naturally adopt an inverted hexagonal phase[23].

## 1.3 Lipid Assembly

The previous section described how small changes to a lipid headgroup can lead to substantially different liposome properties. This section takes a step backward and looks at the process of going from a lipid to a liposome, and focuses on the factors limiting the formation of small-diameter vesicles. Lipids and amphiphiles in general, can

adopt a wide variety of supramolecular structures, such as spherical micelles, tubular micelles, toroids, bilayer tubes, hexagonal phases, and vesicles with a variety of diameters.

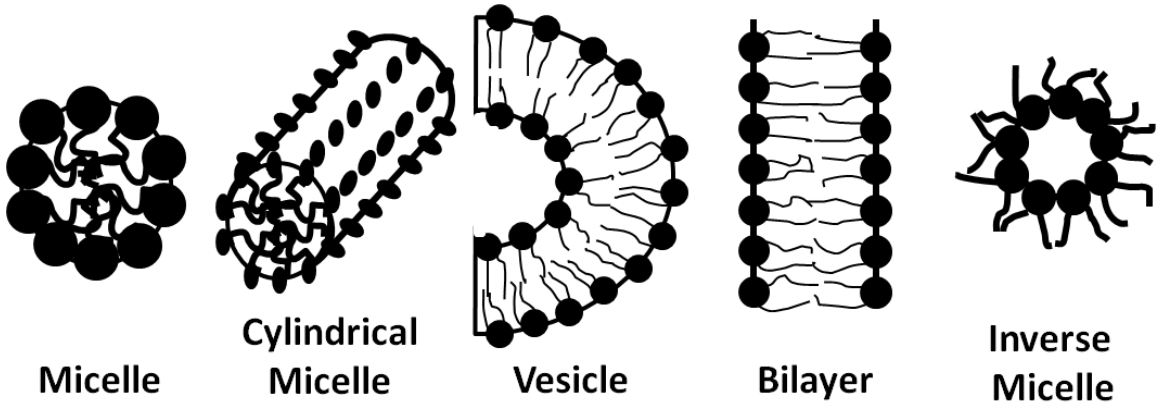


**Figure 1-2: Examples of possible lipid aggregates**

Predicting the aggregate phase a given lipid will adopt can be tricky. In addition to the lipids themselves, the method of liposome preparation can impact both the size and phase of the final assembly—both of which are central to a system's success as a drug carrier. It would be immensely beneficial to be able to predict, *a priori* if a lipid could form liposomes and at in what size range. Unfortunately, a cohesive theory correlating lipid structure to aggregate phase and diameter has yet to be developed. This is primarily due to the tendency of these systems to adopt kinetically trapped structures, making thermodynamic predictions of limited use. The variety of different preparation techniques and starting conditions, the range of lipid solubility and the temperature-dependent changes to their hydrophobic chains, further complicate the treatment.

Some lipid systems can be governed primarily by thermodynamic forces, while others have a greater tendency to become kinetically trapped. The distinguishing factor between these two sets of lipids is their solubility in water. For a solution of lipids to

reach a thermodynamic equilibrium, the monomer lipids must be able to freely exchange from one aggregate phase to another in order to achieve an equilibrium state. If the energetic cost of a lipid leaving an aggregate is too high, all possible configurations will not be accessible to it and the solution will not be able to find its equilibrium configuration. Most diacyl phospholipids have a low solubility in water and they become kinetically trapped in local energetic minimums when hydrated and only rearrange upon the addition of energy, typically in the form of sonication, heat, or vortexing. Kinetically trapped vesicles are preferred for the majority of applications, because they remain intact when diluted (i.e. when injected into the bloodstream or an *in-vitro* cell culture). By definition, equilibrium systems respond to changes in their environment and when a solution of vesicles is diluted, the vesicles can break apart and rearrange into new phases, which could release the encapsulated cargo.

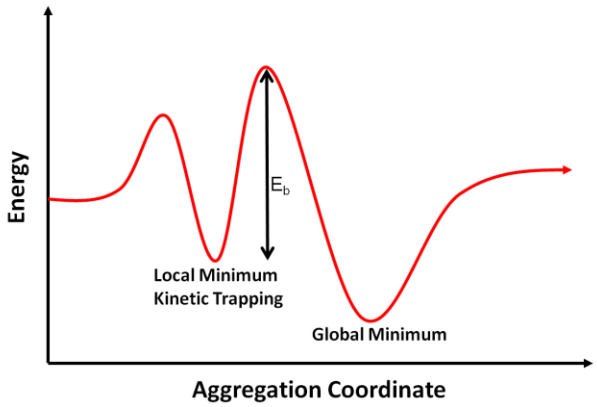


**Figure 1-3: Representative graph of potential kinetic energetic minimums** which can trap an aggregate state, preventing the adoption of the global thermodynamic minimum due to the necessity to overcome the energetic barrier $E_b$.

### 1.3.1 Molecular Free Energies

There are two basic categories of thermodynamic lipid aggregation theory; those beginning at the level of the individual lipid (molecular free energies) and those focused on the bigger picture of the assembled bilayers and membrane curvature. Israelachvili

and others have incorporated geometric considerations into a thermodynamic framework in order to investigate how the physical aspects of a lipid affect the potential energy of a monomer lipid in solution relative to an aggregate. In 1992, Israelachvili[24] published a thorough analysis of lipid aggregates at thermodynamic equilibrium. At equilibrium, all the lipid monomers must have the same free energy regardless of the size of the aggregate (**N** is the number of lipids in a given aggregate). The mean chemical potential for a monomer in an aggregate of size N is $\mu_N = \mu_N^o + (kT/N)Log(X_N/N)$. In this expression, $\boldsymbol{\mu_N^0}$ is the standard partial chemical potential in an aggregate of size **N** monomers, and $\mathbf{X_N}$ is the concentration of the molecules in aggregates containing **N** monomers. For an aggregation to form, the free energy of a lipid in the aggregation phase must be lower than for one in a fully dispersed solution ($\boldsymbol{\mu_1}$).

As written, this expression does not give any predictive information correlating lipid structure with aggregate phase or size. This expression does not yet contain parameters related to structural aspects of the monomer and therefore makes it difficult to translate the concept to an actual system. A more useful expression can be derived if a vesicular structure with spherical geometry is assumed where $N = 4\pi(R_1^3 + R_2^3)/v$, which results in an expression for the free energy of a monomer in an aggregate with **N** monomers of

$$\boldsymbol{\mu_N^o = 4\pi\gamma(R_1^2 + R_2^2 + a^2(n_1^2/(R_1(R_1+D)) + n_2^2/(R_2(R_2-D))))}. \qquad \textbf{Eq. 1}$$

$\mathbf{R_1}$ and $\mathbf{R_2}$ are the radii for the inner and outer monolayers of the bilayer respectively and $\mathbf{n_1}$ and $\mathbf{n_2}$ are the number of monomers in those bilayers respectively. Finally, $a^2 = e^2D/(2\varepsilon\gamma)$, where $\boldsymbol{\gamma}$ is the interfacial free energy per unit area (approximately 50 erg/cm$^2$ for phospholipid bilayers[25], **a** is the area per headgroup measured at the

hydrophobic/hydrophilic interface, **e** is the charge per polar headgroup, **D** is the separation of the two charges, and ε is the dielectric constant. This expression only applies to a one-component bilayer system and neglects both curvature energies and the entropic effects of chain packing. Eq.1 can be used along with the relationships $\mathbf{a_l} = 4\pi R_1^2/n$, $a_2 = 4\pi R_2^2/n_2$, and the bilayer thickness (t), $t = R_1 - R_2$, to find an expression for the minimum free energy for a particular **N** or $\mathbf{R_1}$ (see Appendix in Israelachvili[25]),

$$\mu_{Nmin}^{o} = 2a\gamma[(1-2\pi Dt)/Na_o] \qquad \textbf{Eq. 2}$$

which, when plotted as a function of **N** or $\mathbf{R_1}$, will give you the specific **N** or $\mathbf{R_1}$ value that results in the lowest energy state. According to Israelachvili, thermodynamics will always favor many small vesicles, and it is the incorporation of packing constraints that puts a lower limit on vesicle diameter. As the radius of the vesicle decreases, the lipid headgroups on the exterior of the vesicle must expand beyond their preferred headgroup area of **a**. This increases the energy of the bilayer and prevents a further decrease in size.

Moving from Eq. 2 to a lipid design is not straightforward. Calculating the required parameters is difficult and measuring them is not helpful, because if the lipid is already synthesized, it makes more sense to just run the experiment. Additionally, Eq. 2 only applies if the lipid forms a vesicular phase, which is not always the case.

### 1.3.2 Curvature Energies

In theories based on curvature, the geometry of the individual lipid is not explicitly included, but the lipid structure still determines the characteristics of the bilayer as a whole and is, therefore, incorporated implicitly. Curvature studies generally view a liposome as a thin, spherical film, although some have taken into account a finite bilayer

thickness[26, 27]. Most curvature-based analyses begin with the equation for the elastic energy of bending per unit area ($\gamma$) of a thin film derived by Helfrich[28],

$$\gamma = 2k_c[H - H_o]^2 + kK \qquad \textbf{Eq. 3}$$

where $H = \frac{1}{2}(C_1 + C_2)$, $K = C_1C_2$, $\mathbf{C_1}$ and $\mathbf{C_2}$ are the principle membrane curvatures at a single point on the surface where $C_1 = 1/R_1$ and $C_2 = 1/R_2$. $\mathbf{H_o}$ is the spontaneous curvature of the bilayer and can only have a non-zero value for cases of transbilayer asymmetry[29].

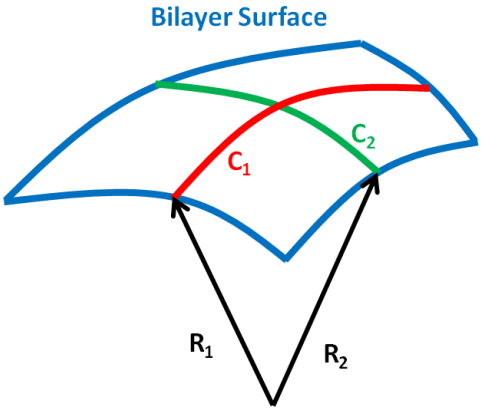


**Figure 1-4: Graphic depicting bilayer curvature.**

$\mathbf{k_c}$ is the mean bending constant and $\mathbf{k}$ is the Gaussian bending constant. $\mathbf{H_o}$ determines the sign and magnitude of the preferred curvature; $\mathbf{k_c}$ reflects the resistance of the bilayer to deviate from $\mathbf{H_o}$ ($k_c > 0$ for stable bilayers); and the value of $\mathbf{k}$ determines whether the curvature is negative or positive at any point on the surface—or more simply, the topology of the aggregate (in all liposomes $k < 0$)[26].

**Table 1-1 Effect of bilayer changes on bending constants**

| Alteration to Bilayer | $H_0$ (spontaneous curvature) | $k_c$ (Gaussian bending constant) | \|k\| (absolute value of the mean bending constant) |
|---|---|---|---|
| Increasing Bilayer Stiffness | No Information | Increases | No Information |
| Adding a 2nd Amphiphile | No change when symmetric | Decreases | No change |
| Increasing Headgroup Size | Increases | Increases then Decreases | Increases |
| Increasing Tail Length | Decreases | Increases | Increases |
| Increasing Bilayer Thickness ($\xi$) | Decreases | Increases as $\xi^2$ | Increases |
| Increasing Ionic Strength of Solution | Case by case | Can Increase or Decrease | Decrease |

In the absence of spontaneous curvature, Helfrich's expression simplifies to $\gamma A = 8\pi k_c + 4\pi k$ , which is the energy required to bend a bilayer into a vesicle of surface area, **A**[30]. For a single component system that forms spherical liposomes, $C_o = 0$ due to the identical composition of each monolayer, which leads to the cancellation of each monolayer's inherent curvature. In bilayers with a spontaneous curvature, ($H_o \neq 0$), this simplified version of the Helfrich expression no longer applies. The vesicle bending energy is often reported as $8\pi k_c$[31] due to typically small **k**-values for phospholipid systems, but it has been shown that at low ionic strengths the constants are of similar magnitude[32]. Since $k_c > 0$ and $k < 0$ for stable vesicles, the energy required to form a vesicle is a balance between the magnitudes of the two bending constants.

Thermodynamic stability can be either entropic or enthalpic. Entropically stabilized systems are often characterized by a less rigid bilayer without spontaneous

curvature, and a broad size distribution, determined by the membrane persistent length, which is dependent on the lipid concentration[32]. Vesicle mixtures stabilized by enthalpy typically have more rigid bilayers, and narrow size distributions, due to a spontaneous curvature[29, 32]. A large $\mathbf{k_c}$, perhaps resulting from a rigid, thick, tightly packed bilayer, leads to a higher bending energy, and may prevent entropic stabilization of the vesicles. If $\mathbf{k_c}$ and $\mathbf{k}$ are close in magnitude, the bending energy is close to zero and translational motion and undulations can be enough to entropically stabilize the vesicles.

Bergstrom has calculated several aspects of the lipid/solvent system that influence $\mathbf{k_c}$, $\mathbf{k}$, and $\mathbf{H_0}$[26, 27, 33]. He determined that headgroup size, tail length, and, for ionic surfactants, solvent ionic strength were of great importance. $\mathbf{H_0}$ increases with larger headgroup size and shorter tails, but both the magnitudes of $\mathbf{k_c}$ and $\mathbf{k}$ increase with increasing tail length. Additionally, $\mathbf{k_c}$ exhibits a maximum in relation to headgroup size, whereas $\mathbf{k}$ increases in magnitude with increasing headgroup size[26]. He also has found that $\mathbf{k_c}$ is reduced in magnitude by mixing a second lipid into the bilayer and that this effect increases as the differences between the tail groups (volume, rigidity, etc) and headgroups (size, charge, etc) of the two lipids increase[27, 34]. This may be due in part to disruption of the packing order, which would decrease the rigidity of the bilayer. All three parameters are affected by bilayer thickness ($\xi$), a parameter that is often left out of curvature calculations. $\mathbf{k_c}$ increases proportional to $\xi^2$, and k also increases in magnitude (becomes more negative) with increasing $\xi$, and $\mathbf{H_0}$ decreases with increasing $\xi$[27].

The ionic strength of the solution determines the Debye screening length and therefore impacts the behavior of the charged headgroups[35]. A high ionic strength can virtually convert the behavior of a charged lipid to that of a neutral one[32]. Shielding the

headgroup charges will also decrease the Gaussian bending constant, **k**, and can either increase the mean bending constant, $\mathbf{k_c}$, by allowing the chains to pack more closely or decrease $\mathbf{k_c}$ by removing the repulsive headgroup interactions that can stiffen the membrane. Because this is a tradeoff, there is typically a minimum $\mathbf{k_c}$ value for a range of ionic strengths.

The above observations identify trends for each of the curvature constants that can be useful for understanding why certain lipids form vesicles more readily than others. However, like in Section 1.3, it is much more difficult to assign quantitative values of $\mathbf{k_c}$, **k**, and the spontaneous curvature, $\mathbf{H_0}$, to a lipid structure. Some studies have reported on the relationship between the vesicle radius and $\mathbf{k_c}$, but only in terms of a scaling principle[27, 33]. It would be ideal to take the computed values of each parameter required for a desired radius and translate those numbers into a specific lipid structure. One reason that going from a computational result to lipid design is difficult is that many structural aspects of the lipid can affect each parameter in a different way. Also, measuring or calculating these parameters for real world systems can be tricky and/or tedious[26, 35, 36]. Furthermore, for multi-component systems, it can be more complicated, because even if the bending constants for each pure state are known, it is difficult to predict how the lipids will interact with each other and how they will distribute across the bilayer.

Although the above analyses could not predict if a given lipid would adopt a vesicular phase, they do provide some general principles for predicting ease of liposome formation and liposome diameter. For small vesicles, spontaneous curvature is desirable and the most advantageous corresponding value of $\mathbf{k_c}$ depends on the degree of curvature.

If the bilayer is highly curved then a larger $\mathbf{k_c}$ is best, because it will resist deviations from $\mathbf{H_o}$, and preserve the high degree of curvature. If $\mathbf{H_o}$ is small, then it is best if $\mathbf{k_c}$ is low so that a higher degree of curvature can be obtained while avoiding a significant increase in the bending energy. . A large negative value of **k** also works to lower the bending energy, and in theory, it should make forming small vesicles easier. Indeed, for systems with little or no spontaneous curvature, a large $\mathbf{k_c}$ results in larger vesicles[32]

### 1.3.3 Geometric Considerations

The above treatments of lipid assembly are complicated and do not predict the phase a lipid will adopt when dispersed in water. A contrast to those theories is Israelachvili's concept of the packing parameter, which is simple and aims to predict the lipid phase. The packing parameter (**P**) is based solely on the geometry of the lipid and is calculated from the volume of the hydrocarbon chain **(v**), the area of the headgroup (**a**), and the length of the extended hydrocarbon chain (**l**), where $P = v/(al)$[25, 37]. Israelachivili hypothesizes that certain **P**-values regularly produce specific aggregate forms. Values for the packing parameter and the predicted aggregation form are shown in Figure. 1-5. This method provides insight into the relationship between lipid geometry and the resulting aggregate structure and can be used for some multi-component systems where the asymmetry between the two monolayers is minimal[38, 39]. However, this theory should be considered a set of general principles, not hard and fast rules, as it neglects parameters like headgroup repulsion and chain repulsion or rigidity.

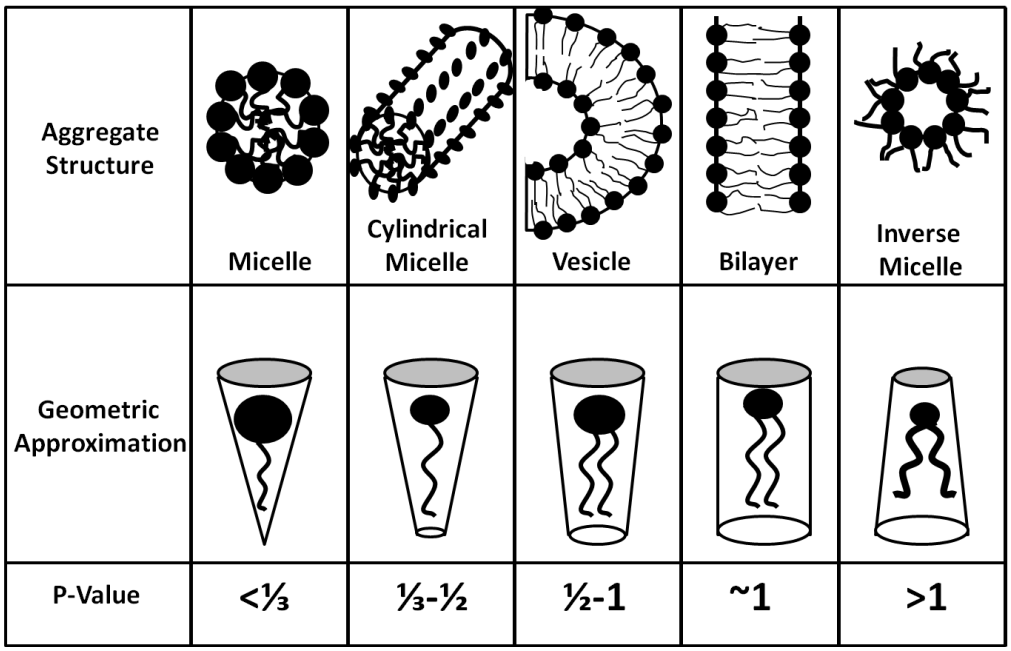


**Figure 1-5: The relationship between lipid structure, P-value and aggregate phase**

This geometric approach also ignores bending energies and the fact that in a bilayer liposome, one monolayer must assume a curvature opposite of the other monolayer (which for a one component bilayer, would mean at least one layer is at an unfavorable bending energy). The advantage of the geometric treatment of aggregate formation is that only the structure of the lipid is required, but the downside is that the lipid geometry is all that is taken into consideration and many other factors play important roles in the process. Geometric analysis can work well for micellular aggregates[25, 40] due to the absence of the second monolayer.

### 1.3.4 Kinetic Influences and the Process of Vesicle Formation

The low solubility of most lipids prevents them from freely exchanging between different aggregate structures, which limits their ability to find the thermodynamic minimum and in turn promotes kinetic trapping. Vesicular aggregates can form from a number of different preparation techniques, and depending on the type and intensity of energy input and the path of formation, can result in a variety of kinetically trapped

states. Generally, vesicle preparations begin with the lipids as a dehydrated film or in an alcohol solution. Some vesicles will form spontaneously when hydrated, but the vast majority require some form of energy input either by physical agitation (stirring/vortexing), heat, sonication, extrusion, or a combination of the four to fully disperse the vesicles[31]. Other techniques include dilution from ethanol into an aqueous buffer, surfactant removal, reverse phase evaporation, freeze-thaw cycles, or pH cycles.

The method of preparation is very important for lipids with low water solubility, because most of the liposomes they form will show a path-dependent size distribution[31, 41, 42]. For instance, Mahbabir[41] has shown that formulations of DMPC/DHPC/DMPG form 77 nm vesicles upon slow annealing and ~170 nm vesicles with an abrupt jump in temperature. The resulting vesicles are then stable to changing lipid and solute concentrations[43]. Clearly in this example, both formulations cannot be in the same thermodynamic minimum, one, or both, must be in a kinetically trapped state.

In order to understand how different preparation techniques may result in different vesicle size distributions, it is helpful to examine the physical mechanism of vesicle formation. There are two main theories for vesicle formation; the budding off of smaller vesicles from larger or multi-lamellar vesicles and the breaking up of bilayers into fragments which then close up to form vesicles[5, 44] (Fig. 1-6). In order for budding to occur, a transbilayer asymmetry from either differing lipid compositions or hydration of one monolayer (resulting in larger headgroups) must be present[45]. Bilayer fragments can be created by breaking apart an existing planar bilayer through sonication, cyclic changes (pH, temperature), and extrusion, or by building them up from lipid monomers via detergent depletion, injection methods, or reverse phase evaporation[46]. It is likely that

both budding and fragmentation play a role in many methods of vesicle formation. One example of this is the commonly used method of rehydration and sonication. As the dried planar bilayers are rehydrated and agitated, vesicles can bud off the planar bilayers and fragmentation can occur during the sonication phase.

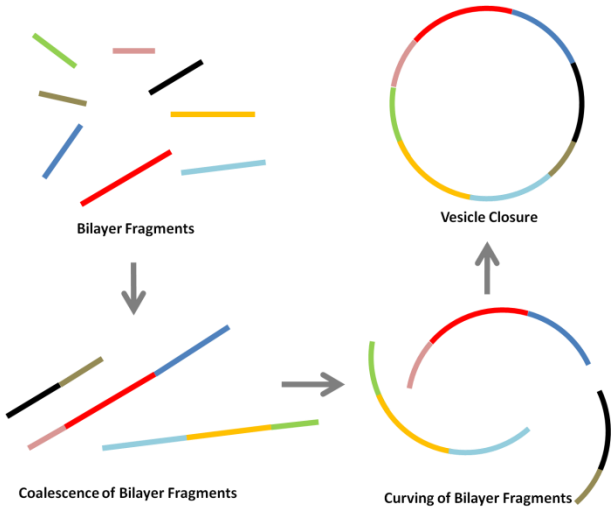


**Figure 1-6: Process of vesicle formation according to the bilayer fragment theory**

Lasic postulates that bilayer fragments are a common step in all of the above-mentioned vesicle formation processes[31, 46]. Experimental work by Fromherz and Rüppel[44] in which they monitored the conversion of bilayer fragments into vesicles by TEM following sonication, supports the bilayer fragment theory. The pathway from bilayer fragment to vesicle is primarily governed by a balance between two energies; (1) the edge energy of the fragment which results from the exposure of the hydrophobic chains to water at the fragments periphery, and (2) the inherent curvature energy of the fragment. The curvature energy refers to the energy associated with a deviation in curvature away from the fragment's inherent preferred curvature state. The edge energy is equal to $\mathbf{A}\gamma$, where **A** is the edge area and $\gamma$ is the surface tension between the hydrophobic chains and water, favors the coalescence of bilayer fragments to reduce the overall exposed hydrophobic surface area. The edge energy is zero for a vesicle, which

has no exposed edges. For small bilayer fragments, the curvature energy can be very high and Lasic proposes that a fragment with a radius (**r**) of r < 2R, where R is the critical radius (~10 nm for egg-PC lipids), will not curve into closed vesicles due to the unfavorable changes in headgoup area on both sides of the bilayer (compression on the interior and expansion on the exterior)[47].

While these two energies influence the formation of vesicles from the bilayer fragments, the overall race between the rates of bilayer fragment coalescence and vesicle closure[48] often result in kinetically trapped vesicles. These rates can be affected by parameters, such as temperature (higher temperatures increase the vesicle closure rate)[48] and the presence of detergents (these can stabilize the bilayer fragments by covering the exposed edges, thus allowing them to grow larger)[44].

The size of the fragments produced also plays an important role, because a vesicle of a certain area ($4\pi r_{vesicle}^2$) can only be made if a bilayer fragment with that area ($\pi r_{bilayer}^2$) is also made. Changes in parameters like intensity of sonication, the pressure of extrusion, and the velocity of injection of an alcohol/lipid solution into water are known to affect the size of the vesicles produced[45, 49]. Rapid injections of dilute lipid solutions in alcohol have been shown to produce smaller vesicles as opposed to slower injections or more concentrated solutions[49]. Jahn attributes the decrease in vesicle size upon faster mixing to the increase in convective mixing versus diffusion of the alcohol into the bulk aqueous volume. Convective mixing quickly creates unstable, small bilayer fragments, whereas in the slower diffusion process, the bilayer fragments are stabilized by the presence of alcohol molecules at the bilayer edge, preventing their interaction with water and allowing them exist for longer times. The longer a bilayer fragment exists, the

more likely it is to coalesce with another fragment. Similarly, Sun[50] reported that for mixtures of egg-PC and **3**-[(3-cholamidopropyl)dimethylammonio]-1-propane sulfonate (CHAPS) mixtures, there was a decrease in vesicle diameter from 380 nm to 40 nm upon changing from slow dilution or dialysis to rapid dilution.

Temperature can also affect the stability of the resulting bilayer fragements by changing the physical characteristics of the lipids themselves. At different temperatures, packed lipid chains behave differently, and at a specific transition temperature, $T_m$, they become fluid. Many phospholipid vesicles are stable above their $T_m$, but below their $T_m$, they fuse rather quickly. It is reasonable to assume that the transition from a rigid hydrocarbon bilayer to a fluid one will change the bilayer rigidity and resistance to changes in its inherent curvature state. Therefore, both the thermodynamically and kinetically favored states will differ depending on the chain fluidity.

According to the bilayer fragment theory of vesicle formation, the size of the bilayer fragments and their inherent curvature, as well as the surface tension of the hydrophobic region all impact the final liposome diameter. The use of high temperatures, high intensity sonication, hydrophobic chains that create a high edge energy, and multi-component systems that align asymmetrically across a bilayer all decrease vesicle diameter. Chapters 4 and 5 describe the design of a lipid-like molecule, a bolaamphiphile, which forms small-diameter vesicles. The bolaamphiphiles in the Chapters 4 and 5 have two different hydrophilic headgroup connected by a hemifluorinated hydrophobic chain. These lipids were designed to assembly into an asymmetric monolayer and have hydrophobic regions with high edge energies

(incorporation of a fluorocarbon), both of which are listed above as attributes that can promote the formation of small vesicles.

### 1.4 Conclusion

Although the steps between identifying a beneficial liposome property and actually creating such a liposome are complex, the more synthetic structures that are tested, the more the field will learn and the more predictable structure-function relationships will hopefully become. Each region of the lipid is important and a change to any part can have a significant effect on efficacy of the drug delivery system in ways that are often unpredictable until tested experimentally. As such, a fair amount of lipid design is done by trial and error. Computer simulations may better take into account different starting configurations and identify kinetic traps, although identifying the true thermodynamic minimum remain beyond the scope of computation today. There is a need for models that can incorporate both atomistic and coarse-grained length scales to the extent that small changes in lipid structure (i.e. changes in saturation or from a sulfonate to a phosphate headgroup) are reflected in the resulting aggregate. As computational programs and processing power continue to advance more insight into the systems and their important characteristics will emerge. As I show in my thesis, there remains a wide chemical space open to new lipid structures and as new lipids are synthesized, the likelihood that they can improve lipid-based therapeutics is quite promising.

### 1.5 References


1. A. D. Bangham, M. M. Standish and J. C. Watkins, *Journal of Molecular Biology*, 1965, **13**, 238-IN227.
2. N. Maurer, D. B. Fenske and P. R. Cullis, *Expert Opinion on Biological Therapy*, 2001, **1**, 923-947.

3. S. C. Semple, A. Akinc, J. Chen, A. P. Sandhu, B. L. Mui, C. K. Cho, D. W. Y. Sah, D. Stebbing, E. J. Crosley, E. Yaworski, I. M. Hafez, J. R. Dorkin, J. Qin, K. Lam, K. G. Rajeev, K. F. Wong, L. B. Jeffs, L. Nechev, M. L. Eisenhardt, M. Jayaraman, M. Kazem, M. A. Maier, M. Srinivasulu, M. J. Weinstein, Q. Chen, R. Alvarez, S. A. Barros, S. De, S. K. Klimuk, T. Borland, V. Kosovrasti, W. L. Cantley, Y. K. Tam, M. Manoharan, M. A. Ciufolini, M. A. Tracy, A. de Fougerolles, I. MacLachlan, P. R. Cullis, T. D. Madden and M. J. Hope, *Nat Biotech*, 2010, **28**, 172-176.
4. T. Lian and R. J. Y. Ho, *Journal of Pharmaceutical Sciences*, 2001, **90**, 667-680.
5. D. D. Lasic, *Biochem. J.*, 1988, **256**, 1-11.
6. H. Lv, S. Zhang, B. Wang, S. Cui and J. Yan, *Journal of Controlled Release*, 2006, **114**, 100-109.
7. S.-D. Li and L. Huang, *Molecular Pharmaceutics*, 2008, **5**, 496-504.
8. T. S. Levchenko, R. Rammohan, A. N. Lukyanov, K. R. Whiteman and V. P. Torchilin, *International Journal of Pharmaceutics*, 2002, **240**, 95-102.
9. J. Senior, J. C. W. Crawley and G. Gregoriadis, *Biochimica et Biophysica Acta (BBA) - General Subjects*, 1985, **839**, 1-8.
10. D. V. Devine, K. Wong, K. Serrano, A. Chonn and P. R. Cullis, *Biochimica et Biophysica Acta (BBA) - Biomembranes*, 1994, **1191**, 43-51.
11. N. N. Desai, H. Zhang, A. Olivera, M. E. Mattie and S. Spiegel, *Journal of Biological Chemistry*, 1992, **267**, 23122-23128.
12. S. Deborah W, *Biochemical and Biophysical Research Communications*, 1987, **145**, 228-233.
13. D. Papahadjopoulos, S. Nir and N. Düzgünes, *Journal of Bioenergetics and Biomembranes*, 1990, **22**, 157-179.
14. P. Wan, Y. Zhao, H. Tong, Z. Yang, Z. Zhu, X. Shen and J. Hu, *Materials Science and Engineering: C*, 2009, **29**, 222-227.
15. R. K. Scheule, J. A. S. George, R. G. Bagley, J. Marshall, J. M. Kaplan, G. Y. Akita, K. X. Wang, E. R. Lee, D. J. Harris, C. Jiang, N. S. Yew, A. E. Smith and S. H. Cheng, *Human Gene Therapy*, 1997, **8**, 689-707.
16. I. V. Khavrutskii, A. A. Gorfe, B. Lu and J. A. McCammon, *Journal of the American Chemical Society*, 2009, **131**, 1706-1716.
17. J. C. Mathai, S. Tristram-Nagle, J. F. Nagle and M. L. Zeidel, *The Journal of General Physiology*, 2008, **131**, 69-76.
18. V. P. Torchilin and V. Weissig, *Liposomes: a practical approach*, Oxford University Press, 2003.
19. R. Homan and H. J. Pownall, *Biochimica et Biophysica Acta (BBA) - Biomembranes*, 1988, **938**, 155-166.
20. C. Huang, Z.-q. Wang, H.-n. Lin, E. E. Brumbaugh and S. Li, *Biochimica et Biophysica Acta (BBA) - Biomembranes*, 1994, **1189**, 7-12.
21. H. Eibl and A. Blume, *Biochimica et Biophysica Acta (BBA) - Biomembranes*, 1979, **553**, 476-488.
22. J. M. Boggs, *Canadian Journal of Biochemistry*, 1980, **58**, 755-770.
23. H. Ellens, J. Bentz and F. C. Szoka, *Biochemistry*, 1986, **25**, 285-294.
24. J. N. Israelachvili, *Intermolecular And Surface Forces*, Academic Press, 2010.

25. J. N. Israelachvili, D. J. Mitchell and B. W. Ninham, *Journal of the Chemical Society, Faraday Transactions 2: Molecular and Chemical Physics*, 1976, **72**, 1525-1568.
26. B. L. Magnus, *Journal of Colloid and Interface Science*, 2006, **293**, 181-193.
27. L. M. Bergström, *Langmuir*, 2006, **22**, 6796-6813.
28. W. Helfrich, *Z. Naturforsch.*, 1973, **28c**, 693-703
29. D. C. Morse and S. T. Milner, *Physical Review E*, 1995, **52**, 5918-5945.
30. M. Winterhalter and D. D. Lasic, *Chemistry and Physics of Lipids*, 1993, **64**, 35-43.
31. L. D.D, *Journal of Colloid and Interface Science*, 1990, **140**, 302-304.
32. M. M. A. E. Claessens, B. F. van Oort, F. A. M. Leermakers, F. A. Hoekstra and M. A. Cohen Stuart, *Physical Review E*, 2007, **76**, 011903.
33. B. Magnus, *Journal of Colloid and Interface Science*, 2001, **240**, 294-306.
34. A. P. Gonzalez, *The Journal of Chemical Physics*, 2004, **120**, 11267-11284.
35. L. M. Bergström, *Langmuir*, 2009, **25**, 1949-1960.
36. M. M. Kamal, D. Mills, M. Grzybek and J. Howard, *Proceedings of the National Academy of Sciences*, 2009, **106**, 22245-22250.
37. J. N. Israelachvili and D. J. Mitchell, *Biochimica et Biophysica Acta (BBA) - Biomembranes*, 1975, **389**, 13-19.
38. V. Kumar, *PNAS*, 1991, **88**, 444-448.
39. E. F. Marques, O. Regev, A. Khan and B. Lindman, *Advances in Colloid and Interface Science*, 2003, **100-102**, 83-104.
40. R. Nagarajan and E. Ruckenstein, *Langmuir*, 1991, **7**, 2934-2969.
41. S. Mahabir, W. Wan, J. Katsaras and M.-P. Nieh, *The Journal of Physical Chemistry B*, 2010, **114**, 5729-5735.
42. M.-P. Nieh, J. Katsaras and X. Qi, *Biochimica et Biophysica Acta (BBA) - Biomembranes*, 2008, **1778**, 1467-1471.
43. B. Yue, C.-Y. Huang, M.-P. Nieh, C. J. Glinka and J. Katsaras, *The Journal of Physical Chemistry B*, 2004, **109**, 609-616.
44. P. Fromherz and D. Ruppel, *FEBS Letters*, 1985, **179**, 155-159.
45. D. Lasic and D. Papahadjopoulos, *Science*, 1995, **267**, 1275-1276.
46. D. D. Lasic, *Journal of Liposome Research*, 1999, **9**, 43-52.
47. L. Danilo D, *Biochimica et Biophysica Acta (BBA) - Biomembranes*, 1982, **692**, 501-502.
48. J. M. Zook and W. N. Vreeland, *Soft Matter*, 2010, **6**, 1352-1360.
49. A. Jahn, S. M. Stavis, J. S. Hong, W. N. Vreeland, D. L. DeVoe and M. Gaitan, *ACS Nano*, 2010, **4**, 2077-2087.
50. C. Sun and M. Ueno, *Colloid & Polymer Science*, 2000, **278**, 855-863.

CHAPTER 2

# Inverse-phosphocholine lipids: A remix of a common phospholipid

## 2.1 Abstract

Zwitterionic inverse-phosphocholine (CP) lipids contain headgroups with an inverted charge orientation relative to phosphocholine (PC) lipids. The CP lipid headgroup has a quaternary amine adjacent to the bilayer and a phosphate that extends into the aqueous phase. The surface potential of neutral CP liposomes remains negative across a broad pH range and in the presence of up to 10 mM $Ca^{2+}$. Anionic CP liposomes aggregate in the presence of $Ca^{2+}$, but at a slower rate than other anionic lipids above 4 mM $Ca^{2+}$ and are susceptible to hydrolysis by alkaline phosphatase which generates a cationic lipid. CP liposomes release encapsulated carboxyfluorescein faster than PC liposomes and mixed CP/PC liposomes have intermediate release rates demonstrating the feasibility of an adjustable release system. CP lipids afford a unique opportunity to investigate the biophysical and bioactivity-related ramifications of a charge inversion at the bilayer surface.

## 2.2 Introduction

Zwitterionic phosphatidylcholine (PC) lipids are the major component in most bilayer membranes that compartmentalize cells. The PC headgroup is exceptionally well hydrated, maintains the zwitterionic character over a broad pH range and interacts weakly with divalent ions; all properties that make it ideal for its central role in cell membranes. In this report, we investigate how an inversion of the PC headgroup—moving the positively charged quaternary amine adjacent to the bilayer; and extending the anionic phosphate into aqueous interfacial region, alters the chemical and physical properties of

the bilayer. We synthesized a family of inverse phosphocholine (CP) lipids (Fig. 2-1) and characterized their; response to changes in pH, interaction with calcium and permeability properties to the anionic water-soluble reporter, carboxyfluorescein and susceptibility to hydrolysis by alkaline phosphatase.

Lipids have three primary regions for potential modification: the hydrophobic tails, the linker region between the tails, and the hydrophilic headgroup. Changes to PC lipids at these three sites have been explored by many groups[1-15]; however, to our knowledge, the locations of the choline and phosphate moieties have not been inverted, nor are such modifications observed in nature. Generally, naturally occurring lipids with anionic headgroups, such as phosphatidic acid (PA), phosphatidylserine (PS), phosphotidyl inositol (PI), sphingosine-1-phosphate (S1P), and ceramide-1-phosphate (C1P) play more than a just a structural role. PA, PI, S1P, and C1P have been identified as key bioactive agents in a variety of signaling pathways[16, 17] such as cell growth/apoptosis[18-20], lymphocyte trafficking[21], chemotaxis[22], and calcium release[19]. Additionally, monophosphoryl lipid A, obtained from gram-negative bacteria, also has a terminal phosphate, and behaves as an adjuvant when used in vaccines[23-25]. Based on the biological roles of these naturally occurring phosphorylated lipids, it is possible that either the anionic CP or the zwitter-neutral CPe lipids could exhibit similar activities, allowing them to adopt a therapeutic role as well as serving as a structural component in a liposome bilayer. In addition to their potential for biological activity, CP lipids are also an exceptionally useful tool for exploring the role of charge orientation at the bilayer interface.

## 2.3 Results and Discussion

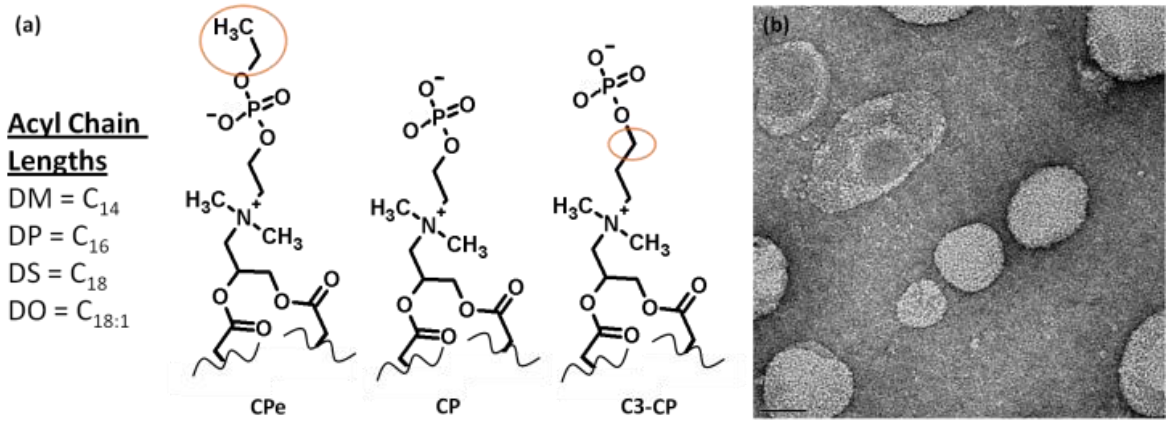


**Figure 2-1: Lipid structure and vesicle formation** (a) General structure of CP lipids (b) TEM image of DPCPe/Cholesterol (6:4) liposomes 65 nm in diameter by light scattering, scale bar = 50 nm.

Dry films of CP lipids hydrated easily in aqueous solution and formed small liposomes upon sonication at temperatures above the transition temperatures ($T_m$) (Fig. 2-1b). The $T_m$ were measured using differential scanning calorimetry (DSC) for the three saturated chain version of the CPe lipids: DMCPe, DPCPe, and DSCPe. The CPe lipid ($C_{14}$, $C_{16}$, $C_{18}$) $T_m$ were 21.4, 41.2, and 53.7 °C respectively (Table 2-1), which are similar to the $T_m$ for DMPC, DPPC, and DSPC which are 24.2, 41.7 and 55.3 °C respectively. Sulfobetaine (SB)[26] lipids and betaine-like (BL)[27] lipids, which have a similar orientation of the charged group at the bilayer interface, have substantially elevated $T_m$ of; 46 °C ($C_{14}$), 59 °C ($C_{16}$), and 68 °C ($C_{18}$) for the SB lipids and 49 °C ($C_{14}$), 58 °C ($C_{16}$), and 67 °C ($C_{18}$) for the BL lipids, when measured under the same conditions as the CPe. Additionally, the SB and BL lipids did not form liposomes at 150 mM NaCl, even above the elevated $T_m$. The increased $T_m$ and difficulty in vesicle formation of the SB and BL lipids were attributed to the ion pairing between adjacent headgroups. The absence of this

effect in the CPe lipids indicates that ion pairing in the headgroups observed in the sulfobetaine liposomes are not present in CPe liposomes.

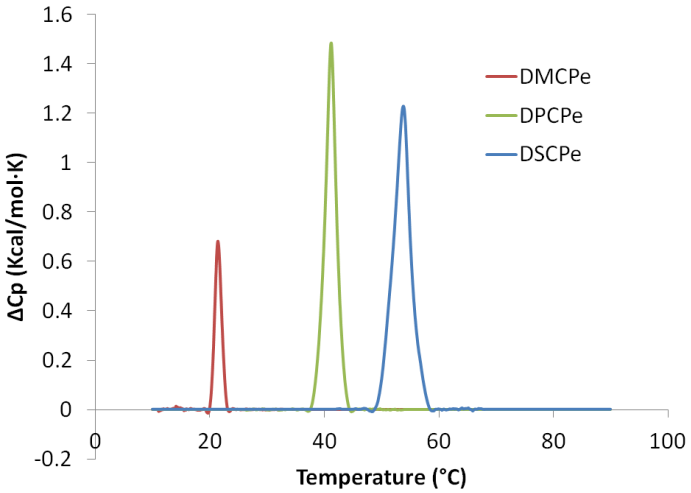


**Figure 2-2: Representative DSC traces for DMCPe, DPCPe, and DSCPe**

**Table 2-1: Transition temperatures (°C) for saturated chain CPe lipids**

| | DMCPe | DPCPe | DSCPe |
|---|---|---|---|
| **Onset** | 20.4 ± 0.2 | 38.4 ± 0.6 | 48.2 ± 3.7 |
| **Peak** | 21.4 ± 0.1 | 41.2 ± 0.1 | 53.7 ± 0.1 |

Average transitions ± standard deviations for 5 measurements

We investigated how the charge inversion of the CP headgroup would affect its overall surface potential. The zwitter-neutral lipids (DOPC and DOCPe) had surface potentials that were slightly negative at high pH and became barely positive (DOPC) or neutral (DOCPe) around a pH of 2. At low pH, DOPC is a slightly more positive than DOCPe, which suggests that the pKa for the phosphate of DOCPe may be lower than for DOPC (typically between 2-3 for PC lipids)[28].

The surface potentials for all three anionic liposomes (POPA, DOCP, and C3-DOCP) start off highly negative and do not differ significantly above pH 5.5. The surface potential of the POPA liposomes, which do not contain a cationic group, remains negative

and constant as the pH decreases. The zeta potential of the CP liposomes should approach neutrality when significantly more than 50% of the phosphate groups have been protonated. The first protonation event in PA headgroups occurs at $pKa_2$~8[29]. The zeta potential for the CP liposomes remains negative well below pH 8, which suggests that the $pKa_2$ of the phosphate in the CP is lower than the $pKa_2$ of the phosphate in PA. The second protonation event for the CP lipids may occur at a pH similar to that for DOCPe. The surface potentials of the two anionic CP liposomes (DOCP and C3-DOCP) do not differ significantly for the majority of the titration, indicating that separating the cationic amine by an additional -$CH_2$- unit does not change the phosphate pKas.

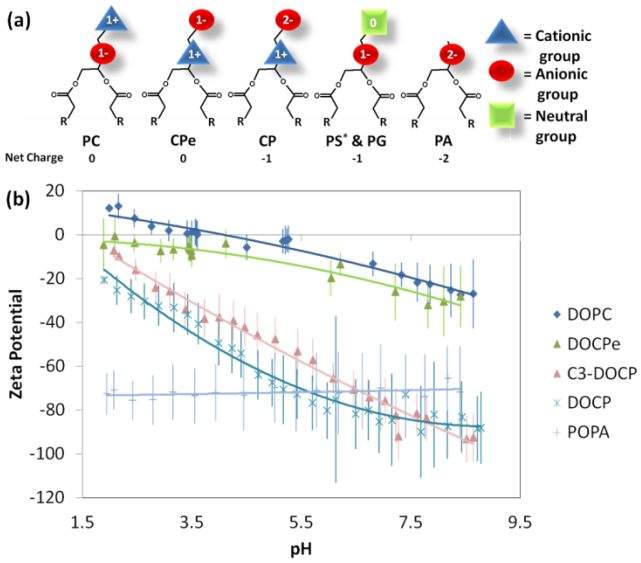


**Figure 2-3: Zeta potential measurements** (a) Graphic of the charge orientation and net charge of naturally occurring phospholipid headgroups (PC, PS, PG, PA) and the IPC lipid headgroups (CPe and CP). * The neutral block of the PS headgroup contains a primary amine and carboxylate that are zwitter-neutral at physiological pH. (b) Change in liposome zeta-potential with changing pH.

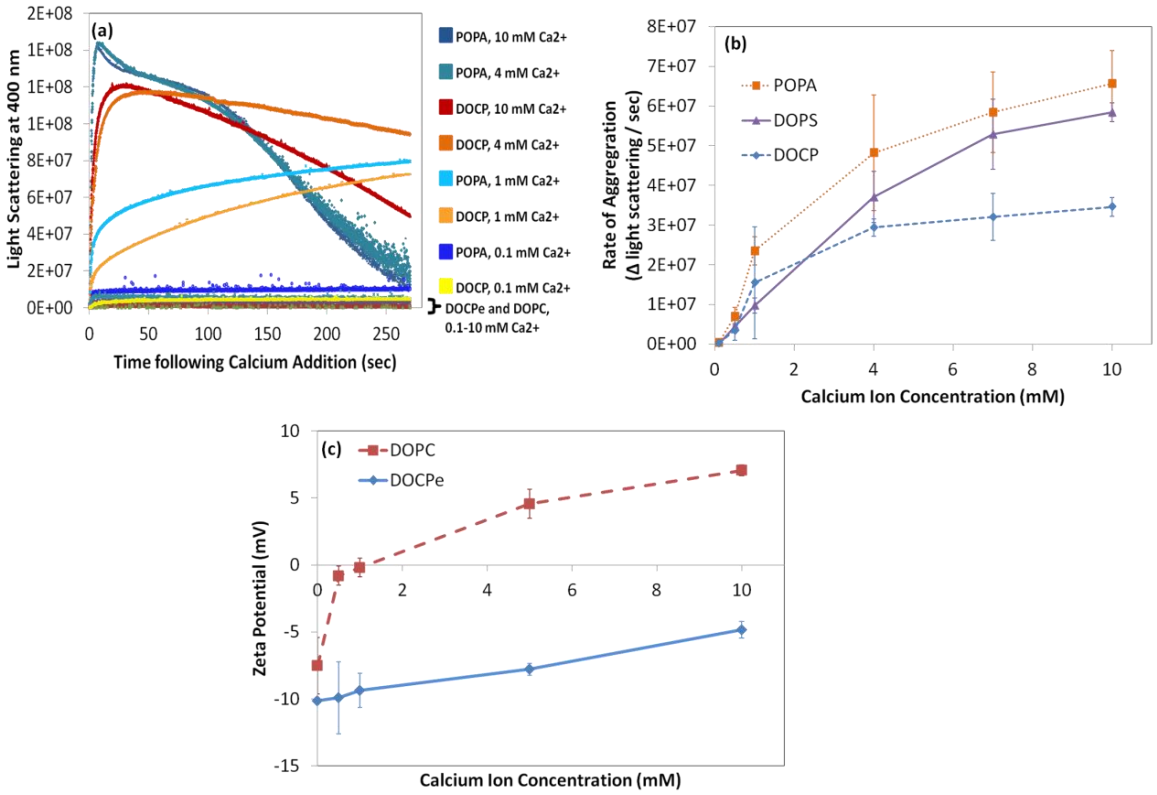


**Figure 2-4: Liposome-$Ca^{2+}$ Interactions** (a) Calcium-induced aggregation profiles of DOCP, POPA, DOPC, and DOCPe (b) Calcium-induced liposome aggregation rates. (c) Shift in zeta potential in the presence of $Ca^{2+}$.

The surface potential measurements revealed subtle differences between the CPe and PC liposomes, but significant differences in the charge properties of CP and PA. Lipids with anionic headgroups like PA and PS coordinate with divalent cations such as $Ca^{2+}$, resulting in aggregation and/or fusion of liposomes containing these anionic lipids[30-33]. To determine how the altered electronic properties of the CP liposomes impact their behavior in the presence of calcium we compared the aggregation of the CPe and CP lipids to traditional zwitter-neutral and anionic lipids (Fig.2-4).

DOCPe and DOPC liposomes did not aggregate at 10 mM $Ca^{2+}$ (Fig. 2-4a). To determine if $Ca^{2+}$ interacts with DOCPe and DOPC differently, the zeta potentials of the DOCPe and DOPC liposomes were measured in the presence of various concentrations of

$Ca^{2+}$ (Fig. 2-4a). The surface potential of the DOPC liposomes becomes increasingly positive as the $Ca^{2+}$ concentration increases, which is in agreement with previous reports[34]. The surface potential of the DOCPe liposomes also becomes more positive as the $Ca^{2+}$ concentration is increased, however; there is no immediate increase between 0 mM $Ca^{2+}$ and 0.1 mM $Ca^{2+}$ and the overall magnitude of the increase is less. Additionally, the surface potential of the DOCPe liposomes remains negative up to 10 mM $Ca^{2+}$. It is possible that $Ca^{2+}$ interacts more strongly with the surface of the DOPC liposomes due to the location of the anionic group. We hypothesize that because the phosphate in the PC headgroup is located at the bilayer interface, they are better oriented and more ordered than the phosphate in the CPe headgroup which extends into the aqueous phase. Calcium could then bind more avidly to one or two phosphates in the DOPC liposomes than in the DOCPe liposomes, where the phosphate has a greater freedom of motion.

CP liposomes aggregate in the presence of calcium (Fig. 2-4c). Calcium-induced aggregation occurs when $Ca^{2+}$ ions form bridges between the outer membranes of two liposomes[35]. The rate of bridge formation is affected by the rate of association/dissociation of the $Ca^{2+}$ ions with the phosphate of the lipid headgroup, as well as the rate of dimerization of the two liposomes[36]. The association/dissociation rates and the $Ca^{2+}$ concentration dictate the amount of $Ca^{2+}$ bound to the liposome surface at any given time. The aggregation rate will increase as the $Ca^{2+}$-phosphate interaction increases and as the $Ca^{2+}$ concentration increases.

The aggregation rates of DOCP liposomes differs from what is observed using DOPS or DOPA (Fig. 2-4b) in that the rate does not significantly increase above 4 mM

$Ca^{2+}$. The increased aggregation rates for DOPS and POPA relative to DOCP at higher $Ca^{2+}$ concentrations and the plateau effect for DOCP suggest some sort of saturation of the $Ca^{2+}$-DOCP interaction that is not observed for POPA or DOPS and could result from the formal positive charge on DOCP.

The $Ca^{2+}$ aggregation and interaction studies demonstrate that the inverted charge orientation changes how the CP liposomes interact with ions in solution compared to PC liposomes. Monovalent ions ($Na^+$ and $Cl^-$) can also coordinate to the bilayer interface and for PC liposomes, $Na^+$ ions interact preferentially over $Cl^-$ due to the electrostatic attraction between the $Na^+$ and the anionic phosphate[37]. This phenomenon, which attracts positively charged molecules or ions toward and sometimes into the bilayer, results in an increased permeability for $Na^+$ over $Cl^-$ for PC liposomes[38]. In the case of the CPs, the positively charged quaternary amine is located at the bilayer interface and should have the opposite affect; attracting anionic compounds to the surface and increasing their permeability relative to cations. The release rate for an anionic compound should be greater from CPe liposomes than from PC liposomes. We tested this hypothesis by measuring the release rates of an encapsulated model anionic compound, carboxyfluorescein (CF)(Fig. 2-5).

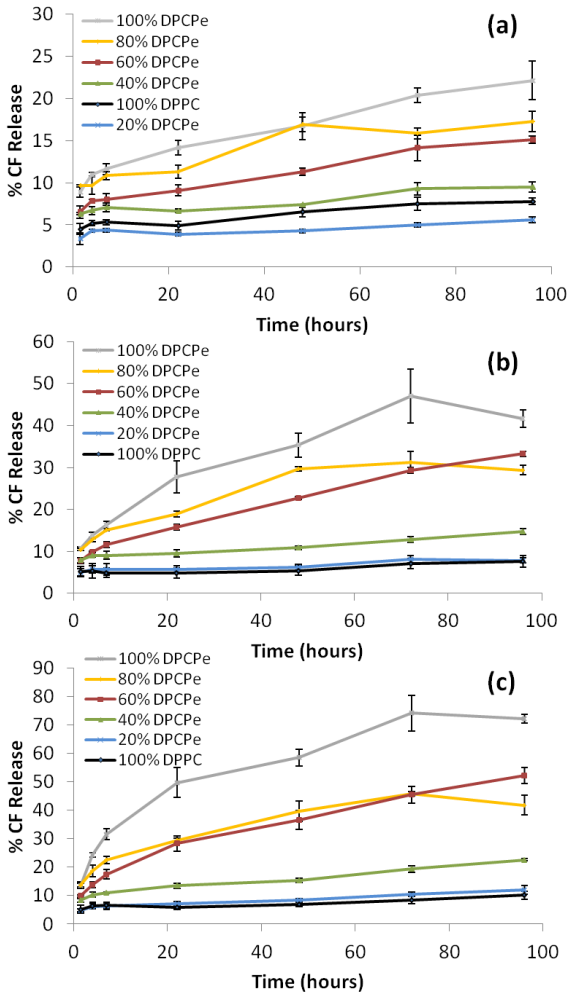


**Figure 2-5: CF release profiles of liposomes** with 5:4 molar diacyl lipid/cholesterol and varying ratios of DPCPe and DPPC.

As predicted, the DPCPe liposomes released CF at a much faster rate than DPPC liposomes at all temperatures (25, 37, and 50 °C) (Fig. 2-5). Furthermore, as the percentage of DPCPe in the liposome increased, the release rate also increased. Further biophysical studies are required to learn if this is a general phenomenon. If so, then mixed DPCPe/DPPC liposomes could be used to create a liposome with an adjustable release profile for an anionic compound. Adjustable release kinetics for liposomal delivery could enhance both existing therapies and aid in the development of new approaches to liposomal drug delivery.

**Table 2-2: Percent dephosphorylation ± standard deviations for CPs in the presence of an alkaline phosphatase (AP).**

| | C3-DOCP w/AP | C3-DOCP | DOCP w/AP | DOCP | DOCPe w/AP | DOCPe |
|---|---|---|---|---|---|---|
| **% Dephosphorylation** | 77±16 | 21±8 | 102±3 | 3±2 | 3±3 | 1±12 |

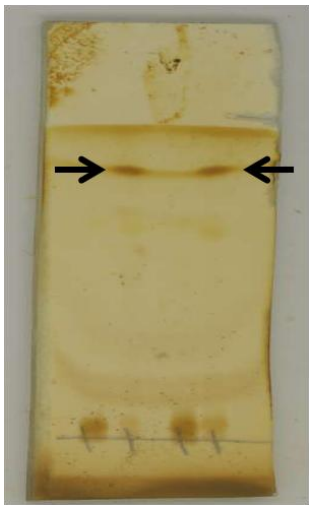

**Figure 2-6: CP lipids before and after treatment with AP**. Lanes from left to right are: DOCP before, DOCP after AP, C3-DOCP before and C3-DOCP after AP. TLC plate was run in chloroform/methanol/ammonium hydroxide (80:30:4).

Finally, to test if the CP lipids exhibited a level of bioactivity, we determined if the CP lipids were substrates for an alkaline phosphatase. Table 2-2 reports the percentage of dephosphorylation relative to the theoretical maximum (the value if the phosphates of every lipid in solution were cleaved) for three CP lipids, C3-DOCP, DOCP, and DOCPe in the presence of AP. The anionic headgroups were either fully (DOCP) or near fully (C3-DOCP) dephosphorylated in the presence of AP. The CPe lipids with and without AP and the C3-DOCP and DOCP preparations without AP showed a minimal increase in absorbance in the Malachite green assay. TLCs of the C3-DOCP and DOCP reactions (Fig. 2-6) following extraction into chloroform correlate with the data in Table 2-2. The low dephosphorylation levels for the DOCPe in the presence of AP suggest that it is not a substrate for the AP, while C3-DOCP and DOCP are

substrates. At the end of the phosphatase incubation period, the small anionic CP liposomes had aggregated into larger, visible structures.

## 2.4 Conclusion

We have synthesized a new class of zwitter-ionic phospholipids, with an inverted charge orientation in the headgroup relative to traditional PC lipids. CP liposomes have negative surface potentials across a broad pH range, and in their neutral form (CPe), do not appreciably interact with $Ca^{2+}$. The CP lipids have a terminal phosphate group which is similar to that found in many biologically active lipids. Furthermore, alkaline phosphatase can remove the phosphate from anionic CP lipids to generate a cationic lipid. This can be exploited to make a chameleon liposome which may be useful for cytoplasmic delivery of encapsulated contents. These CP lipids provide additional opportunities to study the influence of overall headgroup charge versus the location of the phosphate in the headgroup (i.e the importance of the location terminal of the phosphate relative to the negative charge) on the intrinsic biological activity of anionic signaling lipids.

## 2.5 Materials

DOPC, POPA, DOPS and POPG were purchased from Avanti Polar Lipid. Solvents were purchased from VWR Scientific. Trialkylphosphites were purchased from Alfa Aesar and used unmodified. All other chemicals were purchased from Sigma Aldrich. All buffers were made with MilliQ water and passed through a filtration system. NMR measurements were taken on a Bruker 300 MHz Avance system and analyzed with Topspin software. Chemical shifts are expressed as parts per million with tetramethylsilane as internal standard. HPFC column purifications were performed on a

Reveleris Flash System (Grace Division Biosciences) with pre-packed GraceResolv silica cartridges (67 Å, 40.5 μm). All sonication was performed in a G112SP1 Special Ultrasonic Cleaner from Laboratory Supplies Co., Inc (Hicksville, NY).

## 2.6 Methods

### 2.6.1 Synthetic Schemes

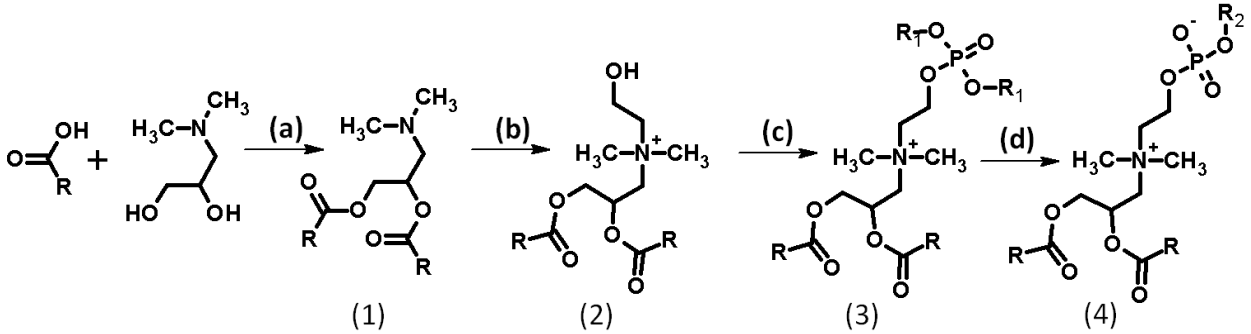


**Figure 2-6: Synthesis of DOCPe and DOCP a)** oleic acid, DCC, DMAP, $CH_2Cl_2$. **b)** 2-bromoethanol, DIPEA, 40° C. **c)** 1) trimethylphosphite (3a) or triethylphosphite (3b), $I_2$, pyridine/$CH_2Cl_2$ (2:5). **d)** TMS-Cl, NaI in acetonitrile, reflux or (4a) or LiBr in acetone, reflux (4b). R = oleyl chain, R1 = methyl (3a) or ethyl (3b) and $R_2$ = hydrogen (4a, DOCP) or ethyl (4b, DOCPe).

Synthesis of **(1)**: To 1 g 3-dimethylamino-1,2-propanediol (0.008 moles) was combined with 2.1 equivalents oleic acid (0.018 moles) in $CH_2Cl_2$ with 0.5 g dimethylaminopyridine (DMAP) and 2.1 equivalents N,N'-Dicyclohexylcarbodiimide (0.018 moles) and the reaction was stirred at room temperature for 4 hours. The reaction was then filtered to remove precipitated dicyclohexylurea and then washed with 1 M HCl (2X) to remove DMAP. The organic layer was collected, dried with sodium sulfate and concentrated under vacuum to yield a clear oil. No further purification was done with this material, which contained minor impurities of excess oleic acid and mono-substituted product. Estimated yield = 90%.

Synthesis of **(2)** from **(1)**: To 1 g of (1) (MW 648, 0.0015 moles) was added 5 equivalents of 2-bromoethanol (0.008 moles) in 3 mL $CH_2Cl_2$/methanol (2:1) with 0.5 mL diisopropylethylamine and stirred while heating at 40° C for 18 hours. The reaction was then diluted in $CH_2Cl_2$ and washed with 1 M HCl (2X) and concentrated under vacuum. **(2)** was isolated by flash chromatography with a Reveleris Flash System (Grace Division Biosciences) by elution at 15% methanol and $CH_2Cl_2$ with some unreacted **(1)** impurities present. Estimated yield = 60 %.

Synthesis of **(4a)** from **(2)**: 0.7 g of **(2)** (MW 692, 0.001 moles) was dissolved in 10 mL $CH_2Cl_2$/pyridine (5:1) and stirred in an acetone/dry ice bath. In a separate flask, also in an acetone/dry ice bath, 1.0 g $I_2$ (0.004 moles) was dissolved in 4 mL $CH_2Cl_2$ and to it was slowly added 0.5 g trimethylphosphite (0.004 moles) and the solution was stirred until colorless. The iodine mixture was then added dropwise to the first flask in the acetone/dry ice bath and the reaction was stirred for another 30 minutes and allowed to warm to room temperature. The reaction was then diluted with $CH_2Cl_2$ and washed with 1 M HCl (2X) and the organic layer was collected, dried with sodium sulfate and concentrated under vacuum. This material, **(3a)**, was then directly taken up into anhydrous acetonitrile with a catalytic amount of NaI added. Trimethylsilyl chloride (0.006 moles) was then added slowly to the reaction while stirring at room temperature. The reaction was then refluxed for 45 minutes, cooled to room temperature and concentrated under vacuum. To the concentrated solution, aqueous methanol was added and the reaction was stirred for 30 minutes. The reaction was then diluted with $CH_2Cl_2$ and washed with a 1 M sodium carbonate solution, dried with sodium sulfate and

concentrated under vacuum. The final product **(4a)** was taken up in minimal $CH_2Cl_2$ and precipitated in cold acetone. This was repeated 4X to yield the final product in a 15% yield from **(2)** – **(4a)**. MALDI-MS calc'd mass 774, found 772. $^1$H NMR ($CDCl_3$): δ 0.87 (t, 6H); δ 1.26 (m, 40H); δ 1.55 (m, 4H); δ 2.00 (m, 8H); δ 2.28 (m, 4H); δ 3.34 (d, 6H); δ 3.7-4.5 (m, 8H); δ 5.32 (m, 4H); δ 5.66 (m, 1H).

Synthesis of **(4b)** from **(2)**: 0.7 g of **(2)** (MW 692, 0.001 moles) was dissolved in 10 mL $CH_2Cl_2$/pyridine (5:1) and stirred in an acetone/dry ice bath. In a separate flask, also in an acetone/dry ice bath, 1.0 g $I_2$ (0.004 moles) was dissolved in 4 mL $CH_2Cl_2$ and to it was slowly added 0.5 g triethylphosphite (0.004 moles) and the solution was stirred until colorless. The iodine mixture was then added dropwise to the first flask in the acetone/dry ice bath and the reaction was stirred for another 30 minutes and allowed to warm to room temperature. The reaction was then diluted with $CH_2Cl_2$ and washed with 1 M HCl (2X) and the organic layer was collected, dried with sodium sulfate and concentrated under vacuum. This material, **(3b)**, was then directly taken up into 10 mL acetone with 0.3 g LiBr and refluxed for 30 minutes and then cooled to room temperature and concentrated under vacuum. The reaction was then diluted with $CH_2Cl_2$ and washed with a 1 M sodium carbonate solution, dried with sodium sulfate and concentrated under vacuum. The final product **(4b)** was purified by flash chromatography and eluted 35% methanol/ammonium hydroxide (35:5) in $CH_2Cl_2$ to yield a clear oil in a 10% yield for **(2)** – **(4b)**. MALDI-MS calc'd mass 800, found 801. $^1$H NMR ($CDCl_3$): δ 0.87 (t, 6H); δ 1.26 (m, 40H); δ 1.55 (m, 4H); δ 2.00 (m, 8H); δ 2.28 (m, 4H); δ 3.34 (d, 6H); δ 3.8-3.93 (m, 4H); δ 4.11 (m, 2H); δ 4.28 (m, 2H); δ 4.55 (m, 2H); δ 5.03 (m, 1H); δ 5.34 (m, 4H).

Synthesis of C3-DOCP: The procedure for the synthesis of 4a was followed with the only deviation occurring in step (b) where 3-bromopropanol was used in place of 2-bromoethanol. Following this step, the properties of the C3-DOCP did not differ significantly from those of DOCP in terms of solubility or purification. C3-DOCP was purified in the final step through acetone precipitation with a 16% yield for steps (b)-(d). MALDI-MS calc'd mass 786, found 786. $^{1}$H NMR ($CDCl_3$): δ 0.9 (t, 6H); δ 1.30 (m, 40H); δ 1.59 (m, 4H); δ 2.03 (m, 8H); δ 2.31 (m, 6H); δ 3.28-3.34 (d, 6H); δ 3.77 (m, 3H); δ 4.31 (m, 4H); δ 4.53 (m, 1H); δ 5.36 (m, 4H); δ 5.67 (m, 1H).

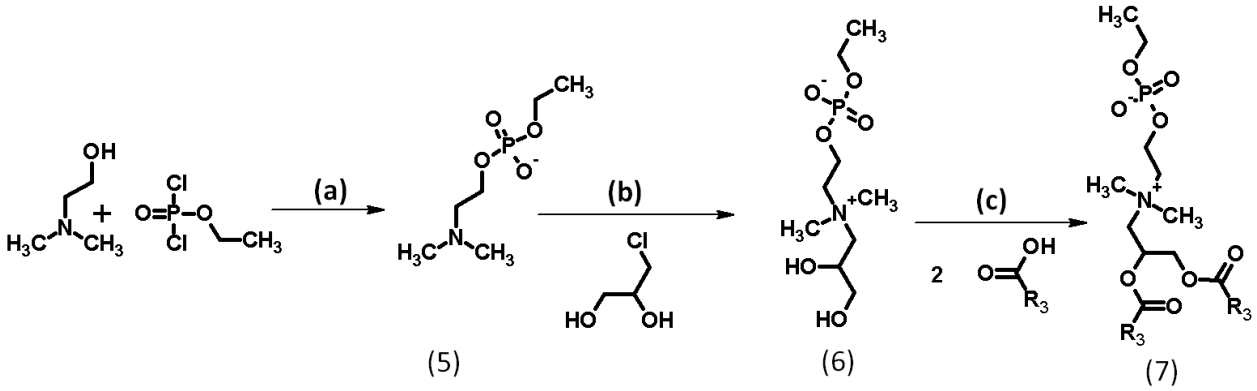


**Figure 2-7 Saturated chain CPe synthesis a)** Pyridine, $H_2O$ **b)** DIPEA, MeOH, heat **c)** DCC, DMAP, Pyridine, DMF.

The synthesis of the CPe lipids has not been optimized and we are currently working on an improved synthesis that increases the yield of the overall reaction. Currently, much of the yield for the overall synthesis is lost in step (b) (Fig. 2-7). General Procedure: To a flask with 70 mL $CH_2Cl_2$, 12 g of N,N-Diisopropylethylamine (DIPEA) (MW 129.25 g/mol, 0.09 moles) in an ice bath at 0° C, was added 5.2 g of ethyl dichlorophosphate (MW 162.94, 0.09 moles) slowly. In a separate flask, 4g N,N-Dimethylaminoethanol (MW 89.14 g/mol, 0.045 moles) was dissolved in $CH_2Cl_2$ and then added dropwise to the first flask while stirring at 0° C. The reaction was stirred for

1 hour following the addition and was allowed to warm to room temperature. Then, the reaction was placed back into the ice bath and a solution of tetrahydrofuran/water (5:1) was added dropwise until the reaction was quenched. The reaction was stirred for another 20 minutes and brought to room temperature. The reaction volume was then reduced under vacuum to approximately 20 mL and then acetone was added to precipitate the product and the acetone solution was decanted. This product was moved forward without further purification.

To (1) was added 7.4 g of 3-chloro-1,2-propanediol (MW 110.54, 0.067 moles) with 5.8 g DIPEA in 5 mL methanol. The reaction was stirred at 45° C for 16 hours and the methanol was removed under vacuum. The reaction mixture was then taken up into 30 mL $CH_2Cl_2$ and then decanted to remove the precipitate. The $CH_2Cl_2$ solution was then concentrated under vacuum to yield (2) and no further purification was performed.

Compound (2), (2.4 g, MW 272 g/mol, 0.009 moles) was dissolved in 60 mL $CH_2Cl_2$ and to the flask was added 2.5 molar equivalents (0.0225) of either myristic acid (5.13 g, MW 228.37 g/mol), palmitic acid (5.76 g, MW 256.42 g/mol), or stearic acid (6.39 g, MW 284.48 g/mol). When the acid chain had dissolved, 5.6 g of N,N-dicyclohexylcarbodiimide (MW 206.33, 0.027 moles) and 0.5 g of 4-(dimethylamino)pyridine (MW 122.17 g/mol, 0.004 moles) were added to the reaction. The reaction was stirred at room temperature for 4 hours or until completion was confirmed by loss of lyso-product on MALDI. The reaction was then filtered to remove dicyclohexylurea byproduct and washed with 1 M HCl. Products were purified on a 40g HPFC silica gel column and were eluted at 50% methanol in chloroform. The percent

yields were calculated for the entire synthesis (steps (a)-(c)), with the most significant loss in yield in step (b). All synthesis had approximately 2% total yield.

DMCPe: $^1$H NMR ($CDCl_3$/$CD_3OD$ ~10:1): δ 0.89 (t, 6H); δ 1.27 (m, 43H); δ 1.60 (m, 4H); δ 2.33 (m, 4H); δ 3.43 (s, 6H); δ 3.85 (m, 1H); δ 4.01 (m, 5H); δ 4.30-4.34 (d, 1H); δ 4.50 (m, 3H); δ 5.67 (m, 1H). MALDI-MS calc'd mass 691, found 692.

DPCPe: $^1$H NMR ($CDCl_3$/$CD_3OD$ ~10:1): δ 0.90 (t, 6H); δ 1.28 (m, 51H); δ 1.60 (m, 4H); δ 2.34 (m, 4H); δ 3.43 (s, 6H); δ 3.64-3.67 (d, 1H); δ 3.83 (m, 1H); δ 4.04-4.14 (m, 5H); δ 4.30-4.35 (d, 1H); δ 4.50 (m, 2H); δ 5.67 (m, 1H). MALDI-MS calc'd mass 748, found 749.

DSCPe: $^1$H NMR ($CDCl_3$/$CD_3OD$ ~10:1): δ 0.91 (t, 6H); δ 1.26 (m, 59H); δ 1.61 (m, 4H); δ 2.36 (m, 4H); δ 3.45 (s, 6H); δ 3.69 (m, 1H); δ 3.88 (m, 1H); δ 4.1 (m, 4H); δ 4.55 (d, 3H); δ 5.67 (m, 1H). MALDI-MS calc'd mass 804, found 804.

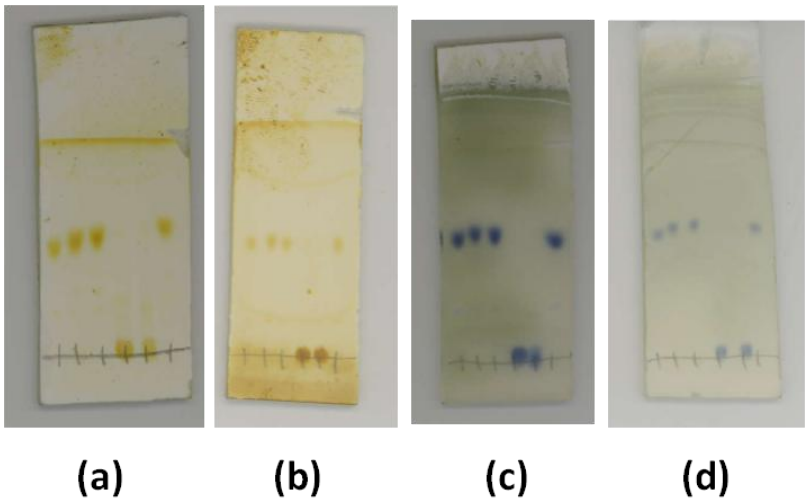


**Figure 2-8: TLC of CP Lipids** with $I_2$ stain (a) and (b) and Dittmer phosphate stain[39] (c) and (d) spotted from 10 mM solutions (a) and (c) and after a 20-fold dilution (b) and (d). Lanes from right to left: DMCPe, DPCPe, DSCPe, C3-DOCP, DOCP, and DOCPe. TLC plates were run in chloroform/methanol/ammonium hydroxide (80:30:4). Lipid purities were estimated to be > 95 %.

### 2.6.2 Dependence of zeta potential on changes in pH.

Liposomes were prepared from thin films in a glass test tube. The lipid films were hydrated to a concentration of 10 mM lipid in a 5 mM Tris, 5 mM NaCl, pH 8.6 buffer. The preparations were sonicated at 50 C for approximately 5 minutes. Then 100 uL of the liposome solution was added to 7.5 mL of the same buffer and this solution used in the auto-titration. A Malvern auto-titration accessory was used in conjunction with a Malvern Nanosizer instrument. The titration was run from pH 8.5 to pH 1.9 with a 0.1 pH tolerance for each measurement. Each lipid was run separately and exported to Excel for plotting and each data set has been fit with a second degree polynomial estimation for a clearer depiction of the trend for each lipid. Standard deviations are provided by the output and represent multiple readings during each individual lipid titration experiment.

### 2.6.3 Calcium-Induced Zeta Potential Shift

Liposomes were prepared as above in the zeta potential shift experiment at 10 mM lipid in a 20 mM MES 20 mM HEPES, pH 7.4 buffer. Twenty microliters of each liposome formulation were added to 3 mL of a 10 mM HEPES, pH 7.4 buffer with various amounts of $CaCl_2$ and NaCl added. NaCl was added along with $CaCl_2$ to maintain a constant ionic strength across all $Ca^{2+}$ concentrations. Ionic strengths were calculated according to the Debye-Hückel model, where the ionic strength (I) = $\frac{1}{2}(4[Ca^{2+}] + [Cl^-] + [Na^+])$, where brackets denote the total concentration of the enclosed ion. Zeta potential measurements were performed on a Malvern Nanosizer using the Smoluchowski model and run in triplicate.

### 2.6.4 Differential scanning calorimetry, $T_m$ measurements

Liposome formulations were prepared by thin film hydration in 10 mM HEPES, 150 mM NaCl, pH 7.4 to a final concentration of 16 mM lipid, followed by brief sonication to disperse the film into small lipid bilayer fragments. Then 200 uL of each preparation were added into each calorimeter chamber with buffer used in the specific liposome preparation as the standard. The measurements were run on a MC-DSC 4100 (Calorimetry Sciences Corp.) from 10 to 90° C at 1 degree/minute with a heat-cool-heat cycle where the last heating cycle is reported. Data was processed with CpCalc software and transferred to Excel to be graphed.

### 2.6.5 $Ca^{2+}$-induced liposome aggregation

Liposomes were prepared by thin film hydration from chloroform solutions of POPA, DOPS, DOPG, DOPC, DOCP, and DOCPe in a 20 mM MES, 20 mM HEPES buffer to a final lipid concentration of 5 mM. The preparations were then sonicated at 50° C for 10 minutes. Liposome diameters were measured following sonication, prior to use in the aggregation studies on a Malvern Nanosizer with Mark-Houwink parameters. Aggregation studies were run on a Flourolog Fluorimeter (Horiba Scientific) using the kinetic measurement function set to measure 90° C scattering at 400 nm. For each measurement, a 50 μL of the liposome solution under examination was added to 3 mL of the hydration buffer in a stirred cuvette maintained at 25° C. At 30 seconds into a 5 minute run, a concentrated solution of $CaCl_2$ was added by pipette to give the target $Ca^{2+}$ concentration. Scattering was measured for the entire 5 minute run. Each scan was normalized to its own baseline by subtracting the amount of scattering prior to $Ca^{2+}$ addition from each data point collected during the run. Six $Ca^{2+}$ concentrations were

measured; 0.1 mM, 0.5 mM, 1 mM, 4 mM, 7 mM, and 10 mM. Data was exported to Excel for graphing. All $Ca^{2+}$ concentrations were run in triplicate for each lipid. Aggregation rates for each $Ca^{2+}$ concentration were determined by determining the slope from a linear regression fit to the initial 2 seconds of aggregation following $Ca^{2+}$ addition.

### 2.6.6 Carboxyfluorescein (CF) Release

Lipid preparations were dried from chloroform solutions into thin film in a glass test tube at a molar ratio of 5:4 diacyl lipid:cholesterol. Three DPPC/DPCPe combinations were made at 20%, 40% and 60% DPCPe with percentages referring to the molar amount of DPCPe relative to the total moles of diacyl lipid in the formulation. A solution of 100 mM CF, 10 mM Tris, pH 7.4 was then added to each preparation to give a total lipid concentration (diacyl lipid and cholesterol) of 20 mM. The preparations were then sonicated at 50 °C for 10 minutes and free CF was removed by size exclusion chromatography on a PD-10 Sephadex column (GE Health Sciences) by elution in a buffer: 92 mM NaCl, 8 mM $NaN_3$, and 10 mM HEPES, pH 7.4. Then, 100 μL of each purified liposome solution was added to 6 mL of the elution buffer. CF release was measured at three different temperatures, room temperature, 37 °C, and 50 °C. The amount of CF released at each time point was measured on a FLUOstar plate reader (BMG Labtech) with Ex 485 nm and Em 520 nm. Percent leakage values were calculated by measuring the total CF preparation by liposome lysis with $C_{12}E_{10}$ surfactant. All formulation/temperature combinations were run in triplicate. Percent Release was calculated as follows: % Release at time, (t) = (measured fluorescence at time, (t)) / (total fluorescence from lysed liposomes) X 100.

### 2.6.7 Alkaline Phosphatase Susceptibility Assay

A procedure similar to those used previously[40] for cholesterol phosphate was employed to test if the CP lipids are susceptible to hydrolysis by an alkaline phosphatase. C3-DOCP, DOCP, and DPCPe films were rehydrated from a thin film in 10 mM HEPES, 150 mM NaCl, pH 7.4 to a lipid concentration of 1 mM. The preparations were sonicated at 60 °C for 5 minutes and then 50 μL of each solution was diluted into 1 mL of a 5 mM HEPES, 145 mM NaCl, 1 mM $MgCl_2$ buffer at pH 7.4 in a 24 well plate. To each well, 5 μL of alkaline phosphatase (Calf Intestinal Phosphatase, New England Biolabs 10,000 units/mL) was added and the plate was gently shaken and incubated at 37 °C for 24 hours. The extent of dephosphorylation was measured by a Malachite green assay. In a 96 well plate, 10 μL of each reaction was added to a well with 90 μL of the reaction buffer and then 100 μL of a Malachite green solution was added (Malachite green solution contained: 0.7 M HCl, 0.3 g Malachite green, 2 g sodium molybdate and 0.5 g Trition X-100). After 20 minutes, the absorbance of each well at 650 nm was measured. A standard curve was made through serial dilutions of $KHPO_4$ from 100 μM to 1.5 μM in the reaction buffer (total volume 100 μL) and 100 μL of the Malachite green solution. A linear regression was fit to the data to yield an equation of $y = .0172x + 0.0658$ with an $R^2$ of 0.98, where "y" is the absorbance at 650 nm and "x" is equal to the concentration of phosphate in solution (μM). The linear fit was used to predict a maximum theoretical value by substituting the lipid concentration in each well in for x. The maximum theoretical value corresponds to the absorbance at 650 nm if all of the CP headgroups

were cleaved from the lipid. Each lipid was measured in triplicate and the results presented in Table 2-2 represent an average of the three points.

## 2.7 References


1. M. Ma, Y. Gong and D. Bong, *Journal of the American Chemical Society*, 2009, **131**, 16919-16926.
2. Y. Rui, S. Wang, P. S. Low and D. H. Thompson, *Journal of the American Chemical Society*, 1998, **120**, 11213-11218.
3. S. Ali and R. Bittman, *Chemistry and Physics of Lipids*, 1989, **50**, 11-21.
4. A. Arora and C. M. Gupta, *Biochimica et Biophysica Acta (BBA) - Biomembranes*, 1997, **1324**, 61-68.
5. R. Anderson, M. Kates and B. E. Volcani, *Biochimica et Biophysica Acta (BBA) - Lipids and Lipid Metabolism*, 1978, **528**, 89-106.
6. H. H. Mantsch, D. G. Cameron, P. A. Tremblay and M. Kates, *Biochimica et Biophysica Acta (BBA) - Biomembranes*, 1982, **689**, 63-72.
7. I. Lindh and J. Stawinski, *The Journal of Organic Chemistry*, 1989, **54**, 1338-1342.
8. J.-P. Rolland, C. Santaella and P. Vierling, *Chemistry and Physics of Lipids*, 1996, **79**, 71-77.
9. Z. Huang and F. C. Szoka, *Journal of the American Chemical Society*, 2008, **130**, 15702-15712.
10. N. S. Chandrakumar and J. Hajdu, *The Journal of Organic Chemistry*, 1982, **47**, 2144-2147.
11. T. Makiyama, N. Nagasaka, Y. Houjyo, E. Yamaura, H. Nakamura, Y. Koide, A. Nishida and T. Murayama, *Biochemical Pharmacology*, 2010, **80**, 1396-1406.
12. R. Z. Lu, J. G. Turcotte, W. H. Lin, J. M. Steim and R. H. Notter, *Journal of Colloid and Interface Science*, 1992, **154**, 24-34.
13. S. Liu and D. F. O'Brien, *Journal of the American Chemical Society*, 2002, **124**, 6037-6042.
14. B. Jing, N. Tokutake, D. H. McCullough and S. L. Regen, *Journal of the American Chemical Society*, 2004, **126**, 15344-15345.
15. B. A. McNally, E. J. O'Neil, A. Nguyen and B. D. Smith, *Journal of the American Chemical Society*, 2008, **130**, 17274-17275.
16. D. N. Brindley and C. Pilquil, *Journal of Lipid Research*, 2009, **50**, S225-S230.
17. J. M. Boon, T. N. Lambert, A. L. Sisson, A. P. Davis and B. D. Smith, *Journal of the American Chemical Society*, 2003, **125**, 8195-8201.
18. S. Deborah W, *Biochemical and Biophysical Research Communications*, 1987, **145**, 228-233.
19. N. N. Desai, H. Zhang, A. Olivera, M. E. Mattie and S. Spiegel, *Journal of Biological Chemistry*, 1992, **267**, 23122-23128.
20. M. Maceyka, S. G. Payne, S. Milstien and S. Spiegel, *Biochimica et Biophysica Acta (BBA) - Molecular and Cell Biology of Lipids*, 2002, **1585**, 193-201.
21. K. Takabe, S. W. Paugh, S. Milstien and S. Spiegel, *Pharmacological Reviews*, 2008, **60**, 181-195.

22. C. Chalfant and M. D. Poeta, *Sphingolipids as signaling and regulatory molecules*, Springer Science+Business Media, 2010.
23. S. R. Coats, A. B. Berezow, T. T. To, S. Jain, B. W. Bainbridge, K. P. Banani and R. P. Darveau, *Infect. Immun.*, 2011, **79**, 203-210.
24. G. De Becker, V. Moulin, B. Pajak, C. Bruck, M. Francotte, C. Thiriart, J. Urbain and M. Moser, *International Immunology*, 2000, **12**, 807-815.
25. A. G. Johnson, M. Tomai, L. Solem, L. Beck and E. Ribi, *Reviews of Infectious Diseases*, 1987, **9**, S512-S516.
26. E. K. Perttu and F. C. Szoka, *Chemical Communications*, 2011.
27. A. G. a. F. C. S. Kohli, Jr., *In preparation*, 2011.
28. U. Köhler, H. H. Mantsch and H. L. Casal, *Canadian Journal of Chemistry*, 1988, **66**, 983-988.
29. H. Hauser, *Proceedings of the National Academy of Sciences*, 1989, **86**, 5351-5355.
30. J. Wilschut, N. Duzgunes, R. Fraley and D. Papahadjopoulos, *Biochemistry*, 1980, **19**, 6011-6021.
31. D. Papahadjopoulos, S. Nir and N. Düzgünes, *Journal of Bioenergetics and Biomembranes*, 1990, **22**, 157-179.
32. R. Leventis, J. Gagne, N. Fuller, R. Rand and J. Silvius, *Biochemistry*, 1986, **25**, 6978-6987.
33. A. Chauhan, V. P. S. Chauhan and H. Brockerhoff, *Biochemistry*, 1986, **25**, 1569-1573.
34. P. Wan, Y. Zhao, H. Tong, Z. Yang, Z. Zhu, X. Shen and J. Hu, *Materials Science and Engineering: C*, 2009, **29**, 222-227.
35. A. Portis, C. Newton, W. Pangborn and D. Papahadjopoulos, *Biochemistry*, 1979, **18**, 780-790.
36. J. Lansman and D. H. Haynes, *Biochimica et Biophysica Acta (BBA) - Biomembranes*, 1975, **394**, 335-347.
37. H. Hauser, D. Oldani and M. C. Phillips, *Biochemistry*, 1973, **12**, 4507-4517.
38. I. V. Khavrutskii, A. A. Gorfe, B. Lu and J. A. McCammon, *Journal of the American Chemical Society*, 2009, **131**, 1706-1716.
39. E. K. Ryu and M. MacCoss, *Journal of Lipid Research*, 1979, **20**, 561-563.
40. S. C. Davis and F. C. Szoka, *Bioconjugate Chemistry*, 1998, **9**, 783-792.

Chapter 3

# Zwitterionic Sulfobetaine Lipids that Form Vesicles with Salt-Dependent Thermotropic Properties

## 3.1 Abstract

We describe a class of zwitterionic sulfobetaine (SB) lipids with fascinating salt-dependent properties. SB lipids are zwitter-neutral across a broad pH range; however they have negative surface potentials in the presence of anions and two salt-dependent transition temperatures. These new SB lipids provide insight on the role of charge orientation at the membrane interface and may be useful components in drug delivery systems.

## 3.2 Introduction

Zwitterionic lipids such as phosphatidylcholine (PC) and phosphatidylethanolamine (PE), are the major lipids in the membranes that compartmentalize most organisms from microbes to man. Although there is a large literature on PC, PE, cationic and non-ionic lipids, there are surprisingly few studies on modifications to diacyllipids that retain a zwitterionic neutral headgroup at pH 7.4[12-17]. Therefore, there is a vast chemical space to explore for synthetic lipids that might shed light on the physical properties of membranes formed from non-biological lipids or provide new components for liposome-based therapies.

Here, we describe a novel class of zwitterionic SB lipids that differ structurally from PC lipids in two ways—the locations of the charged headgroup moieties relative to the bilayer, and the nature of the anionic group. SB lipids have an anionic sulfonate that extends into the aqueous media and a cationic amine adjacent to the bilayer, whereas for PC lipids, the anionic phosphate is adjacent to the bilayer and the cationic amine extends

from the liposome surface (Fig. 3-1a). The SB lipids have interesting salt-dependent phase transition temperatures ($T_m$) and liposome-forming properties.

To our knowledge sulfobetaine diacyllipids have not been reported, although a variety of single chain sulfobetaine surfactants are well characterized and used in a variety of applications[18-20]. Investigations into the properties of SB surfactants in the presence of various salts reveal that anions bind preferentially over cations at the micelle interface. In the presence of salt, the otherwise neutrally charged micelles gain an overall negative charge[21, 22]. Marte[22] reports that anions bind to the interface in the following order $OH^- < Cl^- < Br^- < ClO_4^-$, which parallels the Hofmeister series[23].

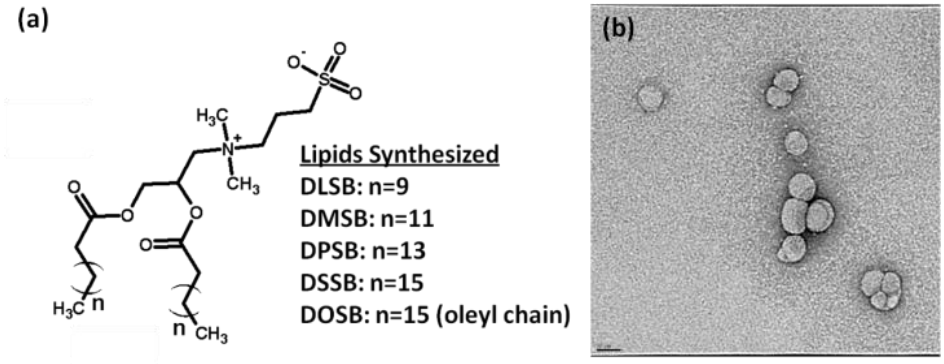


**Figure 3-1: SB lipid structure and liposome TEM** (a) SB lipid structure. (b) TEM Images of DPSB/cholesterol:10/3 mole ratio liposomes. Scale bar is 50 nm. Dynamic light scattering measurements indicated liposome diameters to be 70 nm.

### 3.3 Results and Discussion

Hydration of a dried film of the SB lipids in 150 mM NaCl at a temperature above the $T_m$ of the lipid did not lead to the formation of liposomes. Based upon the findings in the surfactant field we surmised an inner-salt was forming either within the same headgroup or between neighboring headgroups and these interactions were interfering with liposome formation. We increased the NaCl concentration to disrupt the inner-salts

and found that small diameter vesicles formed at NaCl concentrations greater than or equal to 500 mM (Table 3-1).

**Table 3-1 Liposome diameter (nm) and polydispersity in various NaCl concentrations**

| Lipid | 1000 mM NaCl | 500 mM NaCl | 150 mM NaCl | 0 mM NaCl |
|---|---|---|---|---|
| DLSB | 57, [0.4] | 42, [0.3] | 1728, [0.7] | DNF |
| DMSB | 77, [0.2] | 64, [0.4] | DNF | DNF |
| DPSB | 93, [0.3] | 67, [0.3] | DNF | DNF |
| DSSB | 138, [0.4] | 123, [0.3] | DNF | DNF |
| DOSB | 119, [0.2] | 127, [0.2] | DNF | DNF |

Average liposome diameter and polydispersity index, PDI (in brackets), in various concentrations of NaCl. PDI values range from 0-1 with 0 corresponding to a monodisperse population. Liposome preparations were made at 26 mM lipid in 10 mM HEPES buffer, pH 7.4 with the specified salt concentration. All preparations were rehydrated and sonicated at 80 °C for 7 minutes, allowed to cool for 5 minutes and then measured. DNF = Did Not Form, no liposomes formed.

When the counter ion was changed from $Cl^-$ to $ClO_4^-$, $I^-$, or $Br^-$ at 150 mM, liposomes formed regardless of the acyl chain length (Table 3-2) with small variation in diameter between preparations (Table 3-3). Zeta potential measurements of DMSB in the various salt solutions revealed the surface potential of the liposomes varied according to the counter-ion, $ClO_4^- > I^- > Br^- > Cl^-$, specifically: -38, -35, -23, -6 mV respectively, suggesting a higher degree of anion binding in the same order. These results show that as the polarizability of the anion in solution increases, so does its ability to interact with the liposome surface. Lipid films rehydrated in 500 mM NaF, did not form liposomes. We verified the formation of liposomes by transmission electron microscopy (TEM) (Fig. 3-1b), which reveals small, uniform diameter liposomes consistent with the dynamic light scattering data (see Fig. 3-1 legend).

**Table 3-2 Liposome diameter (nm) and polydispersity in various salts following sonication and at 24 Hours**

| Lipid | 150 mM $NaClO_4$ | 150 mM $NaClO_4$ (24h) | 150 mM NaI | 150 mM NaI (24h) | 150 mM KBr | 150 mM KBr (24h) | 150 mM NaF |
|---|---|---|---|---|---|---|---|
| DLSB | 30, [0.2] | 37, [0.3] | 29, [0.2] | 39, [0.2] | 55, [0.3] | 74, [0.3] | DNF |
| DMSB | 42, [0.2] | 44, [0.2] | 35, [0.2] | 39, [0.3] | 29, [0.2] | 32, [0.2] | DNF |
| DPSB | 35, [0.2] | 43, [0.4] | 57, [0.3] | Gel | 64, [0.1] | Precip | DNF |
| DSSB | 42, [0.3] | 72, [0.3] | 43, [0.2] | Gel | 102, [0.1] | Precip | DNF |
| DOSB | 68, [0.3] | 69, [0.2] | 91, [0.2] | 99, [0.3] | 121, [0.3] | 138, [0.4] | DNF |

Average liposome diameter and polydispersity index (in brackets) were measured both five minutes after sonication and at 24 hours. PDI values range from 0-1 with 0 corresponding to a monodisperse population. Gel = Formed Gel, Precip = Liposomes formed polydisperse, large chunks and precipitated, DNF= Did Not Form liposomes.

**Table 3-3 Variation in the diameter of DMSB liposomes**

| Lipid | $NaClO_4$ | $NaClO_4$ (24 hrs) | NaI | NaI (24 hrs) | KBr | KBr (24 hrs) |
|---|---|---|---|---|---|---|
| DMSB | 35 ± 9.4 | 40 ± 5.5 | 33 ± 2.5 | 42 ± 3 | 34 ± 4.3 | 38 ± 5.7 |

Liposome diameter (nm) ± one standard deviation. All salts were in solution at 150 mM.

Since SB liposome formation and stability is largely dependent on salt composition and concentration, we determined if the salt concentration/type influenced the $T_m$ of the lipid colloidal dispersions (Fig. 3-2). We discovered two primary $T_m$ for each SB lipid; a low $T_m$ similar to that of its PC lipid acyl chain analog, and a high $T_m$ similar to its PE lipid counterpart (Table 3-4). $T_m$ measurements were reproducible across multiple experiments (Table 3-5). The more polarizable anions ($Br^-$, $I^-$, and $ClO_4^-$) and high NaCl concentrations (≥ 500 mM) favored the low $T_m$, while low NaCl concentrations and less polarizable anions ($Cl^-$ and $F^-$) resulted in high $T_m$. The transition from high to low $T_m$ appears to be a two-component process with intermediate transitions only observed in DSSB at 150 mM NaCl.

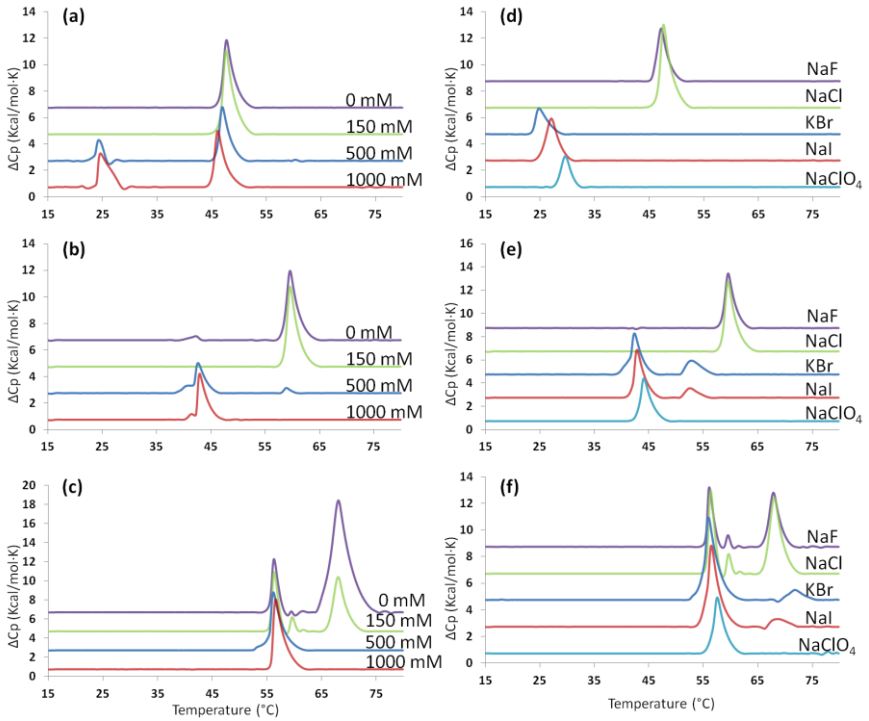


**Figure 3-2: Representative DSC traces for DMSB, DPSB, and DSSB** (a-c) at four NaCl concentrations (a) DMSB, (b) DPSB, (c) DSSB and (d-f) with 150 mM NaF, NaCl, KBr, NaI, and $NaClO_4$ (d) DMSB (e) DPSB (f) DSSB. Repeated measurements have similar thermograms (See Table 4).

**Table 3-4 Transition temperatures (°C) for hypothesized inner and mobile counter-ion salt SB forms compared to PE and PC headgroups**

| Chain Length | PE | SB Inner Salt Onset, Peak | PC | SB Mobile Counter-ion Salt Onset, Peak |
|---|---|---|---|---|
| C14 | 49.4 | 45-46, 46-48 | 24.2 | 23-24, 24-25 |
| C16 | 63.5 | 58-59, 59-60 | 41.7 | 40-41, 43 |
| C18 | 74.4 | 64-66, 68 | 55.3 | 53-56, 56-57 |

Comparison of the transition temperatures of the SBL to literature values[24] for the phase transition temperatures of PE and PC. SB values correspond to the ranges of transition onset or peak values observed across the four NaCl concentrations.

**Table 3-5 Average $T_m$ values with standard deviation for either duplicate or triplicate DSC scans**

| Lipid | NaCl Concentration (mM) | Number of DSC Runs | Low $T_m$ Onset (°C) | Low $T_m$ Peak | High $T_m$ Onset | High $T_m$ Peak |
|---|---|---|---|---|---|---|
| DMSB | 500 | 3 | 23 ± 1 | 24 ± 0 | 45 ± 1.5 | 47 ± 0.6 |
| DPSB | 500 | 3 | 40 ± 0.6 | 42 ± 1.7 | 57 ± 2.6 | 58 ± 1.2 |
| DPSB | 1000 | 2 | 40 ± 2 | 43 ± 0 | Not Pres. | Not Pres. |
| DSSB | 500 | 2 | 52 ± 1.4 | 56 ± 0 | Not Pres. | Not Pres. |
| DSSB | 1000 | 2 | 53 ± 4 | 57 ± 7 | Not Pres. | Not Pres. |

Not Pres. = no peak was observed at the high $T_m$.

The orientation of the fixed charge at the bilayer interface is thought to influence the permeation of ions and charged molecules across the interface[25]. Thus, we compared the leakage rate of a model water soluble anion, carboxyfluorescein (CF), from SB or PC liposomes[26] in two buffers with salt concentrations either equal to or lower than the liposome preparation buffer. If the orientation influences ion permeation, one would expect CF to leak more rapidly from the SB liposomes. The CF release rates for the DPSB and DPPC formulations shown in Fig. 3-3a are slow and similar to each other in the "equal salt" buffer, suggesting only a small effect from the charge orientation. DPSB liposomes have a higher rate of release in the "low salt" buffer which may be due to the dissociation of $Cl^-$ from the liposome surface, resulting in the formation of an inner-salt form and the subsequent destabilization of the bilayer.

The CF release rates for DPPC liposomes are similar for both buffers, which suggest a decreased sensitivity to changing salt conditions relative to DPSB liposomes. DPSB liposomes are fairly stable even when added to a buffer with a lower salt concentration and may be useful for encapsulating and delivering an aqueous drug.

In liposomal drug delivery, temperature induced leakage can allow for site-specific delivery of encapsulated material at a location where the temperature has been

elevated above normal human body temperature (37 °C)[27, 28]. To examine the SB liposomes for potential use in thermally-triggered systems, CF release from DPSB/cholesterol/PEG-DSPE (85:10:5 mole ratio) liposomes was monitored at three different temperatures; physiological (37 °C), near the lower $T_m$ of DPSB (44 °C) (Fig. 3-3b) and at the higher $T_m$ of DPSB (59 °C) (See Fig. 3-5). DPSB liposomes have a more rapid release than DPPC liposomes at 37 °C and do not release to the same extent as DPPC liposomes at 44 °C.

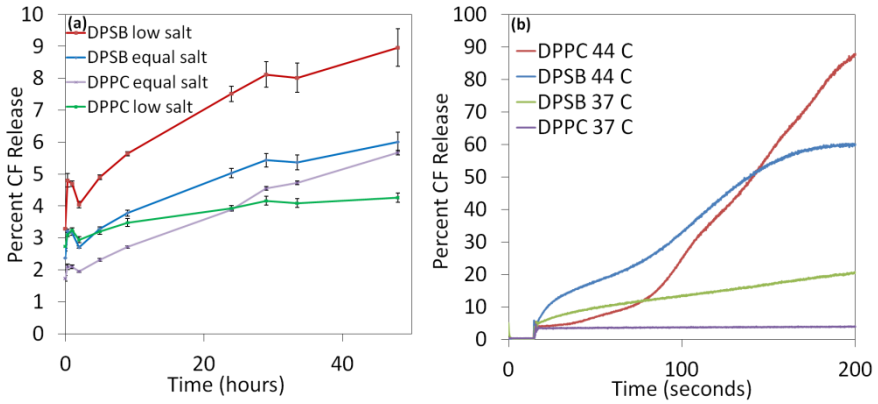


**Figure 3-3: CF release** (a) CF release from DPSB and DPPC liposomes both with 23% cholesterol. (b) Thermal induced CF release from DPSB and DPPC liposomes.

Since the $T_m$ of the SB lipids are salt dependent, we investigated if we could trap the liposomes in one $T_m$ state by preparing them in either NaCl or KBr. We also took liposomes prepared in both salt types and exchanged the outside salt type with the other salt to determine the influence of a salt asymmetry across the bilayer on the thermal release properties (Fig. 3-5). The method is depicted in Fig. 3-4.

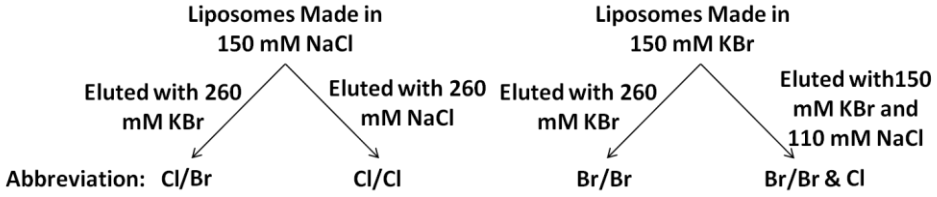


**Figure 3-4: Schematic explaining the nomenclature for the CF release studies** in Fig. 3-5.

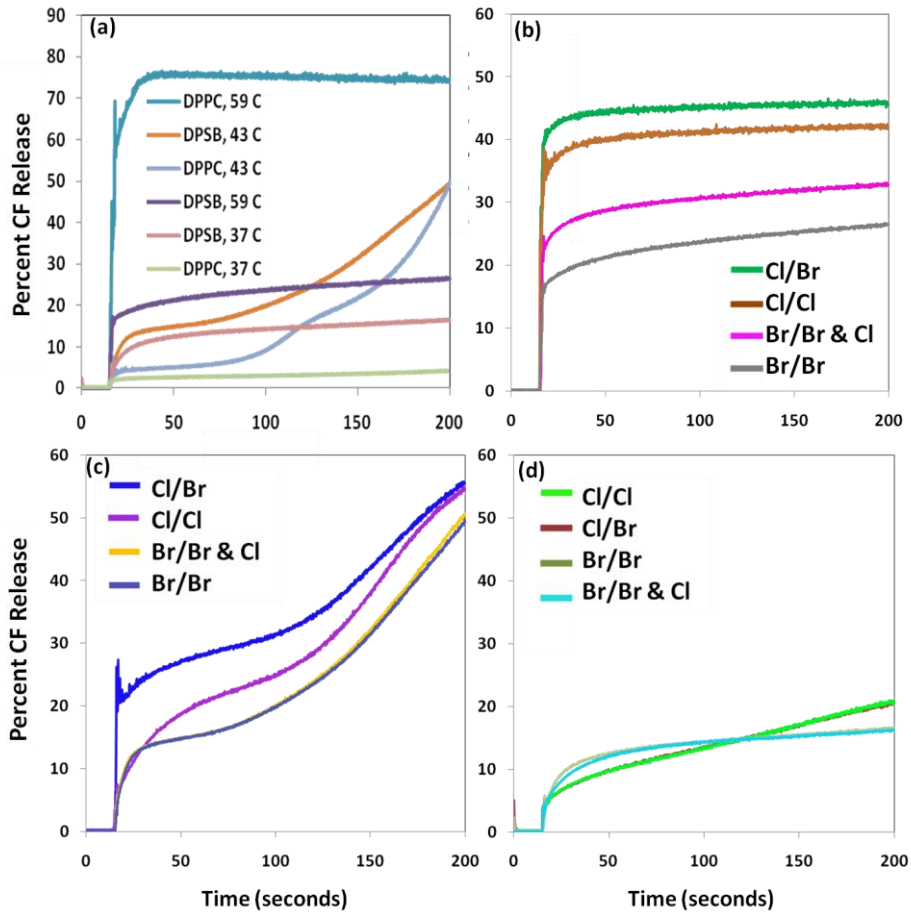


**Figure 3-5: Thermally-triggered CF release from DPSB and DPPC liposomes**. a) Liposomes were prepared as described in the Methods and correspond to the Br/Br preparation in Figure 3-4. Samples were all run in triplicate with average standard deviations of less than 2% for all experiments except DPPC at 59° C, which had a standard deviation of 18.5%. b-d) DPSB Liposomes were prepared as described in the Methods section and as depicted in Figure 3-4. Measurements were performed at 59 °C (b), 43 °C (c), and 37 °C (d). Samples were run in triplicate with average standard deviations of less than 3% for all experiments except for "Br/Br & Cl" at 59 °C, "Cl/Br" at 59 °C, and "Cl/Br" at 43 °C which had average standard deviations between 5-7% and "Cl/Cl" at 59 °C which had an average standard deviation of 10.4%.

Fig. 3-5a shows the CF release profiles of "Br/Br" DPPC and DPSB liposomes at three temperatures, 37, 43 and 59 °C. Fig. 3-5a reveals two release profiles. Both DPSB and DPPC show a sudden release followed by a plateau at 59 and 37 °C, but the magnitude of the initial release is greater at 59 °C than at 37 °C for both lipids. At 59 °C, DPPC releases the majority of its contents in the first seconds following liposome

addition, while DPSB releases only 20 % initially. Although the cause of the sudden release remains unclear, we believe the initial increase in fluorescence is primarily due to CF release after the addition of the liposomes to the cuvette and is not a result of CF release in the liposome stock solution. We believe this because measurements at different temperatures with the same stock solution did not show the same initial increase in fluorescence (data not shown). The immediate jump in fluorescence could be due to a sudden reorganization of the headgroups and melting of the hydrocarbon chains that permit CF release, followed by the formation of stable state that allows the liposome to retain any remaining encapsulated CF. At 43 °C, both DPSB and DPPC show a different type of release profile characterized by a burst release followed by a slow release phase and finally a rapid CF release. This profile may result from a rapid destabilization caused by headgroup rearrangement, followed by a slower release rate as portions of the bilayer begin to transition, and then an increased release rate when the entire bilayer is at the point of transition. At 43 °C, the DPSB and DPPC preparations show similar releases at the end of the measurement.

Fig. 3-5b-d show the CF release rates of DPSB liposomes in which a combination of NaCl and KBr were used in the preparations according to Fig. 3-4. We hypothesized that the "Cl/Cl" liposomes would have the steadiest CF release at the higher $T_m$ (59 °C) and the "Br/Br" liposomes to have the steadiest CF release at the lower $T_m$ (43 °C). However, all the salt combinations had a steady release at 43 °C and not at 59 °C, with the "Cl/Cl" preparation releasing more than either preparation hydrated in KBr. At 59 and 43 °C, all the preparations had similar release profiles with differing maximum values. For all three temperatures, liposomes made with NaCl released more CF than

those made with KBr. At 37 °C, both of the liposome preparations hydrated in NaCl exhibited a third type of release profile, with an immediate burst followed by a single steady release phase. Based on the results in Figure 3-5, it does not appear that the type of salt used in the preparation of the liposomes significantly affects their CF release profile, but liposomes prepared in NaCl are less stable overall than those prepared in KBr. These results do not correlate with the $T_m$ data measured by DSC. DSC measurements were performed predominantly with bilayer fragments, not liposomes, so it is possible that the elevated $T_m$ correspond to an interaction between stacked bilayers. However, many of the DSC measurements show only a low $T_m$ even though bilayer fragments were used.

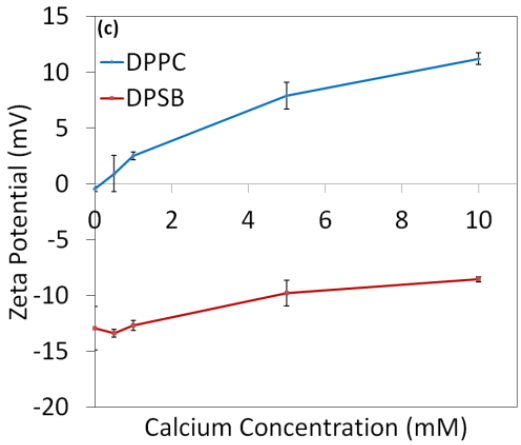


**Figure 3-6 The effect of $Ca^{2+}$ on the zeta potential** of DPSB and DPPC liposomes with cholesterol as in Fig. 3-3a

In biological systems, divalent cations are frequently present and can interact with lipid headgroups to induce aggregation, fusion, or alter the surface potential[29]. We measured the effect of $Ca^{2+}$ concentration on the aggregation and zeta potential of SB liposomes. DMSB liposomes in the presence of up to 300 mM $Ca^{2+}$ did not aggregate whereas DMPC liposomes aggregated at 300 mM $Ca^{2+}$ (data not shown).

As previously reported[30], the surface potential of the PC liposomes becomes increasingly positive as the $Ca^{2+}$ concentration increases (Fig. 3-6). The surface potential of the DPSB formulation also becomes more positive with increasing $Ca^{2+}$ concentration, however the magnitude of the change is less and the zeta potential remains negative up to 10 mM $Ca^{2+}$. This indicates that $Ca^{2+}$ has a weaker interaction with the SB sulfonate, which extends into the aqueous media, than with the PC phosphate anchored at the hydrophobic interface. The ability of SB liposomes to avoid aggregation and remain negative in the presence of elevated $Ca^{2+}$ could be beneficial for drug delivery applications.

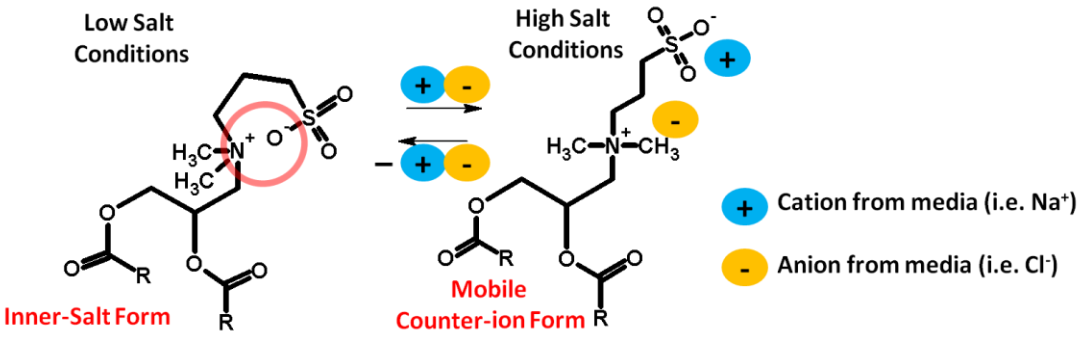


**Figure 3-7: Illustration of inner-salt and mobile counter-ion salt.**

The salt-dependent properties of the SB lipids may be explained by the occurrence of two salt forms; an inner-salt formed within the same (or between neighboring headgroups) and a mobile counter-ion salt formed between the SB headgroup and ions in the surrounding media (Fig. 3-7). These two forms may be responsible for the two $T_m$ observed for the SB lipids.

There are two possible explanations for the increased $T_m$—an increase in the strength of the interactions either between: 1) neighboring headgroups or 2) adjacent acyl chains. Increased acyl chain packing could occur for the case of the self inner-salt due to a decrease in headgroup surface area at the bilayer interface, allowing the hydrophobic

chains to pack more closely. This would also lead to a higher $T_m$ . However, replacing the quaternary amine in PC with either a methyl or t-butyl group, which decreases the headgroup area, does not increase the $T_m$ [31]. This demonstrates that a decrease in headgroup size alone is not enough to produce an elevated $T_m$.

We think it more likely that the observed increase in $T_m$ for the SB lipids is due to strong ionic headgroup interactions. Phospholipids, such as PE[24] and phosphatidic acid (PA)[32,33], have smaller headgroups and elevated transition temperatures relative to PC, but their increased $T_m$ are attributed to hydrogen bonding interactions and not a decrease in headgroup surface area[31, 33]. The hydrogen bonding hypothesis is supported by the decrease in the PE $T_m$ to PC-like values at high pH, where the amine is deprotonated. PA lipids have a maximum $T_m$ around pH 4, where the $pK_1$ hydrogen is 50% deprotonated and the hydrogen bonding ability across the liposome surface is maximized[33]. At pH 11, where the phosphate is almost completely deprotonated, the $T_m$ of PA liposomes is more than 25 °C lower than at pH 4.

Interestingly, PC lipids with a three carbon spacer between the phosphate and quaternary amine[31], similar to the SB lipid headgroup, do not show the same sort of behavior. Therefore, either the interaction of a quaternary amine with a sulfonate instead of a phosphate or the location of the quaternary amine adjacent to the bilayer promotes the inner-salt interactions.

In the mobile counter-ion salt form, the SB headgroup should become more hydrated and exhibit increased degrees of freedom. This would increase the surface area at the bilayer interface and disrupt the attractive headgroup interactions.

## 3.4 Conclusion

In conclusion, a new class of zwitterionic SB lipids has been synthesized that exhibit salt-dependent properties that differ from PC lipids. The SB lipids have an inverse charge orientation at the membrane interface and may provide new ways to create membranes with adjustable, asymmetric properties. SB lipids could also serve as a useful tool for studying membrane biophysics and properties important to drug delivery, such as surface potential and encapsulated ion release.

## 3.5 Materials

DPPC, DSPC, and DSPG were purchased from Avanti Polar Lipid. DiD (D-307) was purchased from Molecular Probes (Eugene, OR). Solvents were purchased from VWR Scientific. All other chemicals were purchased from Sigma Aldrich. All buffers were made with MilliQ water and passed through a filtration system. NMR measurements were taken on a Bruker 300 MHz Avance system and analyzed with Topspin software. Chemical shifts are expressed as parts per million with tetramethylsilane as internal standard. HPFC column purifications were performed on a Reveleris Flash System (Grace Division Biosciences) with pre-packed GraceResolv silica cartridges (67 Å, 40.5 μm). All sonication was performed in a G112SP1 Special Ultrasonic Cleaner from Laboratory Supplies Co., Inc (Hicksville, NY).

## 3.6 Methods

### 3.6.1 Synthesis and Characterization

The SBL library was synthesized from a 3-(dimethylamino)-1,2-propanediol core via a two step synthesis without the need for column purification for the saturated chain versions. After the alkylation with 1,3-propanesultone in the presence of DIPEA, the

reaction was washed with 1 M HCl and 1M $Na_2CO_3$ ,and then precipitated from acetone, hexanes, and acetonitrile sequentially, to afford pure SBL products in moderate yields. Five SBLs were made varying only at the alkyl chains (lauric acid = DLSB ($C_{12}$), myristic acid = DMSB ($C_{14}$), palmitic acid = DPSB ($C_{16}$), stearic acid = DSSB ($C_{18}$), and oleic acid = DOSB ($C_{18:1}$)). This straightforward synthesis requires relatively inexpensive materials and a purification that could make it suitable for cost-effective scale-up and result in a less expensive alternative to PCLs for some applications.

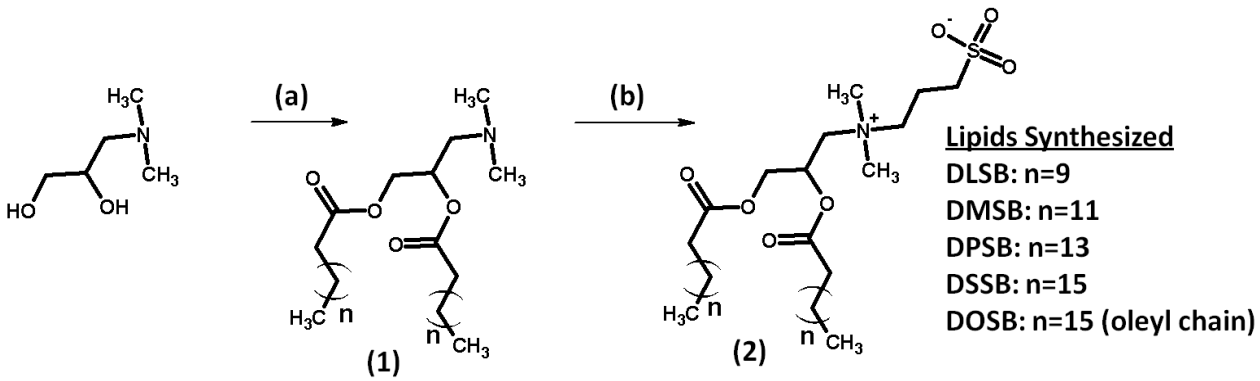


**Figure 3-8: Chemical Synthesis** (a) Cn+3 alkyl acid, DCC, DMAP, CH2Cl2, r.t. 4 hrs. (b) 1,3-Propanesultone, DIPEA, CH2Cl2, MeOH (4:1), 40 °C, 18 hrs.

Synthesis of (1): 1g of N,N-dimethylamino-1,2-propanediol (8.3 mmoles) and 2.2 molar equivalent (18.3 mmoles) of alkyl acid chain (i.e. 4.7 g palmitic acid (MW 256) for DPSB) were dissolved in methylene chloride while stirring at room temperature. Then, 0.1 g 4-dimethylaminopyridine (DMAP) and 2.2 molar equivalent (18.3 mmoles) of *N,N'*-Dicyclohexylcarbodiimide (DCC) (3.78 g) were added and the solution was stirred for 3-4 hours or until complete by TLC. Additional small portions of DCC were added if necessary to drive the reaction to completion. The solution was then filtered to remove the precipitated dicyclohexyuracil and washed 2X with 1M HCl. The organic layer was collected and dried with sodium sulfate and solvent was removed by rotary evaporation.

The di-substituted dimethylaminoglycerol product (1) was moved forward with no further purification.

To all of (1) was added 2 molar equivalents 1,3-propanesultone (2 g, MW 123) with 1.5 mL DIPEA (8.3 mmoles, MW 129) in minimal methylene chloride/methanol (4:1). The reactions were stirred while heating at 40 °C for 18 hours. The solutions were diluted with the reaction solvent mixture and washed with 1M HCl followed by 1 M $Na_2CO_3$. The organic layer was collected and concentrated under rotary evaporation. DLSB, DMSB, DPSB, DSSB were purified through a series of precipitation from methylene chloride in acetone, acetonitrile, and hexanes. Small amounts of product were lost in each precipitation step and overall yields for the entire synthesis were 20%, 66%, 32%, and 38% for the DLSB, DMSB, DPSB, and DSSB respectively. DOSB could not be purified by precipitation and was instead purified by HPFC, and was eluted with 30% methanol in methylene chloride with a yield of 7.6%. Percent yields were calculated according to: Mass collected following purification / expected mass (starting moles of N,N-dimethylamino-1,2-propanediol X Product Molecular Weight). In the DOSB synthesis, a significant amount of side product with a molecular weight corresponding to two additions of the 1,3-propanesultone was observed on MALDI and it is possible that the 1,3-propanesultone was added across the alkene in one of the oleyl chains. DLSB: $^1$H NMR ($CDCl_3$/$CD_3OD$ ~10:3): δ 0.87 (t, 6H); δ 1.26 (m, 32H); δ 1.60 (m, 4H); δ 2.23 (m, 2H); δ 2.32 (m, 4H); δ 2.90 (t, 2H); δ 3.14 (d, 6H); δ 3.66-3.78 (m, 4H); δ 4.05-4.09 (m, 1H); δ 4.43-4.48 (m, 1H); δ 5.60 (m, 1H). MALDI-MS calc'd mass 606.9, found 607.87. Elemental Analysis: 63.4 %C expected, 62.54 % C observed, 10.5 % H expected, 10.72 % H observed, 2.31 % N expected, 2.34 % observed

DMSB:$^{1}$H NMR ($CDCl_3$/$CD_3OD$ ~10:3): δ 0.89 (t, 6H); δ 1.27 (m, 40H); δ 1.62 (m, 4H); δ 2.22 (m, 2H); δ 2.38 (m, 4H); δ 2.87 (t, 2H); δ 3.14 (d, 6H); δ 3.59 (m, 2H); δ 3.71 (m, 2H); δ 4.04-4.08 (m, 1H); δ 4.46-4.47 (m, 1H); δ 5.62 (m, 1H). MALDI-MS calc'd mass 663.02, found 664.62. Elemental Analysis: 65.3%C expected, 64.92 % C observed, 10.8 % H expected, 10.54 % H observed, 2.12 % N expected, 2.13 % observed.

DPSB:$^{1}$H NMR ($CDCl_3$/$CD_3OD$ ~10:3): δ 0.88 (t, 6H); δ 1.26 (m, 48H); δ 1.60 (m, 4H); δ 2.21 (m, 2H); δ 2.33 (m, 4H); δ 2.88 (t, 2H); δ 3.14 (d, 6H); δ 3.60-3.70 (m, 4H); δ 4.02-4.08 (m, 1H); δ 4.43-4.48 (m, 1H); δ 5.60 (m, 1H). MALDI-MS calc'd mass 719.12, found 721.49. Elemental Analysis: 66.9 %C expected, 66.62 % C observed, 11.09 % H expected, 11.31 % H observed, 1.95 % N expected, 1.99 % observed.

DSSB:$^{1}$H NMR ($CDCl_3$/$CD_3OD$ ~10:3): δ 0.83 (t, 6H); δ 1.20 (m, 56H); δ 1.56 (m, 4H); δ 2.15 (m, 2H); δ 2.29 (m, 4H); δ 2.84 (t, 2H); δ 3.07 (d, 6H); δ 3.6 (m, 4H); δ 3.96-4.02 (m, 1H); δ 4.38-4.42 (m, 1H); δ 5.50 (m, 1H). MALDI-MS calc'd mass 775.23, found 776.51. Elemental Analysis: 68.3 %C expected, 68.08 % C observed, 11.3 % H expected, 11.46 % H observed, 1.81 % N expected, 1.84 % observed.

DOSB:$^{1}$H NMR ($CDCl_3$/$CD_3OD$ ~10:3): δ 0.90 (t, 6H); δ 1.30 (m, 40H); δ 1.60 (m, 4H); δ 2.03 (m, 8H); δ 2.33 (m, 6H); δ 2.90 (m, 2H); δ 3.27 (d, 6H); δ 3.6-3.87 (m, 3H); δ 4.00 (m, 1H); δ 4.13 (m, 1H); δ 4.50 (m, 1H); δ 4.36 (m, 4H); δ 5.64 (m, 1H). MALDI-MS calc'd mass 771.20, found 772.88. Elemental Analysis: 68.61 %C expected, 67.4 % C observed, 10.86 % H expected, 10.95 % H observed, 1.82 % N expected, 1.85 % observed.

### 3.6.2 Carboxyfluorescein (CF) release

The CF encapsulation procedure was adapted from Ohno[34]. Lipid formulations were dried down from chloroform solutions in a 10:3 molar ratio ($DiC_{16}$Lipid:cholesterol) in a test tube to form a thin film. The thin film was rehydrated in a 10 mM Tris, 100 mM CF, 500 mM NaCl, pH 7.4 to a final concentration of 25 mM $DiC_{16}$Lipid. Each preparation was sonicated for 10 minutes at 80 °C under argon and then cooled to room temperature. Free carboxyfluorescein was removed by size exclusion chromatography with a PD-10 sephadex column (GE Healthcare) with approximately 10% dilution of the liposome volume. Ten microliters of each liposome solution was added to a well with 200 uL buffer in a 96 well plate. Two isotonic buffers, 10 mM HEPES, 605 mM NaCl, pH 7.4 ("equal salt") and 840 mM HEPES, 150 mM NaCl, pH 7.4 ("low salt"), the first one equal in ionic strength and second with a lower ionic strength were used. Leakage was measured with a FLUOstar plate reader (BMG Labtech) with Ex 485 nm and Em 518 nm over the course of 48 hours. Percent leakage values were calculated by measuring the total CF per well by liposome lysis with $C_{12}E_{10}$ surfactant. All buffer/lipid formulation combinations were run in triplicate. Percent Release was calculated as follows: % Release at time, (t) = (measured fluorescence at time, (t)) / (total fluorescence from lysed liposomes) X 100.

### 3.6.3 Calcium-Induced Zeta-Potential Shift

Liposome preparations used in the CF release study were also used for these measurements. Twenty microliters of each liposome formulation were added to 3 mL of a 10 mM HEPES, pH 7.4 buffer with various amounts of $CaCl_2$ and NaCl added. NaCl was added along with $CaCl_2$ to maintain a constant ionic strength across all $Ca^{2+}$

concentrations. Ionic strengths were calculated according to the Debye-Hückel model, where the ionic strength (I) = ½(4[$Ca^{2+}$] + [$Cl^-$] + [$Na^+$]), where brackets denote the total concentration of the enclosed ion. Zeta potential measurements were performed on a Malvern Nanosizer using the Smoluchowski modelprovided by Malvern's Nanosizer Software and run in triplicate.

### 3.6.4 Liposome vesicle formation at various salt types and concentrations

Liposome preparations were rehydrated from a thin film in a test tube to a final concentration of 26 mM lipid with the specified buffer. Liposome preparations were heated with gentle agitation in an 80 °C heat bath for 2 minutes and then sonicated for 7 minutes at 80 °C under argon. Diameter and zeta potential were measured on a Malvern Nanosizer. Mark-Houwink parameters were used for size measurements and the Smoluchowski model was used for zeta potential measurements as provided by Malvern's Nanosizer software package.

### 3.6.5 Differential scanning calorimetry, $T_m$ measurements

Liposome formulations were prepared as above for size measurements, with 3, 20 second bursts of sonication instead of a 7 minute sonication to disperse the lipid bilayer fragments[17]. Then 200 uL of each preparation were added into each calorimeter chamber with buffer used in the specific liposome preparation as the standard. The measurements were run on a MC-DSC 4100 (Calorimetry Sciences Corp.) from 10 to 80 °C at 1 degree/minute with a heat-cool-heat cycle where the last heating cycle is reported. Data was processed with CpCalc software and transferred to Excel to be graphed.

### 3.6.6 TEM imaging

Preparations of DPSB/Cholesterol (10:3 molar ratio) were prepared in the specified buffer through thin film rehydration to a final DPSB concentration of 20 mM. The preparations were sonicated at 80 °C for 5 minutes. Prior to imaging, the liposome solutions were diluted to half the original concentration with the same buffer. Copper Grids with 400 mesh and Formvar/carbon coatings from Structure Probe, Inc (West Chester, PA) were glow discharged prior to use. Liposome solutions were dropped onto the grid and allowed to adsorb for 1 minute. The liposome solution was then wicked away and the grid surface was washed three times with MilliQ water. Then a 1% solution of uranyl acetate in water was dropped on the grid and allowed to sit for 1 minute. The uranyl acetate solution was then wicked away and the grid was washed once with water and excess water was removed and the grid was allowed to dry. TEM images were collected on a FEI Tecnai 12 transmission electron microscope at the Berkeley Electron Microscopy Lab at UC Berkeley, Berkeley, CA.

### 3.6.7 Thermally-Triggered CF Release

Liposome preparations of $DiC_{16}$Lipid:chol:$PEG_{3000}$DSPE 85:10:5 were dried to a thin film in a test tube and rehydrated in either 150 mM NaCl or 150 mM KBr, both with 100 mM CF and 10 mM Tris, pH 7.4 to a concentration of 20 mM $DiC_{16}$Lipid. The preparations were sonicated at 80 °C for 5 minutes and then cooled to room temperature. Free CF was removed by size exclusion chromatography with a PD-10 sephadex column (GE Healthcare) with mild dilution of the liposome fraction. Two elution buffers were used for each of the initial preparations to investigate the effect of asymmetry of salt form across the bilayer on liposome stability and release. Figure 3-4 provides a schematic of

the liposome formation and purification process. The preparations made in 150 mM KBr were eluted in one of two buffers; one buffer contained 260 mM KBr, 10 mM HEPES, pH 7.4 and the second buffer was 150 mM KBr, 110 mM NaCl, 10 mM HEPES, pH 7.4. The preparations made with 150 mM NaCl were eluted with one of two buffers containing either 260 mM NaCl or 260 mM KBr, both with 10 mM HEPES, pH 7.4. The CF release was then measured for each of the purified liposome samples. Measurements were made on a Flourolog Fluorimeter (Horiba Scientific) using the kinetic measurement function. For each measurement, 10 μL of the liposome sample was added to 2 mL of a 50% fetal bovine serum (FBS), 50% 10 mM HEPES, 150 mM NaCl, pH 7.4 (HBS) solution. Each measurement lasted for 250 seconds and the liposomes were added 15 seconds into the run to insure capture of the initial release. At 200 seconds, 30 μL of $C_{12}E_{10}$ surfactant was added to lyse the liposomes to determine the maximum CF fluorescence. Measurements were done in triplicate and the data was exported to Excel for analysis. Percent Release was calculated as follows: % Release at a time (t) = (measured fluorescence at time (t)) / (total fluorescence from lysed liposomes) X 100.

To measure the release of CF at 37 °C over a longer period of time, release from each preparation made initially in 150 mM KBr was monitored for approximately 4 hours in a 96 well plate. To do this, following the purification of the above liposomes solutions, 10 μL of each liposome solution was added to a well with 200 uL of the 50/50 FBS/HBS buffer in a 96 well plate. The plate was kept in a 37 °C incubator and release was measured with a FLUOstar plate reader (BMG Labtech) with Ex 485 nm and Em 518 nm over the course of 4 hours. Percent release values were calculated by measuring

the total CF per well by liposome lysis with 10 μL of $C_{12}E_{10}$ surfactant. All formulations were run in triplicate.

### 3.7 References


1. A. D. Bangham, M. M. Standish and J. C. Watkins, *Journal of Molecular Biology*, 1965, **13**, 238-IN227.
2. S.-D. Li and L. Huang, *Molecular Pharmaceutics*, 2008, **5**, 496-504.
3. T. S. Levchenko, R. Rammohan, A. N. Lukyanov, K. R. Whiteman and V. P. Torchilin, *International Journal of Pharmaceutics*, 2002, **240**, 95-102.
4. J. Senior, J. C. W. Crawley and G. Gregoriadis, *Biochimica et Biophysica Acta (BBA) - General Subjects*, 1985, **839**, 1-8.
5. R. K. Scheule, J. A. S. George, R. G. Bagley, J. Marshall, J. M. Kaplan, G. Y. Akita, K. X. Wang, E. R. Lee, D. J. Harris, C. Jiang, N. S. Yew, A. E. Smith and S. H. Cheng, *Human Gene Therapy*, 1997, **8**, 689-707.
6. D. V. Devine, K. Wong, K. Serrano, A. Chonn and P. R. Cullis, *Biochimica et Biophysica Acta (BBA) - Biomembranes*, 1994, **1191**, 43-51.
7. T. M. Allen, C. Hansen, F. Martin, C. Redemann and A. Yau-Young, *Biochimica et Biophysica Acta (BBA) - Biomembranes*, 1991, **1066**, 29-36.
8. D. Liu, F. Liu and Y. K. Song, *Biochimica et Biophysica Acta (BBA) - Biomembranes*, 1995, **1235**, 140-146.
9. D. Liu, A. Mori and L. Huang, *Biochimica et Biophysica Acta (BBA) - Biomembranes*, 1992, **1104**, 95-101.
10. R. M. Abra, C. A. Hunt and D. T. Lau, *Journal of Pharmaceutical Sciences*, 1984, **73**, 203-206.
11. R. M. Abra and C. A. Hunt, *Biochimica et Biophysica Acta (BBA) - Lipids and Lipid Metabolism*, 1981, **666**, 493-503.
12. C. A. H. Prata, Y. Li, D. Luo, T. J. McIntosh, P. Barthelemy and M. W. Grinstaff, *Chemical Communications*, 2008, 1566-1568.
13. Y. Obata, S. Tajima and S. Takeoka, *Journal of Controlled Release*, 2010, **142**, 267-276.
14. B. Brazdova, N. Zhang, V. V. Samoshin and X. Guo, *Chemical Communications*, 2008, 4774-4776.
15. M. Ma, S. Chatterjee, M. Zhang and D. Bong, *Chemical Communications*, 2011, **47**, 2853-2855.
16. H. H. Mantsch, D. G. Cameron, P. A. Tremblay and M. Kates, *Biochimica et Biophysica Acta (BBA) - Biomembranes*, 1982, **689**, 63-72.
17. Z. Huang and F. C. Szoka, *Journal of the American Chemical Society*, 2008, **130**, 15702-15712.
18. P. Di Profio, L. Brinchi, R. Germani, G. Savelli, G. Cerichelli and C. A. Bunton, *Journal of the Chemical Society, Perkin Transactions 2*, 2000, 2162-2167.
19. K. K. Ghosh, A. Pandey and S. Roy, *Colloids and Surfaces A: Physicochemical and Engineering Aspects*, 2000, **163**, 293-300.
20. M. del Mar Graciani, A. Rodríguez, M. Muñoz and M. L. Moyá, *Langmuir*, 2005, **21**, 7161-7169.

21. M. d. S. Baptista, I. Cuccovia, H. Chaimovich, M. J. Politi and W. F. Reed, *The Journal of Physical Chemistry*, 1992, **96**, 6442-6449.
22. L. Marte, R. C. Beber, M. A. Farrukh, G. A. Micke, A. C. O. Costa, N. D. Gillitt, C. A. Bunton, P. Di Profio, G. Savelli and F. Nome, *The Journal of Physical Chemistry B*, 2007, **111**, 9762-9769.
23. W. Kunz, J. Henle and B. W. Ninham, *Current Opinion in Colloid & Interface Science*, 2004, **9**, 19-37.
24. C. Huang, Z.-q. Wang, H.-n. Lin, E. E. Brumbaugh and S. Li, *Biochimica et Biophysica Acta (BBA) - Biomembranes*, 1994, **1189**, 7-12.
25. I. V. Khavrutskii, A. A. Gorfe, B. Lu and J. A. McCammon, *Journal of the American Chemical Society*, 2009, **131**, 1706-1716.
26. J. Weinstein, S. Yoshikami, P. Henkart, R. Blumenthal and W. Hagins, *Science*, 1977, **195**, 489-492.
27. D. Needham, G. Anyarambhatla, G. Kong and M. W. Dewhirst, *Cancer Research*, 2000, **60**, 1197-1201.
28. M. Yatvin, J. Weinstein, W. Dennis and R. Blumenthal, *Science*, 1978, **202**, 1290-1293.
29. D. Papahadjopoulos, S. Nir and N. Düzgünes, *Journal of Bioenergetics and Biomembranes*, 1990, **22**, 157-179.
30. P. Wan, Y. Zhao, H. Tong, Z. Yang, Z. Zhu, X. Shen and J. Hu, *Materials Science and Engineering: C*, 2009, **29**, 222-227.
31. J. M. Boggs, *Canadian Journal of Biochemistry*, 1980, **58**, 755-770.
32. K. Jacobson and D. Papahadjopoulos, *Biochemistry*, 1975, **14**, 152-161.
33. H. Eibl and A. Blume, *Biochimica et Biophysica Acta (BBA) - Biomembranes*, 1979, **553**, 476-488.
34. H. Ohno, K. Ukaji and E. Tsuchida, *Journal of Colloid and Interface Science*, 1987, **120**, 486-494.
35. Y. Rui, S. Wang, P. S. Low and D. H. Thompson, *Journal of the American Chemical Society*, 1998, **120**, 11213-11218.
36. S. Ali and R. Bittman, *Chemistry and Physics of Lipids*, 1989, **50**, 11-21.
37. A. Arora and C. M. Gupta, *Biochimica et Biophysica Acta (BBA) - Biomembranes*, 1997, **1324**, 61-68.
38. R. Anderson, M. Kates and B. E. Volcani, *Biochimica et Biophysica Acta (BBA) - Lipids and Lipid Metabolism*, 1978, **528**, 89-106.
39. I. Lindh and J. Stawinski, *The Journal of Organic Chemistry*, 1989, **54**, 1338-1342.
40. J.-P. Rolland, C. Santaella and P. Vierling, *Chemistry and Physics of Lipids*, 1996, **79**, 71-77.
41. N. S. Chandrakumar and J. Hajdu, *The Journal of Organic Chemistry*, 1982, **47**, 2144-2147.
42. T. Makiyama, N. Nagasaka, Y. Houjyo, E. Yamaura, H. Nakamura, Y. Koide, A. Nishida and T. Murayama, *Biochemical Pharmacology*, 2010, **80**, 1396-1406.
43. R. Z. Lu, J. G. Turcotte, W. H. Lin, J. M. Steim and R. H. Notter, *Journal of Colloid and Interface Science*, 1992, **154**, 24-34.
44. S. Liu and D. F. O'Brien, *Journal of the American Chemical Society*, 2002, **124**, 6037-6042.

45. D. N. Brindley and C. Pilquil, *Journal of Lipid Research*, 2009, **50**, S225-S230.
46. S. Deborah W, *Biochemical and Biophysical Research Communications*, 1987, **145**, 228-233.
47. N. N. Desai, H. Zhang, A. Olivera, M. E. Mattie and S. Spiegel, *Journal of Biological Chemistry*, 1992, **267**, 23122-23128.
48. M. Maceyka, S. G. Payne, S. Milstien and S. Spiegel, *Biochimica et Biophysica Acta (BBA) - Molecular and Cell Biology of Lipids*, 2002, **1585**, 193-201.
49. K. Takabe, S. W. Paugh, S. Milstien and S. Spiegel, *Pharmacological Reviews*, 2008, **60**, 181-195.
50. C. Chalfant and M. D. Poeta, *Sphingolipids as signaling and regulatory molecules*, Springer Science+Business Media, 2010.
51. S. R. Coats, A. B. Berezow, T. T. To, S. Jain, B. W. Bainbridge, K. P. Banani and R. P. Darveau, *Infect. Immun.*, 2011, **79**, 203-210.
52. G. De Becker, V. Moulin, B. Pajak, C. Bruck, M. Francotte, C. Thiriart, J. Urbain and M. Moser, *International Immunology*, 2000, **12**, 807-815.
53. A. G. Johnson, M. Tomai, L. Solem, L. Beck and E. Ribi, *Reviews of Infectious Diseases*, 1987, **9**, S512-S516.
54. U. Köhler, H. H. Mantsch and H. L. Casal, *Canadian Journal of Chemistry*, 1988, **66**, 983-988.
55. H. Hauser, *Proceedings of the National Academy of Sciences*, 1989, **86**, 5351-5355.
56. J. Wilschut, N. Duzgunes, R. Fraley and D. Papahadjopoulos, *Biochemistry*, 1980, **19**, 6011-6021.
57. R. Leventis, J. Gagne, N. Fuller, R. Rand and J. Silvius, *Biochemistry*, 1986, **25**, 6978-6987.
58. A. Chauhan, V. P. S. Chauhan and H. Brockerhoff, *Biochemistry*, 1986, **25**, 1569-1573.
59. A. Portis, C. Newton, W. Pangborn and D. Papahadjopoulos, *Biochemistry*, 1979, **18**, 780-790.
60. J. Lansman and D. H. Haynes, *Biochimica et Biophysica Acta (BBA) - Biomembranes*, 1975, **394**, 335-347.
61. H. Hauser, D. Oldani and M. C. Phillips, *Biochemistry*, 1973, **12**, 4507-4517.

Chapter 4

# Hemifluorinated Asymmetric Bolaamphiphiles Design for the Formation of Small-Diameter Vesicles

## 4.1 Abstract

In this chapter, I describe the design of four classes of hemifluorinated bolaamphiphiles devised to form vesicles with small diameters. A number of synthetic routes were attempted resulting in two classes of hemifluorinated bolaamphiphiles that were tested for their ability to form vesicles. The theory behind the general hemifluorinated bolaamphiphile structure as well as the benefits and downsides to each synthesis are discussed. The hemifluorinated bolaamphiphiles may provide insight into lipid architectures that promote the formation of stable, small-diameter vesicles.

## 4.2 Introduction

The size of a nanoparticle can significantly impact its efficacy as a drug delivery system. In general, small vesicles (50-100 nm) circulate longer than large vesicles (>200 nm)[1], in part because serum protein opsonization and clearance by the reticuloendothelial system occurs more rapidly for large vesicles[2]. Vesicles generally accumulate in the liver and spleen with small vesicles favoring the former and larger vesicles the latter[3]. Very large vesicles or vesicle-aggregates can accumulate in the lungs[4] which have a high density of narrow capillaries. Although small vesicles show some favorable pharmacokinetics, they are more difficult to form and tend to be less stable than their larger counterparts when injected in vivo[5]. Most lipid vesicles are formed from bilayers of phospholipids, like PC lipids. These bilayers contain two monolayers with opposing curvatures and for a single-component system; at least one monolayer will be in a heightened energy state. As the diameter of a single-component vesicle decreases, the

strain on the bilayer increases and the vesicles become less stable to interactions with other vesicles and environmental components. The work in this chapter focuses on the development of a lipid-like molecule designed to form highly curved aggregation states and can easily form small-diameter vesicles. This group of lipid-like molecules is collectively referred to as Asymmetric Bolaamphiphiles (ABAs). A bolaamphiphile structure was chosen over a traditional diacyl lipid due to the ability of bolaamphiphiles to form monolayer vesicles, which could alleviate the problem inherent to bilayers, where at least one monolayer is always in an elevated curvature energy state.

### 4.3 Bolaamphiphile Background

The assembly of bolaamphiphiles began in the 1980s, following their discovery in the walls of archaebacteria where they are believed to stabilize bilayers by traversing from one leaflet to another with a continuous hydrocarbon chain[6]. The incorporation of bolaamphiphiles into the archaebacteria bilayers aids in their survival in high salt conditions and at extreme temperatures[7]. Bolaamphiphiles always contain two hydrophilic groups connected by a hydrophobic segment, but they come in a variety of forms. The most commonly used hydrophilic groups are phosphocholine[8, 9], choline[10], sugars[11, 12], and carboxylic acids[13, 14]. The two headgroups can be the same or different and they can be connected by a single hydrocarbon chain (Fig. 4-1 top), two hydrocarbon chains (Fig. 4-1 middle), or one hydrocarbon chain accompanied by two unconnected hydrocarbon chains (Fig. 4-1 bottom).

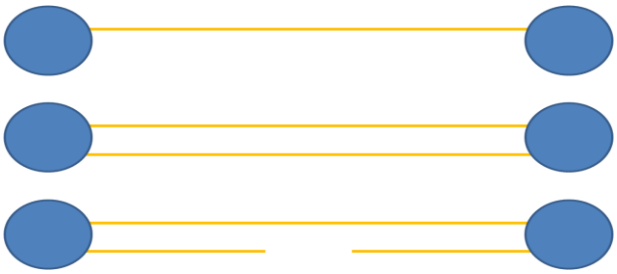

**Figure 4-1: Generic bolaamphiphile structures**. Blue circles representing headgroups and yellow lines representing hydrocarbon chains.

Bolaamphiphiles can form vesicles, micelles, fibers, or tubes when dispersed in water[15, 16]. In the vesicular phase, bolaamphiphiles can either adopt a linear form and extend across the entire hydrophobic region or they can bend into a "U-shape" so that both hydrophilic groups are located on the same leaflet[17, 18] (See Fig. 4-3).

### 4.4 ABA Design Theory

The design of the ABAs is based on the theory that small vesicle formation can be driven by a two-component, asymmetric bilayer, where the lipids on the vesicle interior prefer a negative radius of curvature and the lipids on the vesicle exterior prefer a positive radius of curvature, leaving both lipids in their preferred curvature state. The likelihood of a two-component system assembling into a perfectly asymmetric bilayer is incredibly low due to the associated entropic losses. The ABA design overcomes this hurdle by essentially combining the two different lipids in the asymmetric bilayer into a single bolaamphiphile (Fig. 4-2).

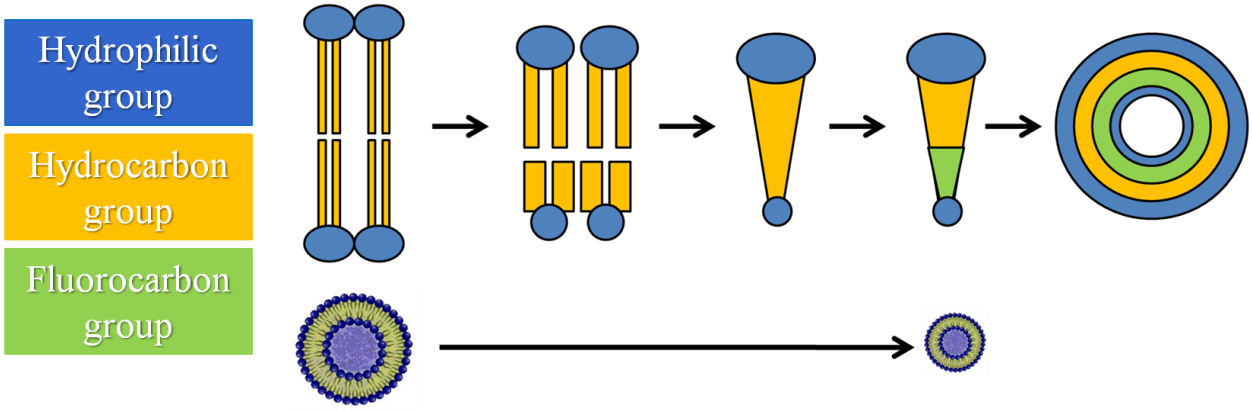


**Figure 4-2: Schematic diagram depicting the theory of ABA small vesicle formation**

Each ABA exhibits an overall "wedge-like" structure with a tapered hydrophobic segment terminated by two hydrophilic moieties that differ in size and have different curvature preferences—one preferring a negative curvature ("small" headgroup end) and one a positive curvature ("large" headgroup end). Therefore, a naturally curved structure can result by the formation of a monolayer in which both hydrophilic ends are in their preferred curvature state ("large" headgroups on the exterior of the vesicle and "small" headgroups on the interior of the vesicle). In each group of ABAs, the tapered hydrophobic segment contains two chains. The first chain is a shorter, fully hydrocarbon chain that can be either a saturated straight chain or contain sterol or other branched structures. The second chain is a linear hemifluorinated chain that terminates with the "small" headgroup.

Unfortunately, bolaamphiphiles are able to adopt several configurations with a vesicle wall and the ABAs can adopt three primary configurations (Fig. 4-3): (1) an asymmetric monolayer, (2) a symmetric monolayer, or (3) a bilayer.

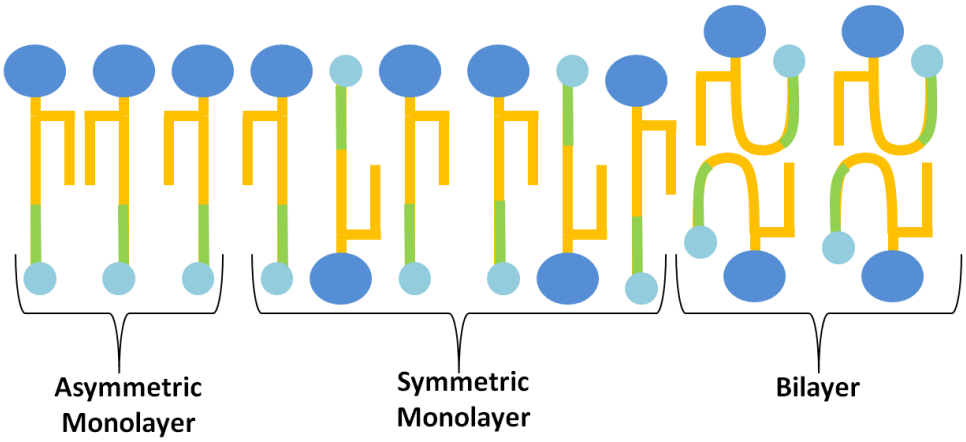


**Figure 4-3: Schematic of the general orientations possible for the ABAs in the vesicle wall**.

According to the proposed theory, the "Asymmetric Monolayer" configuration would best promote the formation of highly-curved monolayers. To increase the likelihood of this preferred orientation, fluorocarbon segments, which phase separate from hydrocarbons for chain lengths of approximately six carbons or more, have been incorporated into the hydrophobic region adjacent to the "small" hydrophilic group[19]. In the "Asymmetric Monolayer" configuration, the fluorocarbon and hydrocarbon self-interactions are maximized.

### 4.5 Synthetic Route

A few different ABA syntheses were attempted throughout the course of this research. The different ABA structures are outlined in Figure 4-4.

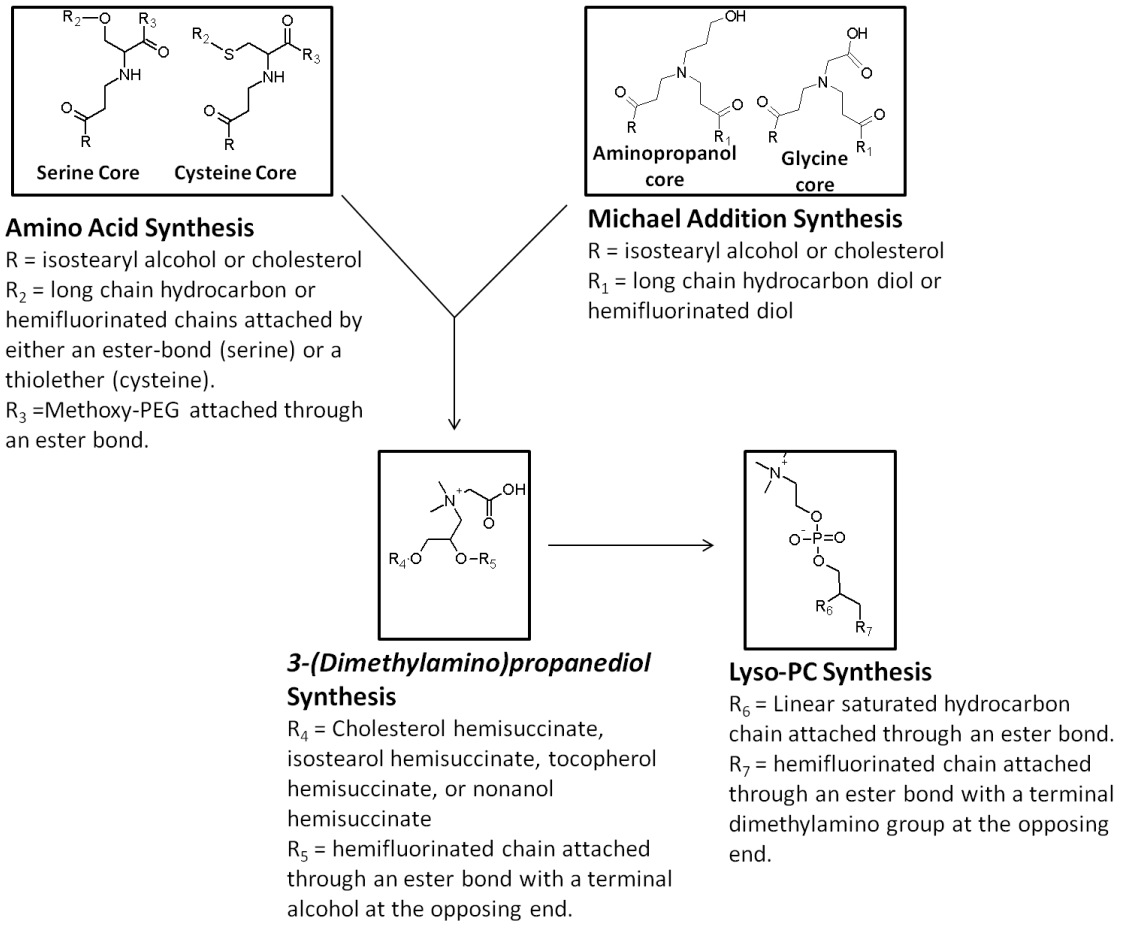


**Figure 4-4: Different synthetic strategies used throughout the ABA project.**

In each of the approaches, the "large" hydrophilic group was added adjacent to the bolaamphiphile core and the "small" hydrophilic group was at the opposite end of the hemifluorinated chain. Each synthesis had its own set of problems, but one unexpected difficulty that affected them all was the unreactive nature of the functional groups on the highly electronegative fluorocarbon chains. This problem was amplified by the limited number of commercially available bifunctional fluorocarbon chains greater than $C_6$ in length. Fluorocarbons with a methylene ($-CH_2-$) spacer between the functional group and the fluorocarbon segment were found to be more reactive than functional groups directly adjacent to the fluorinated chain. Both 1,8-dibromoperfuorooctane and 1,6-divinylperfluorohexane were not reactive to a variety of nucleophilic substitution

conditions and thiol-ene couplings, respectively. Because of this, all the hemifluorinated chains in the ABAs are based off of a 1H, 1H, 10H, 10H-perfluorodecanediol or a 1H, 1H, 12H, 12H-perfluorododecanediol. The Michael Addition, Amino Acid, and 3-(Dimethylamino)propanediol syntheses all use a hemifluorinated chain in which the hydrocarbon and fluorocarbon segments are connected through an ester bond. The presence of an ester group in the hydrophobic region has the potential to disrupt the packing of and bring water into the bilayer or monolayer. Ether linkages would be less disruptive than esters; however, the formation of an ether-linked hemifluorinated chain from 10-bromodecanoic acid and a fluorocarbon diol proved to be difficult, possibly due to the low nucleophilicity of the fluorocarbon hydroxyl. During the synthesis of the PC-ABAs, I discovered that I could functionalize the 1H, 1H, 12H, 12H-perfluorododecanediol with allyl iodide, which could then be used in thiol-ene couplings (See Fig. 4-8). Moving the double bond away from the electronegative fluorocarbon segment restored the ability to perform thiol-ene reactions. Complete removal of the hydrophilic linkages from the hemifluorinated chain would most likely increase the stability of the monolayer or bilayer and reduce the vesicle permeability. Unfortunately, such a hemifluorinated chain could not be easily synthesized during this project.

In the Michael Addition approach, the two hydrophobic chains (in acrylate form) were added to the primary amine of either an aminopropanol or a glycine via a Michael addition. In this strategy, the "large" headgroups were intended to be either a phosphocholine (aminopropanol core) or a PEG chain (glycine core). These syntheses were not successful for a couple of reasons. The first problem arose with the Michael additions. These reactions were run at high temperatures (80 °C) for at least 12 hours and

resulted in many side products, especially during the addition of the hemifluorinated segment. The fluorinated segment was frequently cleaved during the reaction and when heated in the presence of the primary amine, the amine could displace the fluorocarbon segment to form an amide bond with the hydrocarbon segment.

Further problems arose for the aminopropanol core with respect to the order of additions to the core. The presence of both a primary amine and an alcohol requires that either one of the groups is protected or that a reaction selective for one or the other is completed first. Additionally, the PC headgroup has to be added to the core before the hemiflourinated chain, which contains a potentially reactive primary alcohol. Therefore, the fully hydrocarbon chain must be added to the amine first, followed by the addition of the PC headgroup and finally, the hemifluorinated chain. The phosphorylation step did not proceed as desired in the presence of the secondary amine and multiple products were always formed. This synthetic route was not explored further and the focus was shifted to cores with more orthogonal functional groups.

In the glycine core synthesis, both chains were added first through Michael additions and then a methoxy-PEG-OH chain was easily added to the carboxylic acid in the final step using an excess of PEG. When the starting material prior to the PEGylation was not completely pure, it was difficult to separate any PEGylated side-products. Also, the polydispersity of the PEG chains raised concerns regarding the ability to make conclusions on the ABA assembly process since a range of headgroup sizes would be present.

The Amino Acid approach also suffered from a limitation on the order of addition of the lipid components to the core. Expensive functionalized PEGs were avoided in

these syntheses and all PEG chains were added by chemistry on the terminal alcohol of PEG. With the Amino Acid synthesis, the primary amines were functionalized last and were FMOC-protected during the addition of the PEG and hemifluorinated chains. In these syntheses, the functional groups on the core and the components to be added required that PEG be attached first followed by the hemifluorinated chain and finally, the fully hydrocarbon acrylate chain. The purification of the products once the PEG was added was nearly impossible as the chromatographic and solubility properties of the desired product, side-products and the unreacted starting material were all dominated by PEG.

The difficulties in the three strategies above could have been worked through and for each core, it is likely that a successful scheme would have been found. However, the three above syntheses and the 3-(dimethylamino)propanediol synthesis were all done somewhat in unison and when the latter began to show more promise, the other three were dropped.

### 4.6 Betaine-Like Bolaamphiphiles

The lessons learned from troubleshooting the first three strategies were incorporated into the development of the 3-(dimethylamino)propanediol synthesis (Fig. 4-5). This group of bolaamphiphiles contains betaine-like headgroups and they are referred to as Betaine-like Asymmetric Bolaamphiphiles (BLBAs).

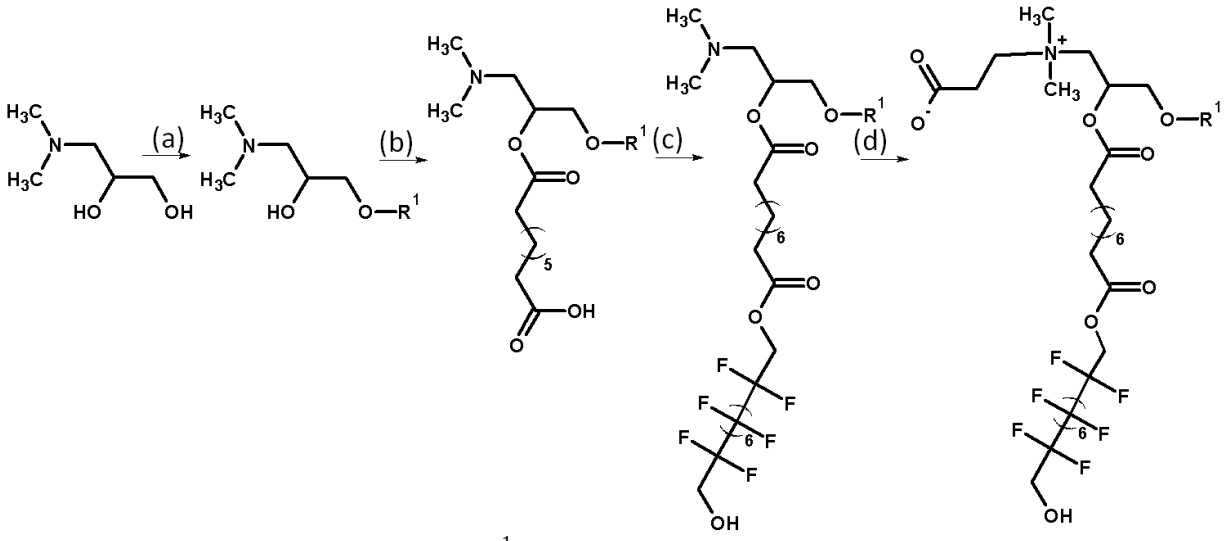


**Figure 4-5: Synthesis of BLBAs** a) $R^1OH$, DCC, DMAP, DCM. b) Sebacic Acid, DCC, DMAP, THF. c) 1,10-decanediol, DCC, DMAP, DCM. d) Acrylic acid, DCM/THF, 40 °C.

The BLBAs do not have a polydisperse PEG headgroup and therefore have a defined chemical structure. Steps (a) through (c) of the synthesis are straightforward and do not require high temperatures or the use of protecting groups. The final step of the synthesis (d), was the most problematic and resulted in the largest decrease in the overall yield. A reasonable amount of product could be formed after reaction times of a week for step (d).

A variety of hydrophobic groups (straight $C_9$ hydrocarbon chain ($C_9$), cholesterol (Chol), isostearol (Iso), and tocopherol (Toc)) were attached to the 1-position of the 3-(dimethylamino)propanediol core to investigate the effect the different structures had on the BLBA aggregation properties (Fig. 4-6). Either a hemiflourinated or a fully hydrocarbon chain was added to the 2-position to examine the impact of the fluorocarbon segment.

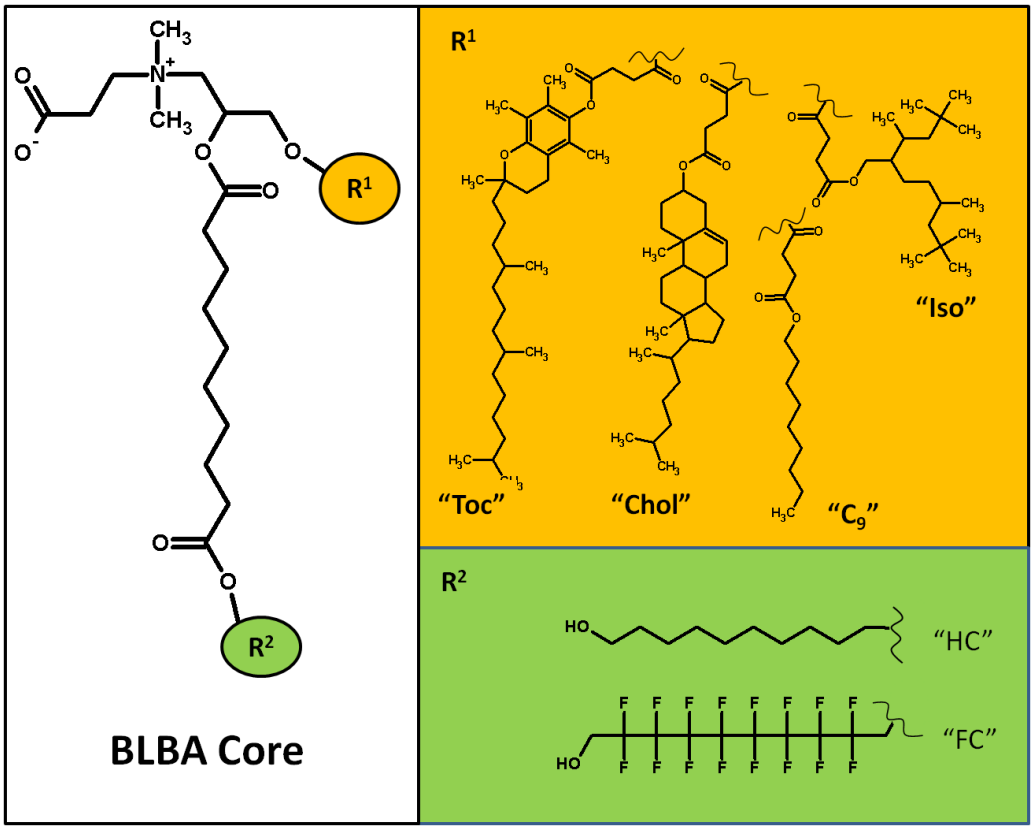


**Figure 4-6: BLBA Structures**

### 4.6.1 BLBA Aggregates

We first examined the ability of the BLBAs to form vesicles upon brief sonication at 57 °C at either pH 3 or 9. The two pHs were selected to determine if the two zwitterionic forms of the betaine headgroup resulted in different assembly properties. At pH 3, the carboxylic acid on the headgroup should be protonated giving the lipid an overall positive charge. At pH 9, the carboxylic acid should be deprotonated resulting in a zwitter-nuetral headgroup.

**Table 4-1 BLBA vesicle diameter at pH 3 and 9**

| BLBA | Diameter (nm) | PDI | pH |
|---|---|---|---|
| Chol-FC | 235 | 0.7 | 3 |
| Chol-FC | 315 | 0.4 | 9 |
| Chol-HC | 102 | 0.1 | 3 |
| Chol-HC | 93 | 0.5 | 9 |
| Toc-HC | 145 | 0.5 | 3 |
| Toc-HC | 269 | 1.0 | 9 |
| Toc-FC | 263 | 0.3 | 3 |
| Toc-FC | 476 | 0.4 | 9 |
| Iso-FC | 235 | 0.6 | 3 |
| Iso-FC | 2048 | 1.0 | 9 |
| $C_9$-FC | 254 | 0.3 | 9 |

BLBA films were rehydrated in 10 mM Tris buffer, pH 9 or a 10mM Glycine buffer, pH 3. Each preparation was sonicated for 10 minutes at 57 °C and then sized by dynamic light scattering. Total lipid concentrations were 5 mM.

Given the results in Table 4-1, it is unclear if the BLBAs form vesicles due to the large diameters and high polydispersities. No trends were observed with respect to pH or between the fluorocarbon and. hydrocarbon chains.

In an effort to promote vesicle formation, mixtures of the BLBAs with diacyl phospholipids were made in a 1:1 molar ratio.

**Table 4-2 Vesicle diameters of mixed BLBA systems**

| Mixture (all 1:1 molar) | Diameter (nm) | PDI | pH |
|---|---|---|---|
| Chol-HC & DLPC | 68 | 0.8 | 9 |
| Chol-HC & DOPC | 97 | 0.2 | 9 |
| Chol-HC & DLPE | 70 | 0.5 | 9 |
| Chol-HC & DOPE | 597 | 1.0 | 9 |
| Chol-HC& DMPC | 65 | 0.6 | 9 |
| $C_9$-FC & DMPC | 47 | 0.2 | 9 |
| Toc-HC & DMPC | 61 | 0.6 | 9 |
| Iso-FC & DMPC | 97 | 0.4 | 9 |
| $C_9$-FC & Chol-FC | 329 | 0.5 | 9 |

BLBA/lipid films were rehydrated in 10 mM Tris buffer, pH 9. Each preparation was sonicated for 10 minutes at 57°C and then measured. Total lipid concentrations were 10 mM. DLPC = 1,2-dilauroyl-*sn*-glycero-3-phosphocholine, DOPC = 1,2-dioleoyl-*sn*-glycero-3-phosphocholine, DMPC = 1,2-myristoyl-*sn*-glycero-3-phosphocholine, DOPE = 1,2-dioleoyl-*sn*-glycero-3-phosphatidylethanolamine, DLPE = 1,2-dilauroyl-*sn*-glycero-3-phosphatidylethanolamine.

The addition of phospholipids to the BLBAs decreased the average diameter of the aggregate but did not decrease the polydispersity significantly. Again, no trend in diameter was observed for either the phospholipid headgroup or chain length. $C_9$-FC with DMPC produced the smallest diameter aggregates at 47 nm and had a relatively low polydispersity (0.2). Without any additional data, it is difficult to determine if the aggregates formed were vesicles or how the BLBAs and phospholipids assembled within them.

To determine if the aggregates were stable over time; their diameters were monitored over a period of 5 days (Fig. 4-7a). When formulated with DMPC, the $C_9$-FC and Chol-FC BLBAs form aggregates with stable and relatively small (~50 nm) diameters. Toc-FC aggregates had initial diameters more than twice as large as $C_9$-FC and Chol-FC and were stable for only a few days.

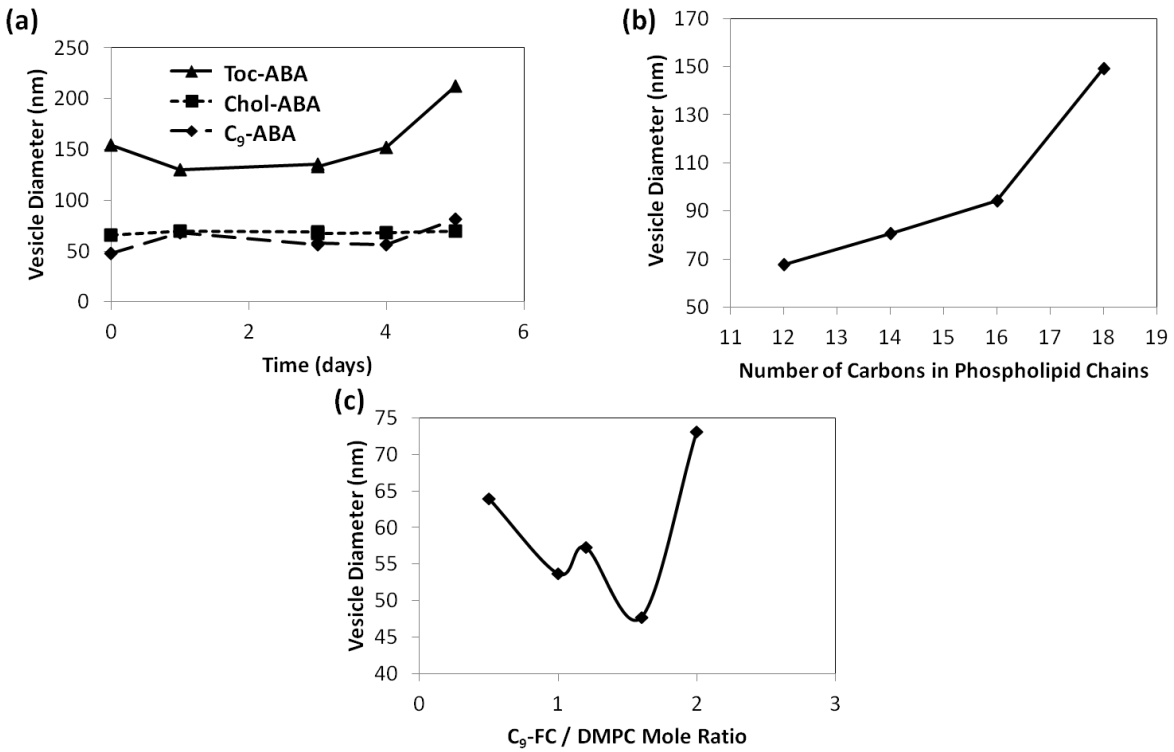


**Figure 4-7: Effect of PC-lipids on BLBA vesicles a)** Aggregate Diameter Stability. BLBAs were combined in a 1:1 ratio with DMPC, rehydrated in a Tris pH 9 buffer and sonicated for 10 min at 57 °C and the diameters were measured daily. **b)** Effect of PC-lipid Chain on Aggregate Diameter. 1:1 mixtures of $C_9$-ABA and a PC-lipid were made as above. **c)** Optimal $C_9$-FC/DMPC Ratio. Aggregates with different ratios of DMPC and $C_9$-ABA were prepared as before. The smallest diameter aggregates were formed at a 1.6:1 ratio of $C_9$-FC/DMPC.

To see how the aggregates were affected by incorporation of a phospholipid, BLBA aggregates were measured in the presence of: (1) phospholipids with different chain lengths and (2) different molar ratios of a single phospholipid. Figure 4-7b suggests that PC-lipids with shorter hydrocarbon chains produce BLBA aggregates with smaller diameters. This may be due to the ability of short chain PC-lipids to pack better with the short chain at the 1-position of the $C_9$-FC. It could also occur due to the ability of shorter chains to naturally form more highly curved structures independent of the presence of the BLBAs.

Table 4-2 shows the ability of the $C_9$-FC to form small aggregates when mixed with DMPC in a 1:1 molar ratio, so we then investigated if a smaller diameter could be found by changing the BLBA/DMPC molar ratio. Figure 4-7c suggests an optimal molar ratio of $C_9$-FC to DMPC of 1.6 for small-diameter aggregates. It is difficult to hypothesize the reason a molar ratio of 1.6 produces the smallest aggregates, because it is unclear how the PC-lipids and the BLBAs interact.

In order to gain insight into the aggregate structure formed by the BLBA/DMPC mixtures, we tested their ability to encapsulate a water-soluble anionic dye, carboxyfluorescein (CF). Typically, liposomes are loaded with CF by hydrating the lipid film in the presence of a high concentration (~100 mM) CF. The unencapsulated CF is then removed by size exclusion chromatography[20]. We were unable to isolate vesicles with enough CF encapsulated to perform a leakage study. Additionally, the collected vesicles rapidly released the remaining CF shortly after elution form the column. There are several potential causes for these observations. It is possible that DMPC vesicles with encapsulated CF form, but are destabilized by the presence of the BLBAs in solution. Alternatively, leaky DMPC/BLBA mixed vesicles with encapsulated CF may form, but quickly release their contents due to poor packing of the two components. It is also possible that a mixture of aggregate structures, such as tubes, vesicles, or micelles are forming, some of which can encapsulate CF, but are not stable due to the interactions with the other components.

## 4.7 The Design of the PC-ABAs

Due to the inability of pure BLBA solutions to form small or uniformly sized vesicles, or aggregates, along with their failure to encapsulate and retain CF, work on the BLBAs was ended. The PC-ABA synthesis was developed to improve upon the BLBA molecules. The PC-ABAs have a standard PC headgroup and are synthesized from a lyso-PC starting material. This greatly reduces the complexity of the synthesis as the formation of the betaine headgroup in the BLBAs was the most time-consuming and lowest-yield step of the synthesis. Since $C_9$-FC formed the smallest particles, the PC-ABAs were designed with only linear hydrocarbon chains of differing lengths and no ring or branched chains were tested. Lastly, the ester group in the BLBA hemifluorinated chain is eliminated in the PC-ABAs, to allow for improved packing of the hydrophobic chains and an increased ability to form pure PC-ABA vesicles.

## 4.8 PC-ABAs

The PC-ABAs were synthesized according to the scheme in Figure 4-8a. Four different lyso-PCs were used to generate four PC-ABAs with different length hydrocarbon segments.

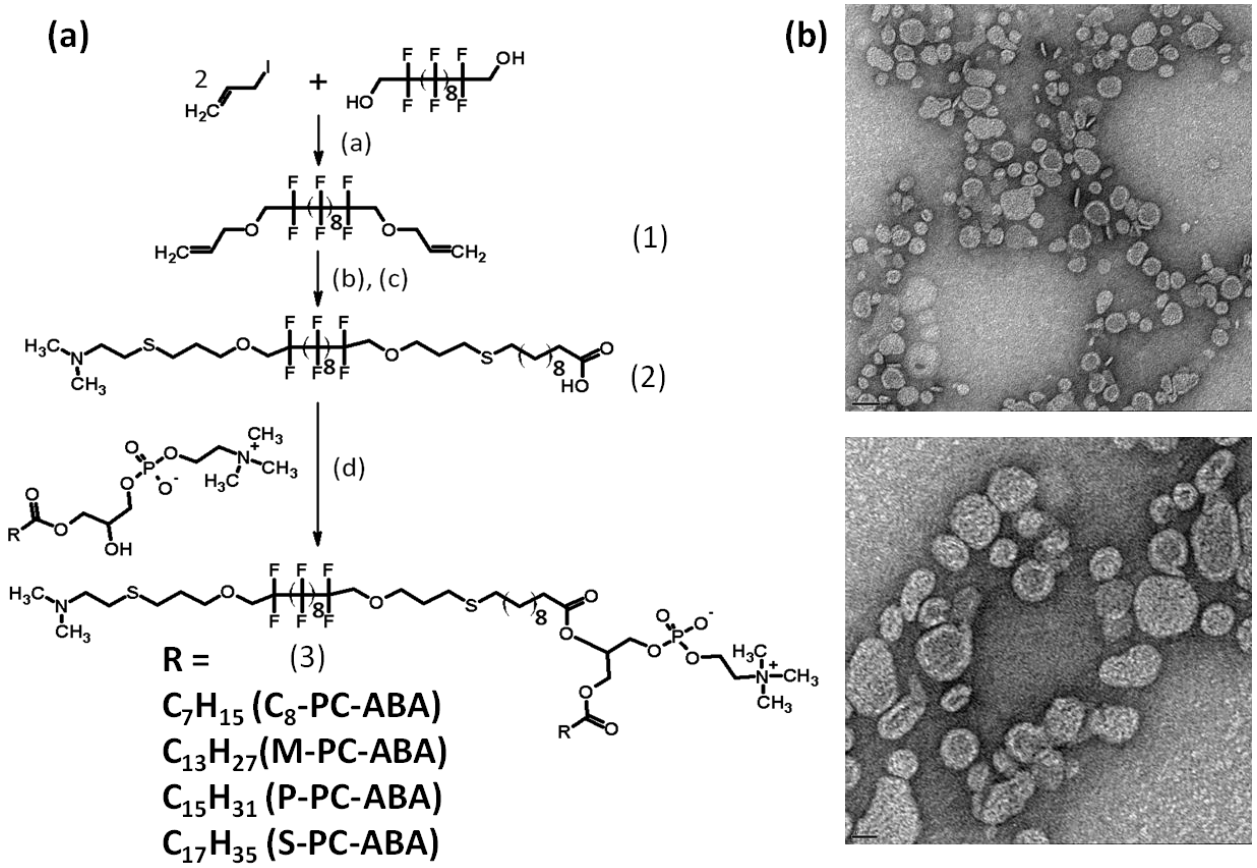


**Figure 4-8: PC-ABA synthesis and liposome TEM (a)** A) KOH, THF B) 2-(Dimethylamino)ethanethiol hydrochloride, 2,2-Dimethoxy-2-phenylacetophenone, $CH_2Cl_2$, MeOH, UV C) 11-mercaptoundecanoic acid, 2,2-Dimethoxy-2-phenylacetophenone, $CH_2Cl_2$, MeOH, UV D) DDC, DMAP, $CH_2Cl_2$, R= $C_7$, $C_{13}$, $C_{15}$, or $C_{17}$. **(b)** TEM images of S-PC-ABA vesicles scale bars 50 nm (top) and 20 nm (bottom).

**Table 4-3: PC-ABA aggregate diameters and zeta-potentials for the PC-ABAs at three pHs**

| Compound | pH | Diameter (nm) | Zeta-Potential (mV) |
|---|---|---|---|
| S-FC | 3 | 51.1 ±0.5 | 28.9 ±0.90 |
| S-FC | 7.4 | 83.7 ±0.8 | 17.0 ±1.75 |
| S-FC | 9 | 60.1 ±1.2 | 4.4 ±1.2 |
| P-FC | 3 | 65.9 ±0.4 | 33.7 ±3.6 |
| P-FC | 7.4 | 68.1 ±3.6 | 16.5 ±1.1 |
| P-FC | 9 | 55.1 ±0.3 | -1.26 ±1.1 |
| M-FC | 3 | 136.7 ±1.2 | 30.5 ±1.6 |
| M-FC | 7.4 | 64.96 ±0.4 | 12.0 ±2.1 |
| M-FC | 9 | 70.7 ±2.5 | 2.2 ±0.8 |
| C8-FC | 3 | 54.5 ±0.1 | 22.9 ±0.7 |
| C8-FC | 7.4 | 62.17 ±2.0 | 16.7 ±3.6 |
| C8-FC | 9 | 1065.3 ±57.1 | 4.3 ±0.5 |

Preparations were made from thin film hydration followed by 5 minutes of sonication at 60 °C. All preparations were made at a concentration of 5 mM total PC-ABA. The buffers used were 1). 10 mM glycine, 150 mM NaCl, pH 3, 2). 10 mM HEPES, 150 mM NaCl, pH 7.4, 3). 10 mM glycine, 150 mM NaCl, pH 9.

### 4.8.1 PC-ABA Vesicle Formation

The diameter and zeta potential of the PC-ABAs were measured following rehydration from a thin film and sonication for 5 minutes at 60 °C. All but two of the PC-ABA/pH combinations formed relatively small aggregates with low polydispersites. Transition electron microscopy (TEM) images of the S-PC-ABA preparation at pH 7.4 corroborate the diameters reported by DLS and reveal a vesicular phase. M-PC-ABA at pH 3 formed vesicles with an average diameter of 136.7 nm and $C_8$-PC-ABA at pH 9 formed a polydisperse phase with a reported diameter of 1065.3 nm. It is unlikely that the $C_8$-PC-ABA at pH 9 formed vesicles, because the preparation was clear and spherical particles of this size result in a cloudy, opaque solution. It is possible that $C_8$-PC-ABA formed tubes or fibers with a narrow diameter as either of these phases could explain the

clarity of the preparation and the large, polydisperse diameter. Overall, we found no correlation between the vesicle diameter and the pH of the solution. However, all the preparations had a neutral zeta potential at pH 9, which then became increasingly positive as the pH decreased. The change in zeta potential most likely resulted from increased protonation of the dimethylamine group. Interestingly, it does not appear as though the adoption of a positive charge on the dimethylamino group resulted in a significant change in diameters of the vesicles produced.

### 4.8.2 PC-ABA Configuration

The results in Table 4-3 and the TEM images in Figure 4-8b suggest the formation of small-diameter vesicles. However, the configuration of the PC-ABAs within the vesicle wall could not be determined from this information alone. The trend in zeta potential indicates the presence of the dimethylamine group on the vesicle exterior where its protonation state has a significant effect on the surface potential of the vesicle. The pH-dependent zeta potential only suggests qualitatively that the dimethylamine groups are on the vesicle exterior, but it does not assign a quantitative value to the percentage. To gain more clarity on the orientation of the PC-ABAs, the distribution of the PC groups between the interior and exterior surfaces of the vesicle was determined using $^{31}$P NMR. We measured the $^{31}$P signal in the phosphocholine group in the absence and presence of the line-broadening agent, $Mn^{2+}$, and used the difference in signal intensity to determine the percent of the PC headgroups on the vesicle exterior. $Mn^{2+}$ transiently coordinates to phosphate groups, at a rate faster than can be detected by the NMR, which broadens the $^{31}$P signal, essentially removing its contribution to the signal integration[21]. By adding $Mn^{2+}$ to pre-formed vesicles just prior to acquiring the NMR

spectrum, only the signal from the phosphates on the exterior of the vesicle are broadened, leaving just the interior phosphate signal. The difference in the phosphate signal before and after addition of the $Mn^{2+}$ is equal to the signal from the phosphates on the vesicle exterior. Through this experiment, we determined that 65% of the phosphate groups were on the exterior of the vesicle, which for a vesicle with a 50 nm diameter and 10 nm vesicle wall, corresponds to a symmetric distribution (Fig. 4-9). Given the presence of both the PC and the dimethylamine group on the vesicle exterior and the symmetric distribution of the PC groups, it is unlikely that asymmetric monolayers are forming. However, it is possible that portions of the vesicle wall adopt an asymmetric configuration, while the entire wall maintains an overall symmetric distribution. The Symmetric Monolayer and Bilayer configurations cannot be ruled out and it is possible that both are present.

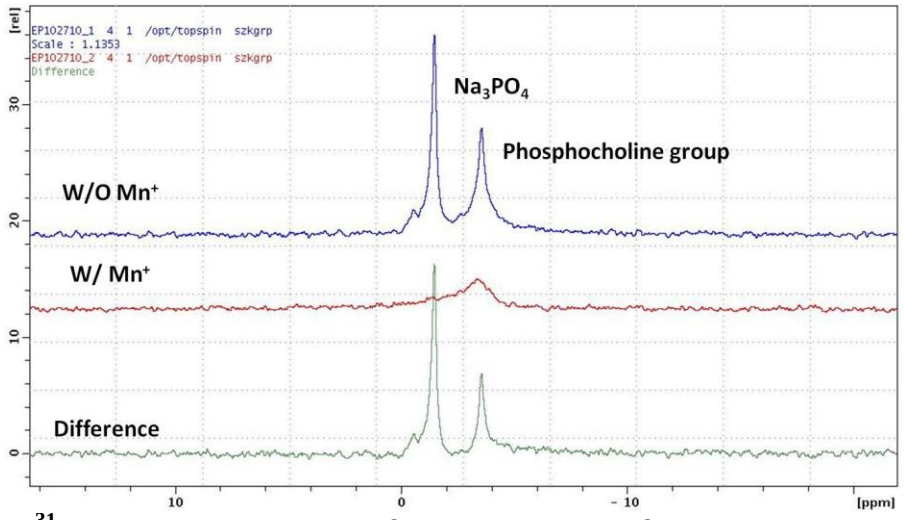


**Figure 4-9: $^{31}$P NMR determination of the Orientation of PC-ABAs within vesicle wall**.

We next used differential scanning calorimetry measurements (DSC) to investigate if the PC-ABAs pack into a crystalline phase and exhibit a phase transition

temperature. Neither pure S-PC-ABA nor P-PC-ABA formulations had a transition temperature between 0-90 °C, which suggests that these systems do not form a crystalline phase above 0 °C. It is unlikely that the Symmetric Monolayer, Bilayer, or a combination phase would readily crystallize due to the neighboring hydrocarbon and fluorocarbon segments and the presence of the ether and thioether linkages. These hydrophilic linkages can both change the geometry of the chains and bring water molecules into the region to disrupt chain packing. Other mixed hydrocarbon/fluorocarbon PC lipids, with comparable chain lengths, had reported transition temperatures of < -25 °C for lipids with one site of unsaturation, and 88 °C for fully saturated chains[22]. The hydrophilic linkers in the PC-ABAs may have an effect similar to the unsaturation in these systems and move the transition temperature below the tested range. Alternatively, it is possible the transition temperature for the lipids is greater than 90 °C, but this is less likely due to the number of ways the packing could be disrupted.

### 4.8.3 PC-ABA vesicle stability

Following the results in Table 4-3 and Figure 4-9b, we next characterized the stability of the PC-ABA vesicles and their ability to encapsulate water-soluble molecules, CF and FITC-Dextran. The results in Fig. 4-10 reveal that PC-ABA vesicles maintain a fairly consist diameter after an initial equilibration period and are quite leaky to small molecules, but gradually release the higher molecular weight FITC-dextran over more than 48 hours.

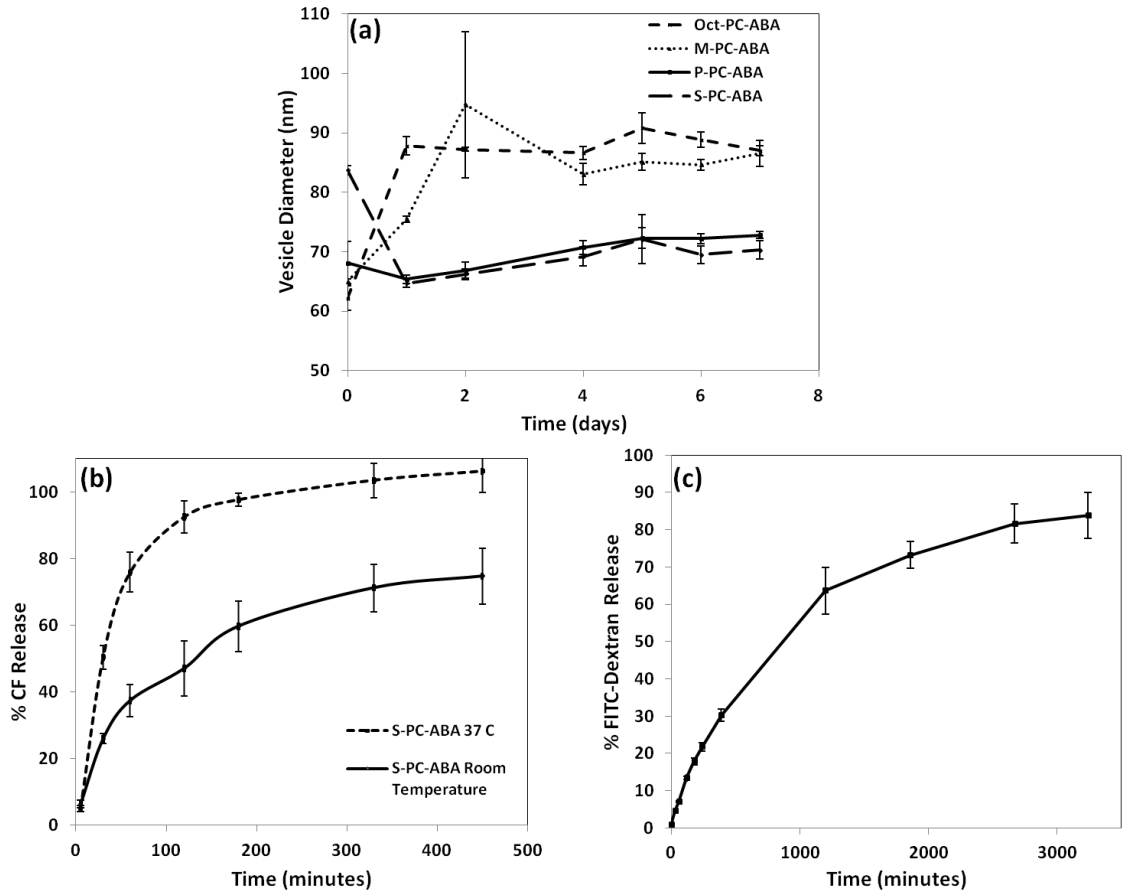


**Figure 4-10: PC-ABA Stability (a)** Variation in vesicle diameter over time. **(b)** Release of encapsulated CF at room temperature and 37 °C. **(c)** Release of FITC-Dextran from S-PC-ABA vesicles at room temperature.

Fig. 4-10a shows that after an initial equilibration, the PC-ABA vesicle diameters are relatively stable for at least a week. The length of the hydrocarbon chain at the 1-position appears to affect the diameter of the resulting vesicles at 24 hours unlike the results in Table 4-3, which were measured shortly after sonication. When the diameters of the formulations have stabilized, the two PC-ABAs with shorter chains at the 1-position, form vesicles of similar sizes and both are larger than the P-PC-ABA and S-PC-ABA vesicles. The change in size following the initial measurement suggests that following sonication, the vesicles are in a metastable state and by the first day, they have transitioned into a stable dispersion of vesicles.

The release studies in Fig. 4-10b,c demonstrate that S-PC-ABA vesicles can encapsulate CF, but quickly release the majority of their content within 400 minutes. At 37 °C, 100% of the CF is released within 8 hours and after 24 hours; the room temperature formulation also released all the CF (data not shown). The fast release of CF may be due to the equilibration phase shown in Fig. 3a for the vesicle diameters. S-PC-ABA vesicles release the macromolecular FITC-Dextran at a slower rate than CF.

**4.9 Conclusions**

Unlike the BLBAs, the PC-ABAs were able to form small-diameter vesicles capable of encapsulating both a small molecule dye and a fluorescently-labeled polymer. The PC-ABAs present a new bolaamphiphile architecture that may provide a basis for the future design of lipids that assemble into small-diameter vesicles. PC-ABA vesicles release both CF and FITC-Dextran more quickly than traditional liposomes, but they do not appear to aggregate or coalesce over the period of a week. It is possible that the PC-ABA vesicles could be made less permeable by removing the hydrophilic linkers (ethers and thioethers) within the bilayer, while retaining the ability to form small vesicles. Future work to create a continuous hydrophobic region, replace the dimethylamine group with alternative hydrophilic groups, and substitute the linear chain at the 1-position for a sterol or branched chain, could provide further insight into the aspects of a bolaamphiphile that promote the formation of small-diameter vesicles.

**4.10 Materials**

All diacyl phospholipids and lyso-PCs were purchased from Avanti Polar Lipid. Solvents were purchased from Fisher Scientific. 1H, 1H, 12H, 12H-perfluorododecanediol was purchased from Synquest Laboratories. All other chemicals were purchased from Sigma

Aldrich. All buffers were made with MilliQ water and passed through a filtration system. NMR measurements were taken on a Bruker 300 MHz Avance system and analyzed with Topspin software. Chemical shifts are expressed as parts per million. HPFC column purifications were performed on a Biotage System (Biotage, LLC Charlotte, NC) with pre-packed Biotage silica cartridges (67 Å, 40.5 μm). All sonication was performed in a G112SP1 Special Ultrasonic Cleaner from Laboratory Supplies Co., Inc (Hicksville, NY).

## 4.11 Methods

### 4.11.1 BLBA Synthesis

BLBA general procedure: N,N-(dimethylamino)-1,2-propanediol was combined with 1 equivalent of $R^1OH$ (see Figure 4-5) in CH2Cl2 with 0.5 g 4-dimethylaminopyridine (DMAP) and 1.2 equivalents of N,N'-Dicyclohexylcarbodiimide (DCC). The reaction was stirred at room temperature for 3 hours and then filtered to remove precipitated dicyclohexylurea. The reaction volume was reduced under vacuum and 2 equivalents of sebacic acid were added and the coupling reaction was run in dry tetrahydrofuran (THF) with 0.5 g DMAP and 1.2 equivalents of DCC. The reaction was stirred for 4 hours at room temperature and then filtered. The THF was removed by rotary evaporation and the product was isolated by flash chromatography and the products were eluted at 3% MeOH in $CHCl_3$. The monosubstituted compound was then dissolved in dry THF and 2 equivalents of 1H, 1H, 10H, 10H-perfluorodecanediol were added along with 0.5 g DMAP and 1.2 equivalents of DCC. For the synthesis of the hydrocarbon derivatives, 1,10-decanediol was used in the place of the fluorocarbon diol. The reaction was stirred for 3 hours and then filtered. The reaction was then washed 2X with 1M HCl to remove

the DMAP. The reaction was reduced in volume and acrylic acid with minimal THF was added and the reaction was heated to 60 °C for several days. The products were purified by flash chromatography and eluted at 12% MeOH in $CHCl_3$ with 2-3% total yields for the entire synthesis. MALDI-MS Chol-FC MW 1296, Toc-FC MW 1338, $C_9$-FC MW 1050, Iso-FC MW 1179, Chol-HC MW 1007. Products were estimated to be on average, 80% pure by NMR with low levels of acrylic acid, sebacic acid, DMAP and dicyclohexylurea as impurities.

### 4.11.2 PC-ABA Synthesis

Compound (1): 1 g 1H, 1H, 12H, 12H-perfluorododecanediol (1.8 mmoles) was dissolved in dry THF with 0.5 g crushed KOH pellets and the solution was stirred for 30 minutes at room temperature. Then 0.75 g of allyl iodide (4.4 mmoles) were added to the reaction along with 0.1 g tetrabutylammonium chloride and the reaction was stirred overnight at room temperature. Then 1 M HCl was added to neutralize the reaction and the organic layer was then collected and dried under rotary evaporation. The product was purified by flash chromatography with a hexane/chloroform system and the product was eluted between at 70 % chloroform in a 15% yield. $^1$H NMR ($CDCl_3$): δ 3.93 (t, 4H); δ 4.15 (d, 4H); δ 5.29 (t, 4H); δ 5.90 (m, 2H).

Compound (2): Compound (1), 2 g (3.1 mmoles) and 0.4 g 2-(Dimethylamino)ethanethiol hydrochloride (3.1 mmoles) 0.8 g and 2,2-Dimethoxy-2-phenylacetophenone (3.1 mmoles) were combined in a flask with 1 mL dichloromethane/methanol (1:1) and reacted under UV light for 10 minutes. Then, 1 g of 11-mercaptoundecanoic acid, (4.95 mmoles) and another 0.8 g 2,2-Dimethoxy-2-phenylacetophenone (3.3 mmoles) were added and the reaction was placed back under

the UV light source for another 10 minutes. . The product was purified by flash chromatography with a chloroform/methanol system and the product was eluted between at 10 % methanol in a 22% yield.

M-PC-ABA: To a flask, 0.2 g 1-myristoyl-sn-glycerol-3-phosphorylcholine (0.43 mmoles) and 0.4 g Compound (2) (0.43 mmoles) were added along with 0.05 g 4-(dimethylamino)pyridine (DMAP) and 0.15 g N,N'-Dicyclohexylcarbodiimide in dichlromethane. The reaction was stirred for 3 hours at room temperature. The product was purified by flash chromatography with a chloroform/methanol/ammonium hydroxide system and the product was eluted between at 35% methanol/ammonium hydroxide (35:5) in a 10% yield. $^{1}$H NMR ($CDCl_3$): δ 0.90 (t, 3H); δ 1.29 (m, 32H); δ 1.60 (m, 6H); δ 1.90 (m, 4H); δ 2.3 (m, 4H); δ 2.51 (m, 2H); δ 2.60 (m, 2H); δ 2.72 (m, 2H); δ 2.90 (s, 6H); δ 3.01 (m, 2H); δ 3.26 (m, 2H); δ 3.45 (s, 9H); δ 3.73 (m, 4H); δ 3.97-4.15 (m, 9H); δ 4.38-4.45 (m, 3H); δ 5.25 (m, 1H). $^{19}$F NMR ($CDCl_3$): δ -123.3 (s, 4F); δ -121.7 (m, 8F); δ -119.4 (s, 4F). MALDI-MS calc'd mass 1415, found 1416.

$C_8$-PC-ABA: $C_8$-PC-ABA was synthesized by the same method as M-PC-ABA with a yield of 67 %. $^{1}$H NMR ($CDCl_3$): δ 0.90 (t, 3H); δ 1.29 (m, 20H); δ 1.59 (m, 6H); δ 1.90 (m, 4H); δ 2.3 (m, 4H); δ 2.51 (m, 2H); δ 2.61 (m, 4H); δ 2.71 (s, 6H); δ 2.85 (m, 2H); δ 3.29 (m, 2H); δ 3.39 (s, 9H); δ 3.7 (m, 4H); δ 3.85-3.96 (m, 8H); δ 4.14 (m, 1H); δ 4.32-4.42 (m, 3H); δ 5.21 (m, 1H). $^{19}$F NMR ($CDCl_3$): δ -123.3 (s, 4F); δ -121.9 to-121.7 (m, 8F); δ -119.5 to -119.4 (s, 4F). MALDI-MS calc'd mass 1331, found 1332.

P-PC-ABA: Oct-PC-ABA was synthesized by the same method as M-PC-ABA with a yield of 12 %. $^{1}$H NMR ($CDCl_3$): δ 0.88 (t, 3H); δ 1.26 (m, 36H); δ 1.58 (m, 6H); δ 1.88 (m, 4H); δ 2.3 (s, 4H); δ 2.50 (m, 2H); δ 2.59-2.66 (m, 4H); δ 2.8 (m, 8H); δ 3.28 (m,

2H); δ 3.31 (s, 9H); δ 3.69 (m, 4H); δ 3.80 (m, 2H); δ 3.94 (m, 5H); δ 4.0-4.2 (m, 2H); δ 4.35 (m, 3H); δ 45.1 (m, 1H). $^{19}$F NMR ($CDCl_3$): δ -123.3 (s, 4F); δ -121.9 to-121.69 (m, 8F); δ -119.5 to -119.4 (s, 4F). MALDI-MS calc'd mass 1443, found 1446.

S-PC-ABA: Oct-PC-ABA was synthesized by the same method as M-PC-ABA with a yield of 33 %. $^{1}$H NMR ($CDCl_3$): δ 0.90 (t, 3H); δ 1.28 (m, 40H); δ 1.59 (m, 6H); δ 1.90 (m, 4H); δ 2.3 (s, 4H); δ 2.52 (m, 2H); δ 2.62 (m, 2H); δ 2.70 (m, 2H); δ 2.85 (s, 6H); δ 2.94 (m, 2H); δ 3.18 (m, 2H); δ 3.43 (s, 9H); δ 3.47 (m, 4H); δ 3.91-3.96 (m, 8H); δ 4.13 (m, 1H); δ 4.34 (m, 3H); δ 5.22 (m, 1H). $^{19}$F NMR ($CDCl_3$): δ -123.3 (s, 4F); δ -121.9 to-121.69 (m, 8F); δ -119.5 to -119.4 (s, 4F). MALDI-MS calc'd mass 1472, found 1473.

### 4.11.3 BLBA Vesicle Formation

Chloroform solutions of lipids were dried in test tubes and the lipid film was rehydrated with 200 μL of either a 10 mM Tris buffer, pH 9.1 or a 10mM Glycine buffer, pH 3.1. Each preparation was sonicated for 10 minutes at 57°C and then measured. Total lipid concentrations were 5 mM for the pure betaine-ABAs and 10 mM for the betaine-ABA-phospholipid formulations. Diameter and zeta potential were measured on a Malvern Zetasizer. Mark-Houwink parameters were used for size measurements and the Smoluchowski model was used for zeta potential measurements as provided by Malvern's Zetasizer software package.

### 4.11.4 BLBA/DMPC Vesicle Diameter Stability Over Time

$C_9$-FC, Chol-FC and Toc-FC were combined in a 1:1 molar ratio with DMPC, rehydrated to a concentration of 10 mM BLBA in a Tris pH 9.1 buffer, sonicated for 10 min at 57 °C. The diameters of the preparations were measured daily as described above.

### 4.11.5 Optimal $C_9$-FC/DMPC ratio

$C_9$-FC/DMPC vesicles with different ratios of DMPC and $C_9$-FC were prepared and measured as above.

### 4.11.6 Effect of PC-lipid Chain Length on Vesicle Size

$C_9$-FC/PC-lipid (1:1 molar) vesicles were prepared and measured as described above.

### 4.11.7 PC-ABA Vesicle Formation at Various pHs

Preparations were rehydrated from a thin film in a test tube to a final concentration of 26 mM lipid with the specified buffer. Preparations were heated with gentle agitation in an 80 °C heat bath for 2 minutes and then sonicated for 7 minutes at 80 °C under argon. Diameter and zeta potential were measured on a Malvern Nanosizer. Mark-Houwink parameters were used for size measurements and the Smoluchowski model was used for zeta potential measurements as provided by Malvern's Nanosizer software package.

### 4.11.8 Variation in PC-ABA Vesicle Diameter Over Time

The vesicle preparations made in pH 7.4 for the initial diameter and zeta potential measurements reported in Table 4-3 were measured in the method above over the course of a week.

### 4.11.9 TEM Imaging of S-PC-ABA

S-PC-ABA vesicles were prepared in the 10 mM HEPES buffer with 150 mM NaCl at pH 7.4 through thin film rehydration to a final PC-ABA concentration of 10 mM. The preparations were heated at 60 °C and sonicated for 5 minutes. Copper Grids with 400 mesh and Formvar/carbon coatings from Structure Probe, Inc (West Chester, PA) were glow discharged prior to use. The S-PC-ABA solution was dropped onto the grid and

allowed to adsorb for 1 minute. The liposome solution was then wicked away and the grid surface was washed three times with MilliQ water. Then a 1% solution of uranyl acetate in water was dropped on the grid and allowed to sit for 1 minute. The uranyl acetate solution was then wicked away and the grid was washed once with water and excess water was removed and the grid was allowed to dry. TEM images were collected on a FEI Tecnai 12 transmission electron microscope at the Berkeley Electron Microscopy Lab at UC Berkeley, Berkeley, CA.

#### 4.11.10 Differential Scanning Calorimetry, Transition Temperature Measurements

PC-ABA dispersions were prepared by thin film hydration in 10 mM HEPES, 150 mM NaCl, pH 7.4 to a final concentration of 10 mM lipid, followed by brief vortex and heating at 60 °C to disperse the film into small lipid bilayer fragments. Then 200 uL of each preparation were added into each calorimeter chamber with buffer used in the specific liposome preparation as the standard. The measurements were run on a MC-DSC 4100 (Calorimetry Sciences Corp.) from 10 to 90° C at 1 degree/minute with a heat-cool-heat cycle where the last heating cycle is reported. Data was processed with CpCalc software and transferred to Excel to be graphed.

#### 4.11.11 S-PC-ABA Carboxyfluorescein (CF) Release

The S-PC-ABA preparation was dried from a chloroform solution into a thin film on a glass test tube and rehydrated in a solution of 100 mM CF, 10 mM Tris, pH 7.4. The preparation was then sonicated for 7 minutes at 60 °C and cooled to room temperature. Free CF was removed by size exclusion chromatography on a PD-10 Sephadex column (GE Health Sciences) by elution in an isotonic buffer: 100 mM NaCl, 10 mM HEPES, pH 7.4. Then, 100 μL of the purified S-PC-ABA vesicle solution was added to 3 mL of

the elution buffer. CF release was measured at two different temperatures, room temperature and 37 °C. The amount of CF released at each time point was measured on a FLUOstar plate reader (BMG Labtech) with Ex 485 nm and Em 520 nm. Percent leakage values were calculated by measuring the total CF preparation by liposome lysis with $C_{12}E_{10}$ surfactant. All measurements were run in triplicate. Percent Release was calculated as follows: % Release at time, (t) = (measured fluorescence at time, (t)) / (total fluorescence from lysed liposomes) X 100.

**4.11.12 $^{31}$P NMR Measurements:**

An S-PC-ABA film was rehydrated in $D_2O$ with 5 mM sodium phosphate. The mixture was sonicated for 10 minutes at 60° C to give a clear solution. The initial spectrum was collected (blue) and then 5μL of a 240 mM $Mn^{2+}$ solution was added to eliminate the phosphorus signal from the phosphates on the exposed exterior of the vesicles, and another spectrum was taken (red). The difference from the first and second spectrums is shown in green. Comparison of the integration of the blue phosphocholine peak and the green phosphocholine peak, with each normalized to their respective sodium phosphate peak integration, reveals the percentage of phosphocholine groups on the exterior of the liposome to be 65%.

**4.11.13 FITC-Dextran Release**

S-PC-ABA was rehydrated from a thin film in 10 mM HEPES with 150 mM NaCl and 40 mg/mL FITC-Dextran (ave. MW 4000), pH 7.4 to a concentration of 7 mM S-PC-ABA. The preparation was sonicated at 60 °C for 5 minutes and then purified by size exclusion using a Sepharose CL-2B resin. The liposome fraction was eluted in 10 mM HEPES, 150 mM NaCl, pH 7.4. The collected fraction was then transferred into a dialysis

cartridge with 10,000 MW cutoff. The cartridge was placed in 100 mL of the elution buffer and the fluorescence of the dialysis buffer was measured over time. The maximum release was calculated by adding the same amount of the formulation to 100 mL elution buffer with 30 μL of a 15% $C_{12}E_{10}$ solution and stirring for 5 minutes. The fluorescence of the lysed solution was then measured. All measurements were taken at Ex. 494 nm and Em. 518 nm. Percent release was calculated by: % Release (t) = (fluorescence at time (t))/(maximum fluorescence) X 100.

### 4.12 References


1. D. V. Devine, K. Wong, K. Serrano, A. Chonn and P. R. Cullis, *Biochimica et Biophysica Acta (BBA) - Biomembranes*, 1994, 1191, 43-51.
2. T. Lian and R. J. Y. Ho, *Journal of Pharmaceutical Sciences*, 2001, 90, 667-680.
3. D. Liu, A. Mori and L. Huang, *Biochimica et Biophysica Acta (BBA) - Biomembranes*, 1992, 1104, 95-101.
4. R. M. Abra, C. A. Hunt and D. T. Lau, *Journal of Pharmaceutical Sciences*, 1984, 73, 203-206.
5. R. M. Abra and C. A. Hunt, *Biochimica et Biophysica Acta (BBA) - Lipids and Lipid Metabolism*, 1981, 666, 493-503.
6. C. E.L, *Biochemical and Biophysical Research Communications*, 1994, 202, 673-679.
7. B. Debora, *Current Opinion in Colloid & Interface Science*, 2006, 11, 74-78.
8. T. Kai, X.-L. Sun, K. M. Faucher, R. P. Apkarian and E. L. Chaikof, *The Journal of Organic Chemistry*, 2005, 70, 2606-2615.
9. A. Meister, S. Drescher, V. M. Garamus, G. r. Karlsson, G. Graf, B. Dobner and A. Blume, *Langmuir*, 2008, 24, 6238-6246.
10. X. Wang, Y. Shen, Y. Pan and Y. Liang, *Langmuir*, 2001, 17, 3162-3167.
11. J. J. Bozell, N. C. Tice, N. Sanyal, D. Thompson, J.-M. Kim and S. b. Vidal, *The Journal of Organic Chemistry*, 2008, 73, 8763-8771.
12. S. Zhou, C. Xu, J. Wang, W. Gao, R. Akhverdiyeva, V. Shah and R. Gross, *Langmuir*, 2004, 20, 7926-7932.
13. Y. Yan, J. Huang, Z. Li, J. Ma, H. Fu and J. Ye, *The Journal of Physical Chemistry B*, 2003, 107, 1479-1482.
14. S. Chen, B. Song, Z. Wang and X. Zhang, *The Journal of Physical Chemistry C*, 2008, 112, 3308-3313.
15. M. Roussel, V. Lognone, D. Plusquellec and T. Benvegnu, *Chemical Communications*, 2006, 3622-3624.
16. C. Zhan, P. Gao and M. Liu, *Chemical Communications*, 2005, 462-464.
17. C. C. Forbes, K. M. DiVittorio and B. D. Smith, *J Am Chem Soc*, 2006, 128, 9211-9218.

18. M. Masuda and T. Shimizu, *Chemical Communications*, 2001, 2442-2443.
19. V. H. Dalvi and P. J. Rossky, *Proceedings of the National Academy of Sciences*, 2010, 107, 13603-13607.
20. J. Weinstein, S. Yoshikami, P. Henkart, R. Blumenthal and W. Hagins, *Science*, 1977, 195, 489-492.
21. H. QUIQUAMPOIX, G. BAČIĆ, B. C. LOUGHMAN and R. G. RATCLIFFE, *Journal of Experimental Botany*, 1993, 44, 1809-1818.
22. V. Ravily, C. Santaella, P. Vierling and A. Gulik, *Biochimica et Biophysica Acta (BBA) - Biomembranes*, 1997, 1324, 1-17.

Chapter 5

# Thesis Summary

The results presented in this thesis highlight the sensitivity of lipid and liposome properties to small changes in lipid architecture and chemistry. In Chapter 2, we showed that an inversion of the traditional PC headgroup results in significantly different surface and permeability properties, even when the overall charge of the headgroup remained unchanged. In Chapter 3, we made a second alteration to the lipid structure by replacing the phosphate in the IPC lipids with a sulfonate (along with an additional carbon in the sulfonate-amine linking region). This substitution led to drastic changes in the ability to form liposomes, the interaction of the liposomes with anions, and the bilayer transition temperature.

In Chapter 4, we describe the process of designing a lipid-like molecule specifically for forming small diameter vesicles. While the end result in Chapter 4 was close to our target vesicle size, we discovered that the theory behind the structure did not hold and was not the driving factor in decreasing the vesicle diameter. Pure formulations of the BLBAs did not form stable, small vesicles and while the pure PC-ABAs did, we determined it was not a result of the fluorocarbon-hydrocarbon phase separation promoting the formation of an asymmetric monolayer.

Many of the new lipid properties discovered in this thesis would have been difficult to predict based on the chemical structure alone and they demonstrate how complicated it is to foretell how significant a given change to a lipid will be. The lipids described in my thesis will provide physical chemists with useful tools for studying the properties of bilayers and other self-assembled architectures. Oftentimes the only way to

know is to make the lipid and measure its properties, which can be incredibly time-consuming. Progress in the liposome field would also gain from other deliberate measures such as the development of more detailed and accurate computer models of the liposome assembly process and a database or toolbox containing lipids—both synthetic and natural—and their known biophysical properties.

Although complex, the continued development of lipid-based therapies is both important and relevant. The ability of liposomes to encase and protect macromolecules from enzymatic degradation and potentially deliver them to a target site makes them a worthy delivery system to pursue. The development of a safe and effective delivery system for biopolymers such as proteins, peptides, RNA and DNA, would provide major advances in the treatment of many diseases and genetic disorders for which small molecules have limited efficacy. I believe there is a diverse and full future for liposomes and other lipid-based therapeutics and hopefully both the specific lipids and the principles developed in this work will provide a small contribution toward it.

**Publishing Agreement**

*It is the policy of the University to encourage the distribution of all theses, dissertations, and manuscripts. Copies of all UCSF theses, dissertations, and manuscripts will be routed to the library via the Graduate Division. The library will make all theses, dissertations, and manuscripts accessible to the public and will preserve these to the best of their abilities, in perpetuity.*

***Please sign the following statement:***

*I hereby grant permission to the Graduate Division of the University of California, San Francisco to release copies of my thesis, dissertation, or manuscript to the Campus Library to provide access and preservation, in whole or in part, in perpetuity.*

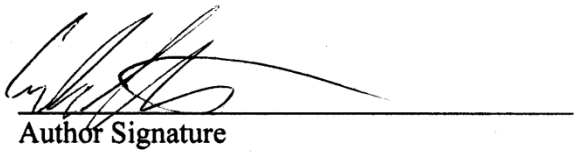

Author Signature

1/12/12

Date